AD-A184 411 FLUTTER ANALYSIS OF A TWO-DIMENSIONAL AIRFOIL CONTAINING STRUCTURAL NONLI (U) NATIONAL AERONAUTICAL ESTABLISHMENT OTTAWA (ONTARIO) B H LEE ET AL MAY 87 1/1

UNCLASSIFIED NAE-LR-618 NRC-27833 N00014-84-C-0132 F/G 1/3 NL

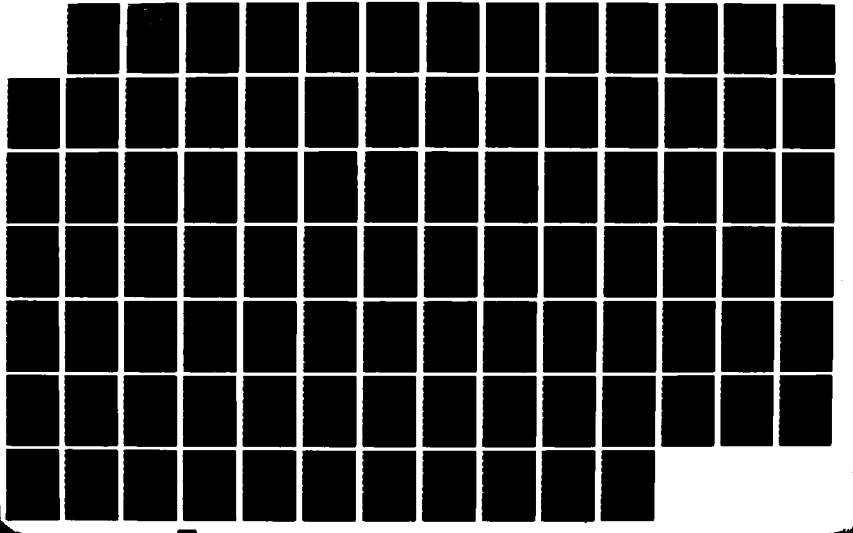

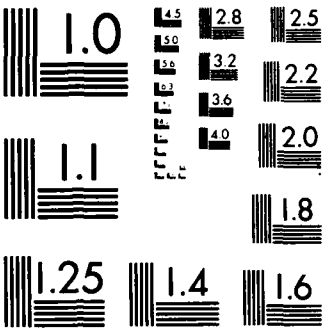

National Research Council Canada

Conseil national de recherches Canada

FLUTTER ANALYSIS OF A TWO-DIMENSIONAL AIRFOIL CONTAINING STRUCTURAL NONLINEARITIES

by

B. H. K. Lee, J. Desrochers

National Aeronautical Establishment

OTTAWA

MAY 1987

AERONAUTICAL REPORT

LR-618

NRC NO. 27833

Canada

NATIONAL AERONAUTICAL ESTABLISHMENT

SCIENTIFIC AND TECHNICAL PUBLICATIONS

AERONAUTICAL REPORTS:

Aeronautical Reports (LR): Scientific and technical information pertaining to aeronautics considered important, complete, and a lasting contribution to existing knowledge.

Mechanical Engineering Reports (MS): Scientific and technical information pertaining to investigations outside aeronautics considered important, complete, and a lasting contribution to existing knowledge.

AERONAUTICAL NOTES (AN): Information less broad in scope but nevertheless of importance as a contribution to existing knowledge.

LABORATORY TECHNICAL REPORTS (LTR): Information receiving limited distribution because of preliminary data, security classification, proprietary, or other reasons.

Details on the availability of these publications may be obtained from:

Publications Section,
National Research Council Canada,
National Aeronautical Establishment,
Bldg. M-16, Room 204,
Montreal Road,
Ottawa, Ontario
K1A 0R6

ÉTABLISSEMENT AÉRONAUTIQUE NATIONAL

PUBLICATIONS SCIENTIFIQUES ET TECHNIQUES

RAPPORTS D'AÉRONAUTIQUE

Rapports d'aéronautique (LR): Informations scientifiques et techniques touchant l'aéronautique jugées importantes, complètes et durables en termes de contribution aux connaissances actuelles.

Rapports de génie mécanique (MS): Informations scientifiques et techniques sur la recherche externe à l'aéronautique jugées importantes, complètes et durables en termes de contribution aux connaissances actuelles.

CAHIERS D'AÉRONAUTIQUE (AN): Informations de moindre portée mais importantes en termes d'accroissement des connaissances.

RAPPORTS TECHNIQUES DE LABORATOIRE (LTR): Informations peu disséminées pour des raisons d'usage secret, de droit de propriété ou autres ou parce qu'elles constituent des données préliminaires.

Les publications ci-dessus peuvent être obtenues à l'adresse suivante:

Section des publications
Conseil national de recherches Canada
Établissement aéronautique national
Im. M-16, pièce 204
Chemin de Montréal
Ottawa (Ontario)
K1A 0R6

FLUTTER ANALYSIS OF A TWO-DIMENSIONAL AIRFOIL CONTAINING STRUCTURAL NONLINEARITIES

ANALYSE DE L'AÉROÉLASTICITÉ D'UN PROFIL D'AILE BIDIMENSIONNEL PRÉSENTANT DES NON-LINÉARITÉS STRUCTURALES

by/par

B.H.K. Lee, J. Desrochers*

* Summer Student/Étudiant, session d'été
McGill University/Université McGill

L.H. Ohman, Head/Chef
High Speed Aerodynamics Laboratory/
Laboratoire d'aérodynamique à hautes vitesses

G.F. Marsters
Director/Directeur

SUMMARY

Nonlinear flutter of a two-dimensional airfoil undergoing plunging and pitching motions is studied using a time marching finite difference scheme. The structural nonlinearity considered is of the type due to a spring with preload and freeplay. Flutter is determined from solutions of the structural dynamic equations of motion when either divergent or limited amplitude oscillations are encountered. Case studies using various airfoil parameters and values of preload and freeplay are carried out. The effect of initial condition, which is important in nonlinear problems, is investigated by varying the displacement from equilibrium of the pitch angle at the beginning of the airfoil motion. For nonzero values of the preload, three types of oscillatory motion are possible, namely: damped, limited amplitude and divergent. The divergent flutter boundary is practically identical to that for the linear flutter case. The location of the limit-cycle flutter boundary varies for different airfoil and spring parameters. For zero preload, damped oscillations are not encountered even for air speeds down to 15 percent of the linear flutter speed which is the lowest used in this study. The limited amplitudes of the pitch and plunge motions are found to be independent of initial angular displacement. The characteristics of the oscillations and the development of higher harmonics in the various regions defined by the flutter boundary curves are investigated.

RÉSUMÉ

L'aéroélasticité non-linéaire d'un profil d'aile bidimensionnel subissant des mouvements de tangage est étudiée au moyen d'un schéma en différences finies en fonction du temps. La non-linéarité structurale étudiée est celle produite par un ressort préchargé et à jeu libre. L'aéroélasticité est déterminée à partir des solutions aux équations dynamiques structurales de mouvement lorsqu'il y a oscillations à amplitude limitée ou divergente. Des études de cas sont menées à partir de divers paramètres de profil d'aile et de diverses valeurs de précharge et de jeu libre. On étudie l'effet de l'état initial, important dans les problèmes de non-linéarité, en faisant varier le mouvement par rapport au point d'équilibre de l'angle de tangage dès que le profil d'aile commence à se déplacer. Pour des valeurs de précharge différentes de zéro, trois types d'oscillation sont possibles, soit: oscillation amortie, oscillation à amplitude limitée et oscillation divergente. La limite d'aéroélasticité divergente est pratiquement identique à celle de l'aéroélasticité linéaire. L'emplacement des oscillations limites d'aéroélasticité varie en fonction des paramètres de profil d'aile et de ressort. Pour une précharge nulle, aucune oscillation amortie n'est relevée, même dans le cas de vitesses aérodynamiques ramenées à 15 pour-cent de la vitesse d'aéroélasticité linéaire, laquelle est la plus faible utilisée dans le cadre de l'étude. On a trouvé que les amplitudes limitées des mouvements de tangage étaient indépendantes du déplacement angulaire initial. Les caractéristiques des oscillations et la production d'harmoniques supérieures dans les diverses zones délimitées par les courbes limites d'aéroélasticité sont étudiées.

CONTENTS

LIST OF ILLUSTRATIONS

Appendices

Table

List of Symbols

Symbol	Definition
a	constant in Equation (11)
a_h	nondimensional distance measured from airfoil mid-chord to elastic axis
b	semi-chord of airfoil; also constant in Equation (11)
c	chord; also constant in Equation (11)
d	constant in Equation (11)
F	defined in Equation (8)
$\bar{F}$	nonlinear function representing restoring moment
F_p	defined in Equation (16)
F_α	defined in Equation (17)
h	plunge displacement
h_{f^+}	value of α at beginning of freeplay
h_{f^-}	value of α at end of freeplay
ℓ	constant defined in Equation (11)
m	mass of airfoil per unit span
$\bar{P}_{11}, \bar{P}_{12}, \bar{P}_{21}, \bar{P}_{22}$	elements of matrix [P] defined in Appendix A
p	defined in Equation (9)
$\bar{Q}_{11}, \bar{Q}_{12}, \bar{Q}_{21}, \bar{Q}_{22}$	elements of matrix [Q] defined in Appendix B
r	defined in Equation (10)
r_α	radius of gyration about elastic axis
t	time
U	free stream velocity
U^*	nondimensional velocity defined in Equation (7)
U_L^*	nondimensional linear flutter speed

Symbol	Definition
V_{f°	preload
x_α	nondimensional distance measured from elastic axis to centre of mass
$\bar{X}_1, \bar{X}_2$	elements of matrix $\{X\}$ defined in Appendix A
$Y_2^{(1)}, Y_2^{(2)}, Y_1^{(3)}, Y_2^{(3)}, Y_1^{(4)}, Y_2^{(4)}$	elements of matrix $\{Y^{(n)}\}$ defined in Appendix B
α	pitch angle
$\bar{\alpha}$	estimated value of α in Equations (16) and (17)
α_A	limited amplitude of α
ζ_α	viscous damping ratio of pitching motion
ζ_ξ	viscous damping ratio of plunging motion
λ	defined in Equation (A8)
μ	airfoil-air mass ratio, $m/\pi\rho b^2$
ξ	nondimensional plunge displacement
ξ_A	limited amplitude of ξ
ρ	air density
τ	nondimensional time
ϕ	Wagner's function
ω	frequency
ω_α	uncoupled natural frequency of pitching motion of linear system
ω_ξ	uncoupled natural frequency of plunging motion of linear system
$\bar{\omega}$	ratio, ω_ξ/ω_α

1.0 Introduction

The assumption of structural linearity is frequently made to enable the use of analytical methods in determining the divergence and flutter characteristics of aerodynamic surfaces. Linear theory will predict the magnitude of dynamic pressure or flight velocity above which the system under consideration becomes unstable and the motion grows exponentially in time. However, aircraft structures often exhibit nonlinearities which affect not only the flutter speed, but also the characteristics of flutter motion. An understanding of the nonlinear behaviour of the system is crucial to the efficient and safe design of aircraft wings and control surfaces.

Reference 1 gives an excellent discussion of the various types of nonlinearities and some of the methods used to treat them. In general, structural nonlinearities can be categorized as either distributed or concentrated. Only the latter is considered in this study because they are more important. An example of this type of nonlinearity, which is investigated in this report, is the freeplay representing a loose hinge or linkage of a control system. The response characteristics are usually functions of the amplitude of oscillation. The system stiffness behaviour changes with amplitude of motion and at some particular flight speed the motion can be self-excited and attain a limited amplitude. The appearance of the phenomenon of limit-cycle flutter is important from the design viewpoint. These oscillations may occur within the divergence and flutter flight envelope, but the amplitude, frequency and duration of these limit-cycle oscillations may have an important impact on the structural integrity of the aerodynamic surfaces.

Woolston et al (Ref. 2) studied the effects of structural nonlinearities on the flutter of a two-dimensional airfoil using an analog computer. There are serious drawbacks in the use of an analog computer to analyse nonlinear flutter and accuracy is often not as great as one would desire. An alternate analytical approach was suggested by Shen (Ref. 3) using the well known Kryloff and Bogoliuboff (Ref. 4) method in nonlinear vibration theory. The original limitation of weak nonlinearities was removed by adopting a modification given by Popov (Ref. 5). Only rigid surfaces with single nonlinearity were treated. Extensions to multiple nonlinearities (Ref. 6, 7) and inclusion of higher harmonic terms (Ref. 8) have been reported in recent studies.

Another method of investigating nonlinear flutter is by numerical time integration of the structural equations of motion. This has the advantage that no assumptions on the type of motion have to be made beforehand. Also, the effect of initial conditions, which is important in nonlinear problems, can readily be investigated.

Flutter analyses of two-dimensional airfoils with aerodynamic nonlinearities and structural nonlinearities of the type due to a cubic spring have been studied by Lee and LeBlanc (Refs. 9 and 10). In that study, Houbolt's (Ref. 11) finite difference scheme was found to be efficient and of sufficient accuracy in determining flutter boundaries. Following the approach used in Ref. 10, the aeroelastic equations for a two-dimensional airfoil performing plunging and pitching motions are written in this report in finife difference form using incompressible aerodynamics in the time domain given by Wagner's function. The effect of initial conditions on nonlinear flutter is

studied by varying the displacement from equilibrium of the pitch angle at the beginning of the airfoil motion. Divergent and limit-cycle flutter are investigated using different airfoil parameters and values of spring preload and freeplay. The characteristics of the oscillations and the development of higher harmonics in the various regions defined by the flutter boundary curves are analysed. The results are useful not only in assessing the validity and accuracies of the method of harmonic balance (Refs. 3-8) commonly used in the study of nonlinear flutter, but also in understanding the impact of limit-cycle oscillations on the structural integrity of aerodynamic surfaces.

2.0 Analysis

2.1 Two-Degree-of-Freedom Motion of a 2-D Airfoil

Figure 1 shows the notations used in the analysis of a two-degree-of-freedom motion of an airfoil oscillating in pitch and in plunge. The plunging deflection is denoted by h, positive in the downward direction, α is the pitch angle about the elastic axis, positive with the nose up. The elastic axis is located at a distance $a_h b$ from the midchord, while the mass centre is located at a distance $x_\alpha b$ from the elastic axis. Both distances are positive when measured towards the trailing edge of the airfoil. The aeroelastic equations of motion for linear springs have been derived by Fung (Ref. 12). For nonlinear restoring moment from a spring with preload and freeplay in the torsional degree of freedom (Figure 2), they can be written as follows:

$$m\ddot{h} + S\ddot{\alpha} + C_h\dot{h} + K_h h = P \tag{1}$$

$$S\ddot{h} + I_\alpha\ddot{\alpha} + C_\alpha\dot{\alpha} + \bar{F}(\alpha) = R \tag{2}$$

where the dot represents differentiation with respect to time. S is the airfoil static moment about the elastic axis, $\bar{F}(\alpha)$ is a nonlinear function representing the restoring moment, P and R are the externally applied force and moment respectively. The symbols m, C_h, K_h, I_α and C_α are the airfoil mass, linear damping coefficient, linear spring constant, wing mass moment of inertia about the elastic axis, and torsional damping constant respectively.

Define $\xi = h/b$, $x_\alpha = S/bm$, $\omega_\xi = (K_h/m)^{\frac{1}{2}}$, $\omega_\alpha = (K_\alpha/I_\alpha)^{\frac{1}{2}}$, $r_\alpha = (I_\alpha/mb^2)^{\frac{1}{2}}$, $\zeta_\xi = C_h/2(mK_h)^{\frac{1}{2}}$, $\zeta_\alpha = C_a/2(I_\alpha K_\alpha)^{\frac{1}{2}}$. Here K_α is the torsional spring constant for the linear part of the moment-displacement curve shown in Figure 2. Equations (1) and (2) can be written in nondimensional form as follows:

$$\xi''(\tau) + x_\alpha\alpha''(\tau) + 2\zeta_\xi\frac{\bar{\omega}}{U^*}\xi'(\tau) + \left[\frac{\bar{\omega}}{U^*}\right]^2\xi(\tau) = p(\tau) \tag{3}$$

$$\frac{x_\alpha}{r_\alpha^2}\xi''(\tau) + \alpha''(\tau) + 2\zeta_\alpha\frac{\alpha'(\tau)}{U^*} + \frac{1}{U^{*2}}F[\alpha(\tau)] = r(\tau) \tag{4}$$

where $p(\tau)$ and $r(\tau)$ are the nondimensional force and moment respectively. The prime denotes differentiation with respect to the non-dimensional time τ defined as

$$\tau = \frac{Ut}{b} \tag{5}$$

In Eqs. (3) and (4), $\bar{\omega}$ is given by

$$\bar{\omega} = \frac{\omega_\xi}{\omega_\alpha} \tag{6}$$

U* is defined as

$$U^* = \frac{U}{b\omega_\alpha} \tag{7}$$

From Figure 2., $F(\alpha)$ can be written as

$$F(\alpha) = \begin{cases} \alpha + V_{f^\circ} - h_{f^+} & \alpha < h_{f^+} \\ V_{f^\circ} & h_{f^+} \leq \alpha \leq h_{f^-} \\ \alpha + V_{f^\circ} - h_{f^-} & h_{f^-} < \alpha \end{cases} \tag{8}$$

For incompressible flow, Fung (Ref. 12) gives the following expressions for $p(\tau)$ and $r(\tau)$:

$$\begin{aligned} p(\tau) = & -\frac{1}{\mu}\left[\xi''(\tau) - a_h\alpha''(\tau) + \alpha'(\tau)\right] \\ & - \frac{2}{\mu}\left[\left\{\alpha(0) + \xi'(0) + \left(\tfrac{1}{2} - a_h\right)\alpha'(0)\right\}\phi(\tau)\right. \\ & \left. + \int_0^\tau \phi(\tau-\sigma)\left[\alpha'(\sigma) + \xi''(\sigma) + \left(\tfrac{1}{2} - a_h\right)\alpha''(\sigma)\right]d\sigma\right] \end{aligned} \tag{9}$$

$$r(\tau) = \frac{2}{\mu r_\alpha^2}\left(\tfrac{1}{2}+a_h\right)\left\{\left[\alpha(0)+\xi'(0)+\left(\tfrac{1}{2}-a_h\right)\alpha'(0)\right]\phi(\tau)\right.$$

$$\left.+\int_0^\tau \phi(\tau-\sigma)\left[\alpha'(\sigma)+\xi''(\sigma)+\left(\tfrac{1}{2}-a_h\right)\alpha''(\sigma)\right]d\sigma\right\}$$

$$+\frac{1}{\mu r_\alpha^2}\left\{a_h\left[\xi''(\tau)-a_h\alpha''(\tau)\right]-\left(\tfrac{1}{2}-a_h\right)\alpha'(\tau)-\frac{1}{8}\alpha''(\tau)\right\} \quad (10)$$

where μ is the airfoil-air mass ratio, and the Wagner's function $\phi(\tau)$ is given by

$$\phi(\tau) = \ell - ae^{-b\tau} - ce^{-d\tau} \quad (11)$$

and for incompressible flow, the constants $\ell = 1$, $a = 0.165$, $b = 0.0455$, $c = 0.335$ and $d = 0.3$ are given in Ref. 12.

2.2 Finite Difference Scheme

For a system with few structural components or the number of vibration modes is small, higher order methods such as the eighth order scheme reported in Ref. 13 does not offer any distinct advantage over Houbolt's (Ref. 11) scheme which is simpler and less cumbersome to use. For this reason, Houbolt's method is used in the present analysis. The derivatives at time $\tau+\Delta\tau$ are replaced with backward difference formulas using values at three previous points. For example,

$$\alpha''(\tau+\Delta\tau) = \frac{1}{\Delta\tau^2}\left[2\alpha(\tau+\Delta\tau)-5\alpha(\tau)+4\alpha(\tau-\Delta\tau)-\alpha(\tau-2\Delta\tau)\right] \quad (12)$$

and

$$\alpha'(\tau+\Delta\tau) = \frac{1}{6\Delta\tau}\left[11\alpha(\tau+\Delta\tau)-18\alpha(\tau)+9\alpha(\tau-\Delta\tau)-2\alpha(\tau-2\Delta\tau)\right] \qquad (13)$$

Similar expressions can be written for $\xi''(\tau+\Delta\tau)$ and $\xi'(\tau+\Delta\tau)$. In difference form, Eqs. (3) and (4) can be expressed as:

$$\bar{P}_{11}\alpha(\tau+\Delta\tau) + \bar{P}_{12}\,\xi(\tau+\Delta\tau) = \bar{X}_1 \qquad (14)$$

$$[\bar{P}_{21} + U^{*-2}\,F_p]\alpha(\tau+\Delta\tau) + \bar{P}_{22}\xi(\tau+\Delta\tau) = \bar{X}_2 - U^{*-2}F_\alpha \qquad (15)$$

In Eq. (15), $F[\alpha(\tau)]$ has been replaced with $F_p(\alpha;\bar{\alpha})\alpha(\tau+\Delta\tau) + F_\alpha(\bar{\alpha})$, where

$$F_p(\alpha;\bar{\alpha}) = \begin{cases} 1 & \bar{\alpha} < h_{f^+},\ h_{f^-} < \bar{\alpha} \\ 0 & \text{otherwise} \end{cases} \qquad (16)$$

and

$$F_\alpha(\bar{\alpha}) = \begin{cases} V_{f^\circ} - h_{f^+} & \bar{\alpha} < h_{f^+} \\ V_{f^\circ} & h_{f^+} \le \bar{\alpha} \le h_{f^-} \\ V_{f^\circ} - h_{f^-} & h_{f^-} < \bar{\alpha} \end{cases} \qquad (17)$$

Here $\bar{\alpha}$ is an estimate of α which can be obtained, for example, by linear extrapolation of α from τ to $\tau+\Delta\tau$. $\bar{P}_{11}$, $\bar{P}_{12}$, $\bar{P}_{21}$, $\bar{P}_{22}$, $\bar{X}_1$ and $\bar{X}_2$ are given in Appendix A.

Renaming the coefficients in Eqs. (14) and (15) yields the following:

$$[P]\begin{Bmatrix}\alpha(\tau+\Delta\tau)\\ \xi(\tau+\Delta\tau)\end{Bmatrix} \simeq \begin{Bmatrix}X_1\\ X_2\end{Bmatrix} \tag{18}$$

which has for solution

$$\begin{Bmatrix}\alpha(\tau+\Delta\tau)\\ \xi(\tau+\Delta\tau)\end{Bmatrix} = [P]^{-1}\begin{Bmatrix}X_1\\ X_2\end{Bmatrix} \tag{19}$$

[P] can take on one of the two forms whereas $\{X\}$ can take on one of three forms depending on the estimated value of $\bar{\alpha}(\tau+\Delta\tau)$.

2.3 Starting Procedure

Houbolt's scheme requires values of α and ξ at times $\tau-2\Delta\tau$, $\tau-\Delta\tau$ and τ in order to determine their values at $\tau+\Delta\tau$. At time $\tau = 0$, a special starting procedure is required. A Taylor series is used to obtain the following:

$$\alpha(-\Delta\tau) = \alpha(0) - \Delta\tau\alpha'(0) + \frac{\Delta\tau^2}{2}\alpha''(0) + O(\Delta\tau^3) \tag{20}$$

$$\alpha(\Delta\tau) = \alpha(0) + \Delta\tau\alpha'(0) + \frac{\Delta\tau^2}{2}\alpha''(0) + O(\Delta\tau^3) \tag{21}$$

with similar expressions for $\xi(-\Delta\tau)$ and $\xi(\Delta\tau)$. The expressions for $\bar{X}_1$ and $\bar{X}_2$ in Appendix A have terms depending on the first and second derivatives of α and ξ, and these derivatives are given as follows:

$$\alpha'(-\Delta\tau) = \alpha'(0) - \Delta\tau\alpha''(0) + \frac{\Delta\tau^2}{2}\alpha''(0) + O(\Delta\tau^3) \tag{22}$$

$$\alpha'(\Delta\tau) = \alpha'(0) + \Delta\tau\alpha''(0) + \frac{\Delta\tau^2}{2}\alpha'''(0) + 0(\Delta\tau^3) \tag{23}$$

and

$$\alpha''(-\Delta\tau) = \alpha''(0) - \Delta\tau\ \alpha'''(0) + \frac{\Delta\tau^2}{2}\alpha^{IV}(0) + 0(\Delta\tau^3) \tag{24}$$

$$\alpha''(\Delta\tau) = \alpha''(0) + \Delta\tau\ \alpha'''(0) + \frac{\Delta\tau^2}{2}\alpha^{IV}(0) + 0(\Delta\tau^3) \tag{25}$$

with expressions of the ξ derivatives written in the same form as those given in Eqs. (22) to (25). The initial conditions $\alpha(0)$, $\alpha'(0)$, $\xi(0)$ and $\xi'(0)$ are known, and the higher derivatives can be obtained from Eqs. (3) and (4) and are given by:

$$[Q] \begin{Bmatrix} \alpha^{(n)}(0) \\ \xi^{(n)}(0) \end{Bmatrix} = \begin{Bmatrix} Y_1^{(n)} \\ Y_2^{(n)} \end{Bmatrix} \tag{26}$$

which has for solution

$$\begin{Bmatrix} \alpha^{(n)}(0) \\ \xi^{(n)}(0) \end{Bmatrix} = [Q]^{-1} \begin{Bmatrix} Y_1^{(n)} \\ Y_2^{(n)} \end{Bmatrix} \tag{27}$$

Here n = 2, 3 and 4. Q_{11}, Q_{12}, Q_{21}, Q_{22}, $Y_1^{(n)}$ and $Y_2^{(n)}$ are given in Appendix B. For the next step, Houbolt's scheme can be used since α and ξ at $\tau = -\Delta\tau$, 0 and $\Delta\tau$ are known.

2.4 A Recurrence Formula

In Eq. (18), the terms X_1 and X_2 contain integrals which have to be evaluated at each time step. To reduce the amount of

computations, a recurrence formula is used. Using Simpson's rule, the integral $I_1(\tau+\Delta\tau)$ in Eq. (A6) of Appendix A can be written as

$$I_1(\tau+\Delta\tau) = e^{-b\Delta\tau}I_1(\tau) + \frac{\Delta\tau}{24}\{9\lambda(\tau+\Delta\tau) + 19\lambda(\tau)e^{-b\Delta\tau} - 5\lambda(\tau-\Delta\tau)e^{-2b\Delta\tau} + \lambda(\tau-2\Delta\tau)e^{-3b\Delta\tau}\} \quad (28)$$

where λ is defined in Eq. (A8).

The starting value for $I_1(\Delta\tau)$ is given by

$$I_1(\Delta\tau) = \frac{\Delta\tau}{6}\{2\lambda(\Delta\tau) + 5\lambda(0)e^{-b\Delta\tau} - \lambda(-\Delta\tau)e^{-2b\Delta\tau}\} \quad (29)$$

Expressions for $I_2(\tau+\Delta\tau)$ and $I_2(\Delta\tau)$ are obtained by substituting b for d in the above equations.

3.0 Results and Discussions

In this report, only nonlinearities in the pitch degree of freedom are considered. The elastic axis of the airfoil is placed at the $\frac{1}{4}$ chord location (that is, $a_h = -0.5$), r_α and x_α are kept constant at 0.5 and 0.25 respectively. The two properties of the airfoil being varied are μ and $\bar{\omega}$. The effects of preload and freeplay are investigated by varying the values of V_{f^o}, h_{f^+} and h_{f^-}. Table 1 shows the combinations of parameters used in this study.

A comparison of cases 1, 2 and 3 shows the effect of preload for constant freeplay, while cases 2, 4 and 5 show the effect of freeplay for constant preload. Cases 6 and 7 are with zero preload and the effect of varying μ can be obtained from cases 2, 8 and 9. The results for increasing $\bar{\omega}$ to a value of 0.8 are given in cases 10 to 16

where the values of preload and freeplay are kept the same as those for cases 1 to 5, 8 and 9 in which $\bar{\omega} = 0.2$. These computations are carried out primarily to study the effect of $\bar{\omega}$ on the binary flutter of the airfoil.

3.1 Effect of Preload on Flutter Boundary

Figures 3 to 5 show the flutter boundaries for cases 1 to 3. The values of μ and $\bar{\omega}$ are kept constant at 100 and 0.2 respectively. The freeplay is 0.5° with the preload V_{f^o} set at 0.25°, 0.5° and 1° respectively. Throughout this study, it is assumed that $h_{f^*} = V_{f^o}$ so that the restoring moment is zero when the displacement $\alpha = 0$.

To determine the flutter boundary, Eq. (19) is solved for given initial conditions. In this report, only $\alpha(0)$ is varied and $\xi(0) = \xi'(0) = \alpha'(0) = 0$. The procedure is to find the linear flutter speed U_L^* first, and this is equivalent to solving the problem for $h_{f^-} = h_{f^*}$. In the nonlinear case, once $\alpha(0)$ is specified, a value of U^* usually greater than U_L^* is selected and α and ξ are obtained by the time marching finite difference scheme. For the type of structural nonlinearity considered, the solution is divergent for $U^* > U_L^*$, and the nonlinear divergent flutter speed is, within the numerical accuracy, the same as U_L^* for these three cases considered. It is observed that for $\alpha(0) > V_{f^o}$ decreasing U^* below U_L^* results in limit-cycle flutter. The oscillation is self-excitated and maintains a constant amplitude which is self-limited. The boundaries between divergent and limit-cycle flutter in Figures 3 to 5 are practically vertical lines at $U^*/U_L^* = 1$ for values of $\alpha(0)$ ranging from -10° to 20°.

As U^* decreases, a value will be reached where any further decrease will result in damped oscillations of the airfoil. Boundaries

can be identified on the $\alpha(0)$ versus U^*/U^*_L plots separating the regions of limit-cycle flutter with the stable regions where the oscillations decay.

Figures 3 to 5 also show that for a freeplay of 0.5° the region of limit-cycle flutter decreases with increasing values of the preload. Another observation is the non-symmetry of the boundaries between decaying oscillation and limit-cycle flutter with initial displacement $\alpha(0)$. For values of initial displacement less than the preload, the system moves on the linear part of the moment-displacement curve shown in Figure 2, and at velocities below the linear flutter speed, the system is stable. Increasing $\alpha(0)$ will have a destablizing effect, but this is only restricted to the limited amplitude oscillation regions.

Figure 3 shows pockets in the damped oscillation region where the airfoil oscillates with constant amplitude. This limit-cycle flutter behaviour is only observed for the smallest preload value of 0.25° and is not detected in the other two cases. The regions of limited amplitude oscillations are determined using a binary search complemented with linear grid scans. This by no means assures that all such regions especially the small ones have been identified, but those that are found can be considered to be quite accurately defined.

Figures 6a to 6j show the time behaviour of α in the various regions corresponding to the locations marked 1 to 10 in Figure 3. Figure 6a is for initial displacement $\alpha(0) = 8°$ and $U^* = 0.7U^*_L$. The airfoil damps out fairly rapidly and the oscillations are mainly sinusoidal and no noticeable harmonics are detected. This is a typical α

decay curve sufficiently far from any limit-cycle futter region. The same behaviour is also observed for the ξ oscillations.

Figure 6b corresponds to location 2 in Figure 3 where $\alpha(0) = 8^\circ$ and $U^*/U_L^* = 0.78$. This type of oscillatory behaviour of α is typical in those pockets where limit-cycle flutter occurs. A strong second harmonic is always present.

At initial displacment $\alpha(0) = 8^\circ$ and $U^*/U_L^* = 0.81$, corresponding to location 3 in Figure 3, the α decay curve is shown in Figure 6c. Higher harmonics can be detected from the oscillatory motion of the airfoil, and this is often the case in the proximity of the limit-cycle flutter regions. Figure 6d is also in the damped oscillation region but it is very close to the limit-cycle flutter boundary. This corresponds to location 4 in Figure 3 with initial displacement $\alpha(0) = 8^\circ$ and $U^*/U_L^* = 0.82$. The airfoil oscillates in pitch (also in plunge) at approximately constant amplitude for a number of cycles (nearly twenty in this case) and suddenly damps out. This is often encountered very close to the limit-cycle flutter boundary.

Figure 6e shows the time variation of α in the limit-cycle flutter region for $\alpha(0) = 8^\circ$ and $U^*/U_L^* = 0.83$ corresponding to location 5 in Figure 3. Again, being close to the flutter boundary, the appearance of a second harmonic can be detected. Sufficiently far away from the limit-cycle flutter boundary, the curves shown in Figures 6f and 6g for limited amplitude oscillations corresponding to locations 6 and 7 in Figure 3 indicate the motion of the airfoil to be practically sinusoidal. This type of motion is typical even if U^*/U_L^* is close to the divergent flutter boundary.

Figure 6h shows the α oscillations at location 8 on Figure 3 for $\alpha(0) = -0.3^\circ$ and $U^*/U_L^* = 0.99785$. For this value of initial displacement, the airfoil motion is on the linear part of the moment-displacement curve shown in Figure 2. This type of decay curve is typical for linear flutter (Ref. 10).

The behaviour of the airfoil motion inside the limit-cycle flutter region at location 9 in Figure 3 is given in Figure 6i. The values of $\alpha(0)$ and U^*/U_L^* are -1.5° and 0.78 respectively. The oscillations behave in a similar manner as those given in Figure 6b. This is characterized by the presence of a strong second harmonic component. It is noted that in all pockets of limnit-cycle flutter within the damped oscillation region, the oscillations of the airfoil are similar to those given in Figure 6b and 6i.

It is observed in Figure 3 that there are bulges on the limit-cycle flutter boundary. For example, for positive values of $\alpha(0)$ and $0.825 \leq U^*/U_L^* \leq 0.86$, the oscillations can either be of limited amplitude or damped depending on the value of $\alpha(0)$. Figure 6j shows the time variation of α corresponding to location 10 in Figure 3 where $\alpha(0) = 1.5$ and $U^*/U_L^* = 0.84$.

In Figures 7-9, the limited amplitudes α_A and ξ_A are plotted against the speed ratio U^*/U_L^* for cases 1-3. It is found that they are independent of the initial displacement $\alpha(0)$. In Figure 7, the curves have breaks at U^*/U_L^* approximately equal to 0.825. To the left of this value of U^*/U_L^*, the amplitudes are obtained from the limit- cycle flutter pockets inside the damped oscillation region. The curves do not join smoothly with those for U^*/U_L^* greater than 0.825 and this

is due to the different oscillatory motion of the airfoil as shown in Figures 6b and 6f. A comparison of the amplitudes for $U^*/U_L^* > 0.87$ in Figure 7 with those in Figures 8 shows that they are identical. Similarly, the results in Figure 9 coincide with those in Figure 7 for $U^*/U_L^* > 0.915$. This indicates that the variations of the limited amplitudes α_A and ξ_A with speed ratio for various values of preload, but with the freeplay fixed, lie on the same curves. The values of U^*/U_L^* where the curves begin depend on the values of the preload.

Throughout this study, the value of the time step $\Delta\tau$ is taken to be 1/128 of the shorter period of the two coupled modes of oscillation of the airfoil in the absence of aerodynamic forces. The periods of the coupled modes are obtained from Equation (3) and (4) for $F[\alpha(\tau)] = \alpha(\tau)$, and $p(\tau) = r(\tau) = 0$. In numerical time integration schemes, Bathe and Wilson (Ref. 14) pointed out that the amplitude decays due to numerical errors and is dependent on $\Delta\tau$. The value of $\Delta\tau$ used in this study is found to be sufficiently small to give good accuracies in determining the flutter boundaries while ensuring the computation time is not excessive.

3.2 Effect of Freeplay on Flutter Boundary

To investigate the effect of freeplay on the flutter boundary, results for cases 2, 4 and 5 of Table 1 are shown in Figures 4, 10 and 11. The preload is constant at 0.5°, and the values of the freeplay are 0.25°, 0.5° and 1° respectively. The boundaries between divergent and limit-cycle flutter are all located at $U^*/U_L^* \simeq 1$. Decreasing the freeplay will decrease the limited amplitude

oscillation region and move the limit-cycle flutter boundary closer to the divergent flutter boundary. In the limit, as the freeplay tends to zero, the two flutter boundaries coincide at $U^*/U_L^* = 1$ which is to be expected since the system is acted on by linear spring forces. Because of the preload, the flutter boundaries are not symmetrical about $\alpha(0) = 0$.

The limited amplitudes α_A and ξ_A motions are given in Figures 8, 12 and 13. They are independent of the initial displacement $\alpha(0)$, but for given speed ratio, higher amplitudes are obtained when the values of the freeplay are increased. The curves in Figure 13 have breaks at U^*/U_L^* approximately equal to 0.825. The amplitudes for $U^*/U_L^* < 0.825$ are determined from the pockets of limit- cycle flutter in the damped oscillation region. The presence of a strong second harmonic is always observed in the oscillatory motion of the airfoil inside these pockets (see Figs. 6b and 6i). This is quite unlike the motions for $U^*/U_L^* > 0.825$ where the oscillations are mainly sinusoidal.

It is interesting to note that when Figure 3 is compared with Figure 11, the flutter boundaries are identical if the vertical scale for $\alpha(0)$ in Figure 3 is multiplied by a factor of 2 which is the ratio of the two values of preload. Similarly, the limited amplitudes α_A and ξ_A in Figure 7 when multiplied by 2 match those given in Figure 13. From the limited results of the two cases considered here, it appears that for a particular combination of preload and freeplay, similar results are obtained for other values of preload and freeplay if the ratio of preload to freeplay is kept the same. The flutter boundary curves can be made identical if the vertical scales are

multiplied by factors equal to the ratio of the preloads. Also, the limited amplitudes of the plunge and pitch oscillations differ from those with other values of preload and free play by the same factors.

3.3 Effect of Zero Preload on Flutter Boundary

For zero preload, cases 6 and 7 of Table 1 are investigated for a freeplay of 1°. The difference bewtween these two cases is in the location of the equilibrium position. Case 6 gives the equilibrium of the airfoil at a point on the linear portion of the moment-displacement curve (Figure 2) just ahead of the freeplay, while in case 7, the equilibrium position is centered in the freeplay.

The flutter boundary for case 6 is given in Figure 14. The boundary originates at $U^*/U_L^* = 1$ and $\alpha(0) = 0$ and rapidly becomes a straight line at $U^*/U_L^* = 0.995$. Unlike the previous cases with positive preload, the figure shows only two regions, namely; divergent and limit-cycle flutter. In this study, no numerical computations have been carried out for $U^*/U_L^* < 0.15$ since the number of cycles needed to determine the limited amplitude becomes larger and larger as the speed ratio decreases, and no drastic change in the behaviour of the airfoil motion is anticipated.

The limited amplitudes α_A and ξ_A are plotted in Figure 15. The curves are discontinuous at $U^*/U_L^* = 0.69$ and Figure 16 show typical pitch oscillations of the airfoil near the discontinuity (Figure 16b) and at a fair distance away (Figure 16a). The mean value of α is not a constant but depends on U^*/U_L^*, and the oscillatory motion of the airfoil is non-symmetrical about the mean. For U^*/U_L^* slightly greater than 0.69, a small second harmonic can be detected, but further

increase in U^*/U_L^* results in oscillations which are practically sinusoidal. For $U^*/U_L^* > 0.69$, the mean value of α is a constant 0.5° which is half the value of the freeplay.

For zero preload and equilibrium position centered in the freeplay, the flutter boundary and limited amplitude curves are identical to Figures 14 and 15 illustrating their dependence only on the value of the freeplay. The mean motion for $U^*/U_L^* < 0.69$ is usually slightly above $\alpha = 0$ although for some values of U^*/U_L^* and $\alpha(0)$, it can be slightly below $\alpha = 0$. However, for $U^*/U_L^* > 0.69$ the mean value of α is always zero. Similar to case 6, a large second harmonic is present in the oscillatory motion of the airfoil for $U^*/U_L^* < 0.69$. The magnitude of the second harmonic is less pronounced in the vicinity of $U^*/U_L^* = 0.69$ and as U^*/U_L^* increases, its value diminishes. The oscillations appear mainly sinusoidal with no noticeable harmonics when $U^*/U_L^* > 0.8$.

3.4 Effect of Airfoil-Air Mass Ratio μ on Flutter Boundary

The effect of airfoil-air mass ratio on the flutter boundary for $\mu = 50$, 100 and 250 are shown in Figures 17, 4 and 18 respectively. The preload and freeplay are both 0.5° in all three cases.

The boundaries for divergent flutter are all approximately at $U^*/U_L^* = 1$ for all three values for μ, while those for limit-cycle flutter move towards $U^*/U_L^* = 1$ for increasing μ. At $\mu = 250$, pockets of limited amplitude oscillations appear in the damped oscillation region. The oscillatory motions of the airfoil in the various regions on the flutter boundary curves are similar to those given in Figure 6.

The limited amplitudes α_A and ξ_A are given in Figures 19, 8 and 20 for the three values of μ considered. Comparison of the curves for α_A shows that the limited amplitude between the limit-cycle and divergent flutter boundaries practically does not change with μ and no differences can be detected. On the other hand, ξ_A is found to increase with μ. This behaviour where μ has an effect on the plunge degree of freedom but with no noticeable effect on the pitch motion is also observed for a cubic nonlinearity in the restoring moment reported in Ref. 10.

3.5 Effect of Uncoupled Plunge to Pitch Natural Frequency Ratio $\bar{\omega}$ on Flutter Boundary

3.5.1 Effect of Preload for Constant Freeplay

In cases 10 to 12 given in Table 1, the value of $\bar{\omega}$ is 0.8 and the preload is set at 0.25°, 0.5° and 1° for a constant freeplay of 0.5°. The flutter boundaries are shown in Figures 21 to 23, and comparison with Figures 3 to 5 for the corresponding values of preload and freeplay at $\bar{\omega}$ = 0.2 gives the effect of $\bar{\omega}$ on the oscillatory motion of the airfoil.

From Figures 3 and 21, bringing the plunge and pitch uncoupled natural frequencies closer to each other seem to eliminate the pockets where limit-cycle flutter occurs. The bulges on the limit-cycle flutter boundary grow with the preload for $\bar{\omega}$ = 0.8. Similar to the observations from cases 1 to 3, it is found that the limited amplitudes α_A and ξ_A given in Figures 24-26 are independent on initial displacement $\alpha(0)$ and preload. However, their values are smaller than those for $\bar{\omega}$ = 0.2 for the same value of the freeplay.

3.5.2 Effect Freeplay for Constant Preload

Figures 27, 22 and 28 show the effect of varying the freeplay on the limit-cycle flutter boundaries for a fixed preload of 0.5° and frequency ratio $\bar{\omega} = 0.8$. Similar to the results for $\bar{\omega} = 0.2$, increasing the freeplay will increase the region where limited amplitude oscillation occurs. It is observed that the bulges on the flutter boundary curves for $\alpha(0) > 0$ diminish as the freeplay is increased. Also, the pockets of limited amplitude oscillations which occur inside the damped oscillation region, as found in case 5, are not present when $\bar{\omega} = 0.8$.

The limited amplitudes α_A and ξ_A are given in Figures 29, 25 and 30 for values of freeplay 0.25°, 0.5° and 1.0° respectively. Again, they are independent of initial displacement $\alpha(0)$. For a given speed ratio, higher amplitudes are obtained for larger values of freeplay. The breaks in the curves, similar to those shown in Figures 13 for $\bar{\omega} = 0.2$, are not found in the corresponding case for $\bar{\omega} = 0.8$ given in Figure 30 because pockets of limited amplitude oscillations are not encountered. Comparisons with results for $\bar{\omega} = 0.2$ given in Figures 12, 8 and 13 show that the amplitudes of oscillation at limit-cycle flutter attain a larger value for the smaller ratio of the natural frequencies $\bar{\omega}$.

In section 3.2, it is observed that at $\bar{\omega} = 0.2$ and for a particular combination of preload and freeplay, the results can be used for other values of preload and freeplay as long as the ratio of preload to freeplay is the same. The vertical scale of the flutter boundaries and limited amplitudes α_A and ξ_A have to be multiplied by a factor equal to the ratio of the preloads. The results for $\bar{\omega} = 0.8$ show the same behaviour.

3.5.3 Effect of Airfoil-Air Mass Ratio μ

The effect of μ on the flutter boundaries can be obained from cases 11, 15 and 16 of Table 1, and the results are shown in Figures ..., 31 and 32. The vertical portions of the boundaries do not appear to be much affected by μ. The most pronounced changes occur in the ridges of the limit-cycle flutter curve. Pockets of limited amplitude oscillations such as those shown in Figure 18 for $\mu = 250$ are not present when $\bar{\omega} = 0.8$.

The limited amplitude α_A given in Figures 25a, 33a and 34a show that α_A is slightly larger when μ is decreased from 250 to 50. There is a much larger increase in amplitude ξ_A for the plunge degree of freedom for this change in μ. This is in contrast to the results for $\bar{\omega} = 0.2$ where no noticeable change in α_A with μ is detectable and ξ_A increases with increasing μ instead.

Period of Limited Amplitude Oscillations

Some computations of the period of oscillations in the limit-cycle flutter regions are given in Figures 35 to 37.

The results for $\mu = 100$, $\bar{\omega} = 0.2$ are shown in Figure 35 for a preload of $-5°$ and three values of the freeplay. Not included in this figure are the periods of oscillations in the pockets where limit-cycle flutter occurs within the damped oscillation region. The period decreases initially as U_L^* increases until a minimum is reached. Thereafter, it increases at a gradual rate. Within the computation accuracy, it appears that the three curves coalesce in the vicinity of U_L^* approximately equal to 6.95. Increasing the value of $\bar{\omega}$ to 0.8 shows a somewhat different behaviour of the period of oscillations. Figure 36 shows the variation of the period with U_L^* for constant

preload of 0.5° and the values of freeplay being 0.5° and 1° respectively. The two curves are identical for $0.885 \leq U^*/U_L^* \leq 1.0$, and the curve for the 1° freeplay extends to $U^*/U_L^* = 0.835$ which is the location of the limit-cycle flutter boundary. Examination of the oscillations for these two cases shows that the second harmonic is too small to be detected even near the limit-cycle flutter boundary.

At zero preload with equilibrium at a point on the linear portion of the moment-displacement curve just ahead of the freeplay (case c of Table 1), Figure 37 shows the period of oscillations for $\mu = 100$, $\bar{\omega} = 0.2$ and 1° freeplay. A discontinuity in the curve occurs at $U^*/U_L^* = 0.69$, which is on the same location as that observed in the limited amplitude curves given in Figure 15. For $U^*/U_L^* < 0.69$, the oscillations are characterized by "kinks" indicating the presence of large harmonics. When U^*/U_L^* is between 0.69 and 1.0, the usual behaviour of the oscillations is observed, that is, small second harmonics are observed near the limit-cycle flutter boundary but their amplitudes diminish quite rapidly as U^*/U_L^* is increased. For preload centered in the freeplay (case 7 of Table 1), the results are similar to those given in Figure 37.

6. Conclusion

Nonlinear flutter of a two-dimensional airfoil undergoing plunging and pitching motion is studied using a numerical time marching finite difference scheme. The structural nonlinearity considered is of the type due to a spring with preload and freeplay. The nonlinearity appears in the pitch degree of freedom only, but extension of the solution to the other degree of freedom can readily be carried out.

For nonzero values of the preload, three types of oscillations are possible, namely; damped, limited amplitude and divergent. Divergent flutter occurs when the nondimensional speed of the airflow past the airfoil U^* is greater than the linear flutter speed U_L^*. In spite of the presence of a structural nonlinearity of the type considered, the nonlinear divergent flutter speed is, within the numerical accuracy, equal to U_L^* for the cases studied. For U^* less than U_L^*, limited amplitude oscillations occur until a value of U^* is reached where further decrease will result in damped oscillations. The location of the limit-cycle flutter boundary depends on the airfoil parameters in addition to the values of the spring preload and freeplay.

For some combinations of preload and freeplay, there are pockets of limit-cycle flutter in the damped oscillation regions. The oscillations inside these pockets are characterized by the presence of large second harmonics. Bringing the uncoupled natural frequencies of the two modes closer to each other seem to eliminate these pockets, but large bulges are detected on the limit-cycle flutter boundary. The oscillations in the limited amplitude region are mainly sinusoidal except very near the limit-cycle flutter boundary where second harmonics are observed.

The limited amplitudes ξ_A and α_A of the plunge and pitch motions respectively for given airfoil parameters are dependent on the values of the freeplay. Larger amplitudes are obtained when the values

of the freeplay are increased. Changes in preload and initial displacement do not appear to have any effect on them. The amplitudes also vary with the ratio of the uncoupled natural frequencies of the plunge to pitch motions $\bar{\omega}$. For the lower value of $\bar{\omega} = 0.2$ considered in this study, larger oscillatory motions in both degrees of freedom are observed than those at $\bar{\omega} = 0.8$. Varying the airfoil-air mass ratio μ at $\bar{\omega} = 0.2$ does not have any noticeable effect on α_A, but ξ_A is found to increase with μ. At $\bar{\omega} = 0.8$, α_A decreases slightly with increasing μ while the corresponding decrease in ξ_A is much larger.

The period of oscillations at the lower value of $\bar{\omega} = 0.2$ decreases as U^* is increased from the limit-cycle flutter boundary until a minimum is reached. Thereafter, it increases at a gradual rate towards the divergent flutter boundary. At the higher value of $\bar{\omega} = 0.8$, only a gradual increase of the period from the limit-cycle flutter boundary to the divergent flutter boundary is observed.

For zero preload, only divergent and limit-cycle flutter are observed. The divergent flutter boundary occurs very close to that for the linear flutter case. Results for $\bar{\omega} = 0.2$ and $\mu = 100$ show that they are independent of the equilibrium position of the freeplay. The limited amplitude curves versus speed ratio have a discontinuity. For speed ratio less than its value at the discontinuity, the oscillations are characterized by the presence of second harmonics, while in the region between the discontinuity and the divergent flutter boundary, the oscillations are practically sinusoidal. The variations of the

period of oscillations with speed ratio in these two regions are quite different. A rapid increase of the period with increasing speed ratio is seen up to the discontinuity. Thereafter, the period changes very little as the divergent flutter boundary is approached.

The results presented in this study on the response characteristics of a two degree of freedom nonlinear system with preload and freeplay are useful to the understanding of the impact of limit-cycle oscillations on the structural integrity of aerodynamic surfaces. They can also be used to assess the validity and accuracies of the method of harmonic balance commonly used in the study of nonlinear flutter.

5.0 References

1. Brietbach, E. — "Effect of Structural Nonlinearities on Aircraft Vibration and Flutter," AGARD Report 665, January 1978.

2. Woolston, D.S. Runyan, H.L. and Andrews, R.E. — "An Investigation of Certain Types of Structural Nonlinearities on Wing and Control Surface Flutter," Journal Aeronautical Sciences, Vol. 24, No 1, 1957, pp. 57-63.

3. Shen, S.F. — "An Approximate Analysis of Nonlinear Flutter Problems," Journal Aeronautical Sciences, Vol. 26, No 1, 1959, pp. 25-32.

4. Kryloff, N. and Bogoliuboff, N. — Introduction to Nonlinear Mechanics Translation by Solomon Lifschitz, Princeton University Press, Princeton, 1947.

5. Popov, E.P. — "On the Use of the Harmonic Linearization Method in Automatic Control Theory," NACA TM 1406, January, 1957.

6. Laurenson, R.M. and Trn, R.M. "Flutter Analysis of Missile Control Surfaces Containing Structural Nonlinearities," AIAA Journal, Vol. 18, No 10, 1980, pp. 1245-1251.

7. Lee, C.L. "An Iterative Procedure for Nonlinear Flutter Analysis," AIAA/ASME/ASCE/AHS 26th Structures, Structural Dynamics and Materials Conference, Orlando, Florida, 15-17 April, 1985, AIAA Paper 85-0688.

8. Laurenson, R.M. Hauenstein, A.J. and Gubser, J.L. "Effects of Structural Nonlinearities of Limit Cycle Response of Aerodynamic Surfaces," AIAA/ASME/ASCE/AHS 27th Structrues, Structural Dynamics and Materials Conference, San Antonio, Texas, 19-21 May, 1986, AIAA Paper 86-0899.

9. Lee, B.H.K. and LeBlanc, P. "Forced Oscillation of a Two-Dimensional Airfoil with Nonlinear Aerodynamic Loads," National Research Council Canada, LR-617, January, 1986.

10. Lee, B.H.K. and LeBlanc, P. "Flutter Analysis of a Two-Dimensional Airfoil with Cubic Nonlinear Restoring Force," National Research Council Canada, NAE-AN-36, February, 1986.

11. Houbolt, J.C. "A Recurrence Matrix Solution for the Dynamic Response of Elastic Aircraft," Journal Aeronautical Sciences, Vol. 17, No 9, 1950, pp. 540-550.

12. Fung, Y.C. An Introduction to the Theory of Aeroelasticity John Wiley and Sons, N.Y., 1955.

13. Jones, D.J. and Lee, B.H.K. "Time Marching Numerical Solution of the Dynamic Response of Nonlinear Systems," National Research Council Canada, NAE-AN-25, January, 1985.

14. Bathe, K.J. and Wilson, E.L. Numerical Methods in Finite Element Analysis Prentice-Hall Inc., Englewood Cliffs, New Jersey, 1976.

Table 1 List of Airfoil and Nonlinear Spring Parameters used in Case Studies

Case	μ	$\bar{\omega}$	V_{f°	h_{f^+}	h_{f^-}
1	100	0.2	0.25°	0.25°	0.75°
2	100	0.2	0.5°	0.5°	1.0°
3	100	0.2	1.0°	1.0°	1.5°
4	100	0.2	0.5°	0.5°	0.75°
5	100	0.2	0.5°	0.5°	1.5°
6	100	0.2	0.0°	0.0°	1.0°
7	100	0.2	0.0°	-0.5°	0.5°
8	50	0.2	0.5°	0.5°	1.0°
9	250	0.2	0.5°	0.5°	1.0°
10	100	0.8	0.25°	0.25°	0.75°
11	100	0.8	0.5°	0.5°	1.0°
12	100	0.8	1.0°	1.0°	1.5°
13	100	0.8	0.5°	0.5°	0.75°
14	100	0.8	0.5°	0.5°	1.5°
15	50	0.8	0.5°	0.5°	1.0°
16	250	0.8	0.5°	0.5°	1.0°

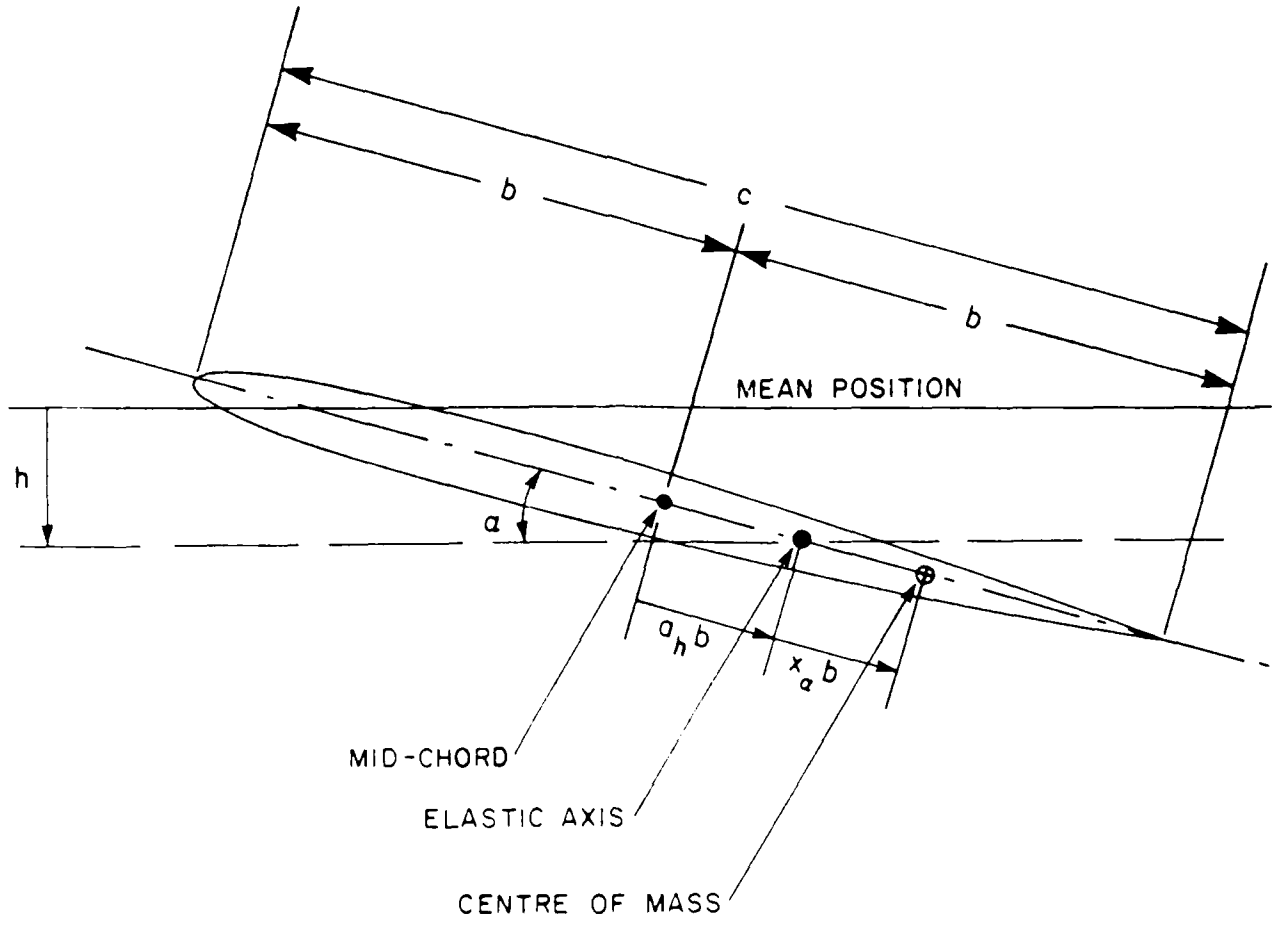

FIG. 1: TWO-DEGREE-OF-FREEDOM AIRFOIL MOTION

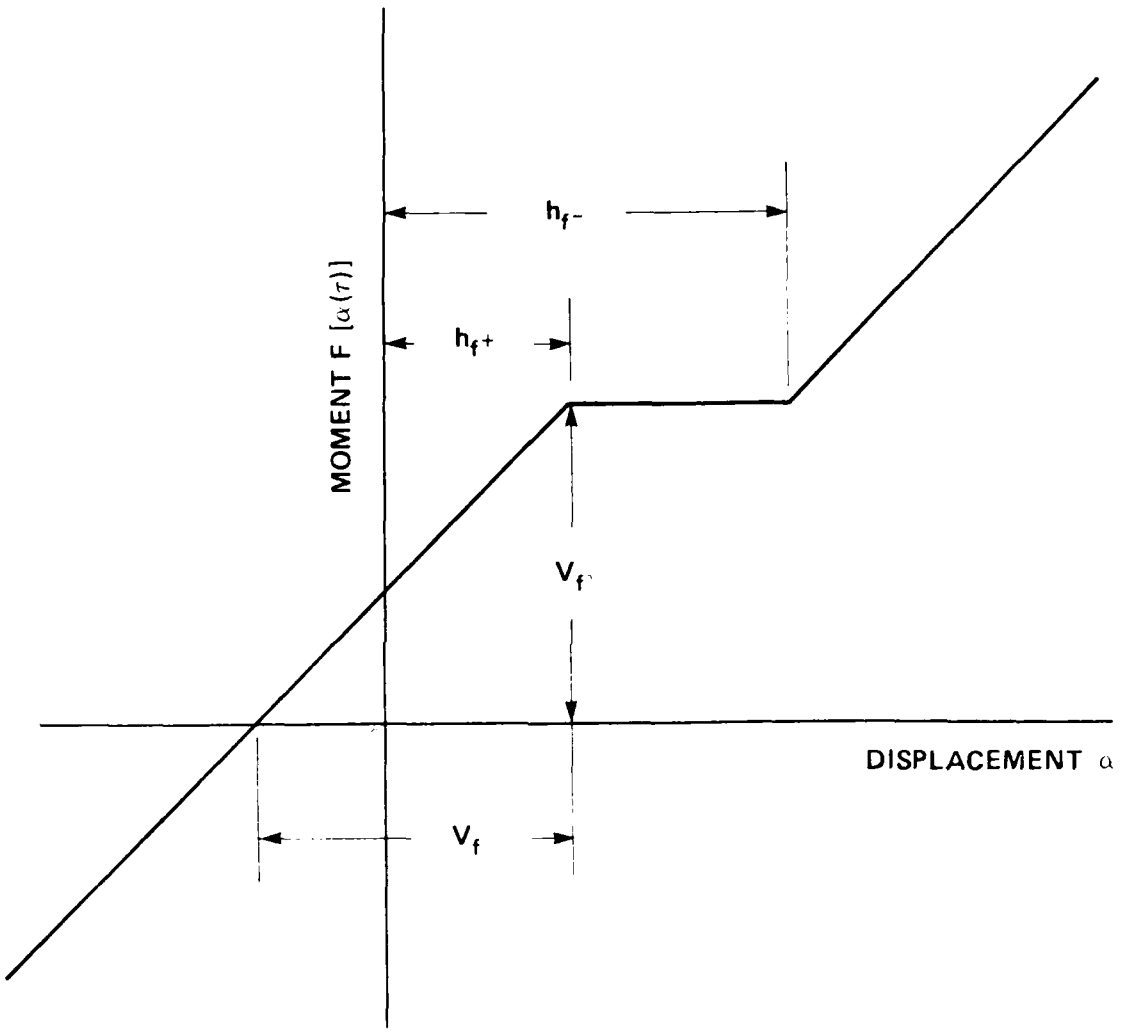

FIG. 2: NONLINEARITY IN PITCH DEGREE-OF-FREEDOM WITH PRELOAD AND FREEPLAY

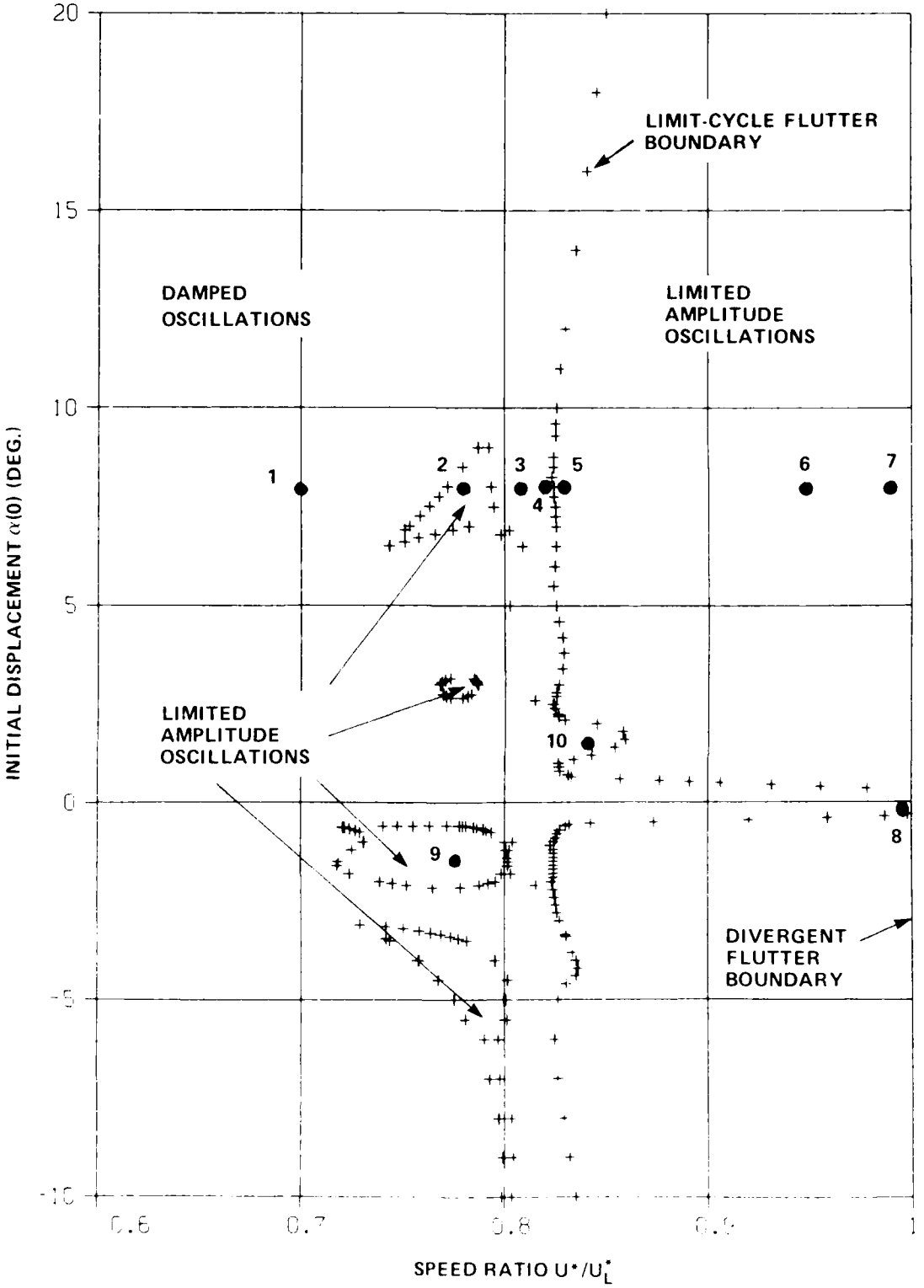

FIG. 3: FLUTTER BOUNDARY FOR $\mu = 100$, $\bar{\omega} = 0.2$, $h_{f+} = 0.25$, $h_{f-} = 0.75$ AND $V_{fc} = 0.25$

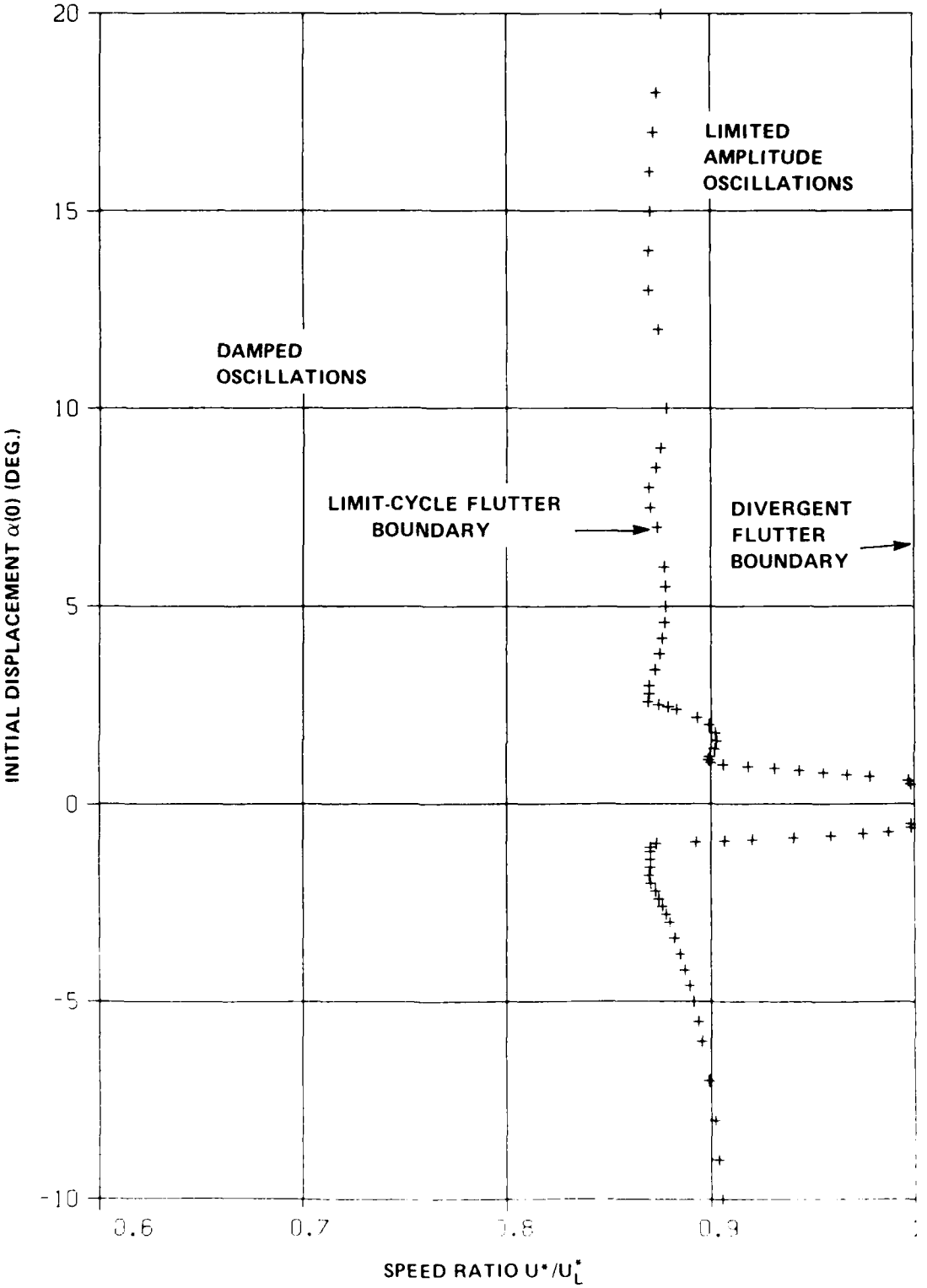

FIG. 4: FLUTTER BOUNDARY FOR $\mu = 100$, $\bar{\omega} = 0.2$, $h_{f+} = 0.5$, $h_{f-} = 1.0$ AND $V_{f\infty} = 0.5$

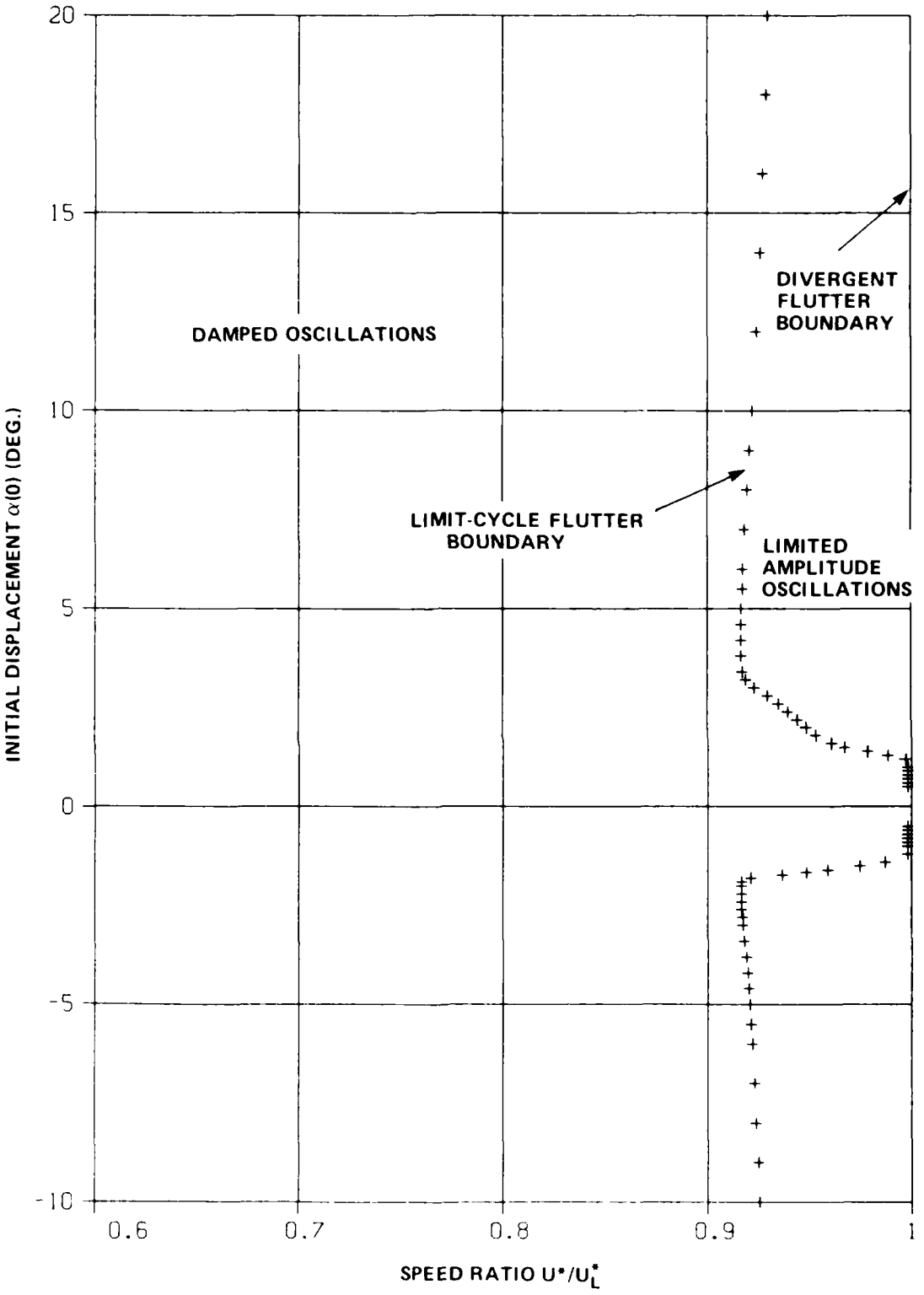

FIG. 5: FLUTTER BOUNDARY FOR $\mu = 100$, $\bar{\omega} = 0.2$, $h_{f+} = 1.0^{\circ}$, $h_{f-} = 1.5^{\circ}$ AND $V_{f^{\circ}} = 1.0^{\circ}$

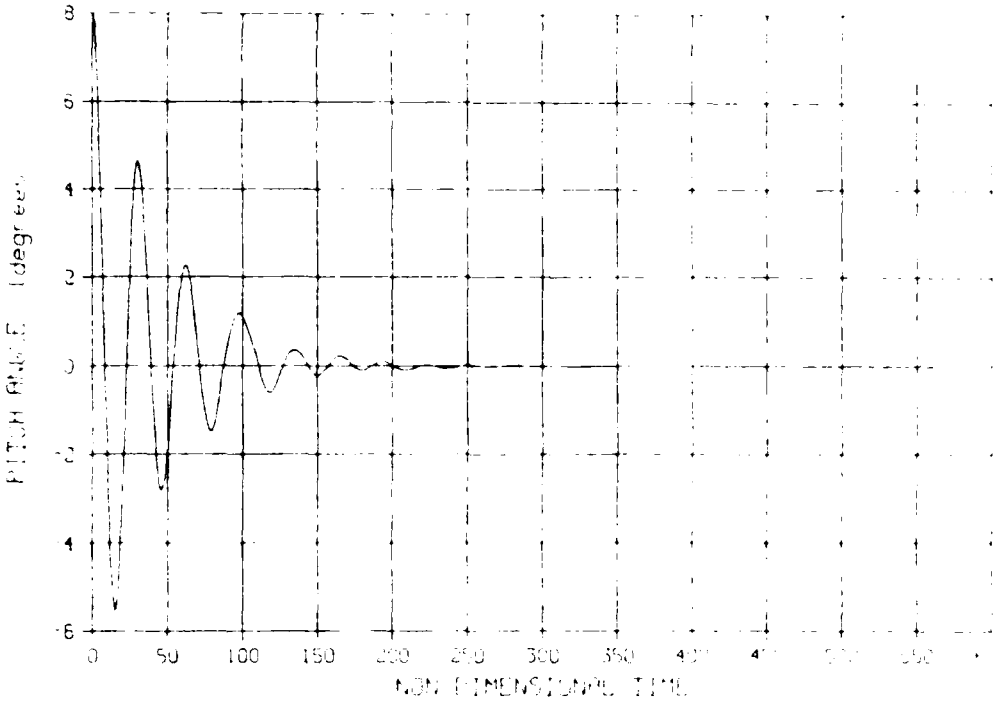

FIG. 6a: TIME VARIATION OF α FOR $\alpha(0) = 8^{\circ}$, $U^*/U_L^* = 0.7$
(CORRESPONDING TO LOCATION 1 IN FIG. 3)

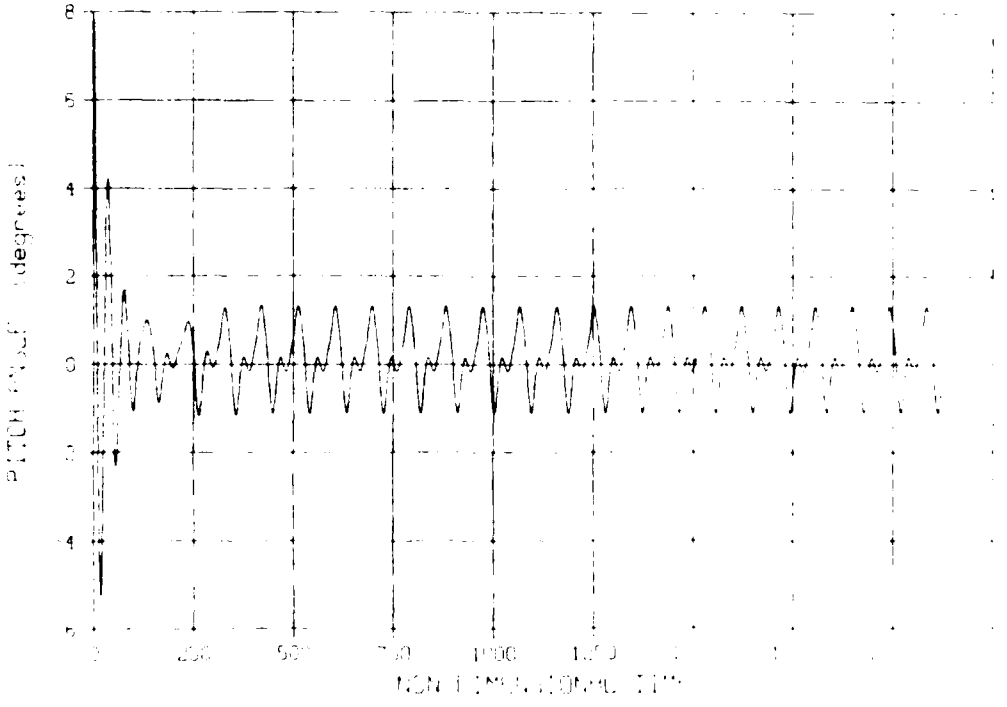

FIG. 6b: TIME VARIATION OF α FOR $\alpha(0)$ 8 , U^*/U_L^* 0.78
(CORRESPONDING TO LOCATION 2 IN FIG. 3)

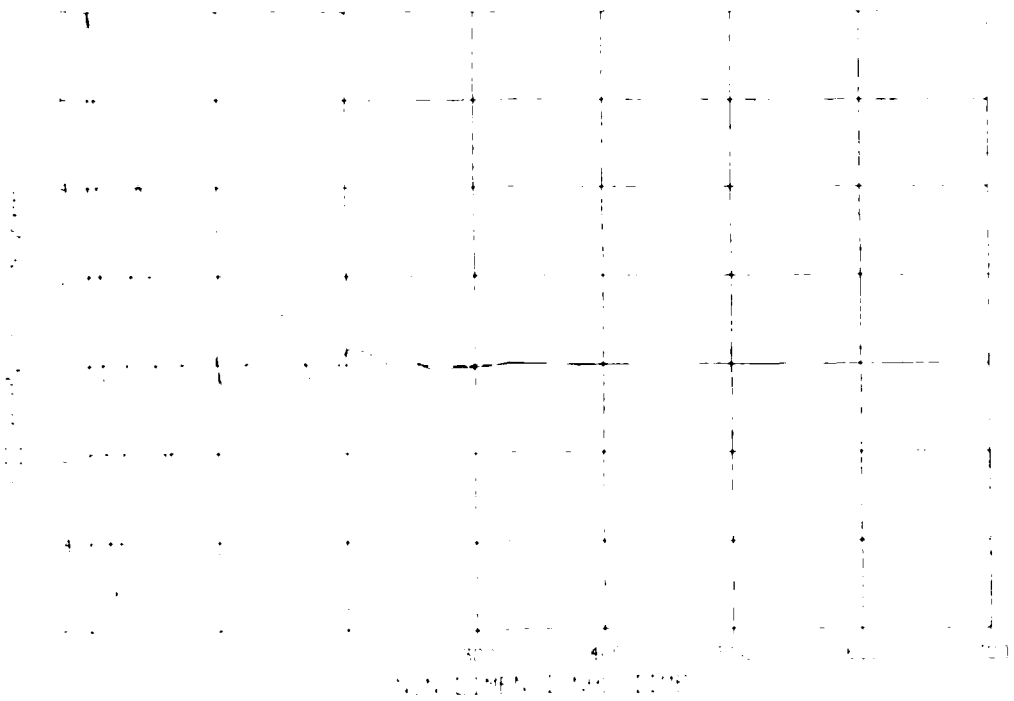

FIG. 6c: TIME VARIATION OF α FOR $\alpha(0) = 8$, $U^*/U_L^* = 0.81$
(CORRESPONDING TO LOCATION 3 IN FIG. 3)

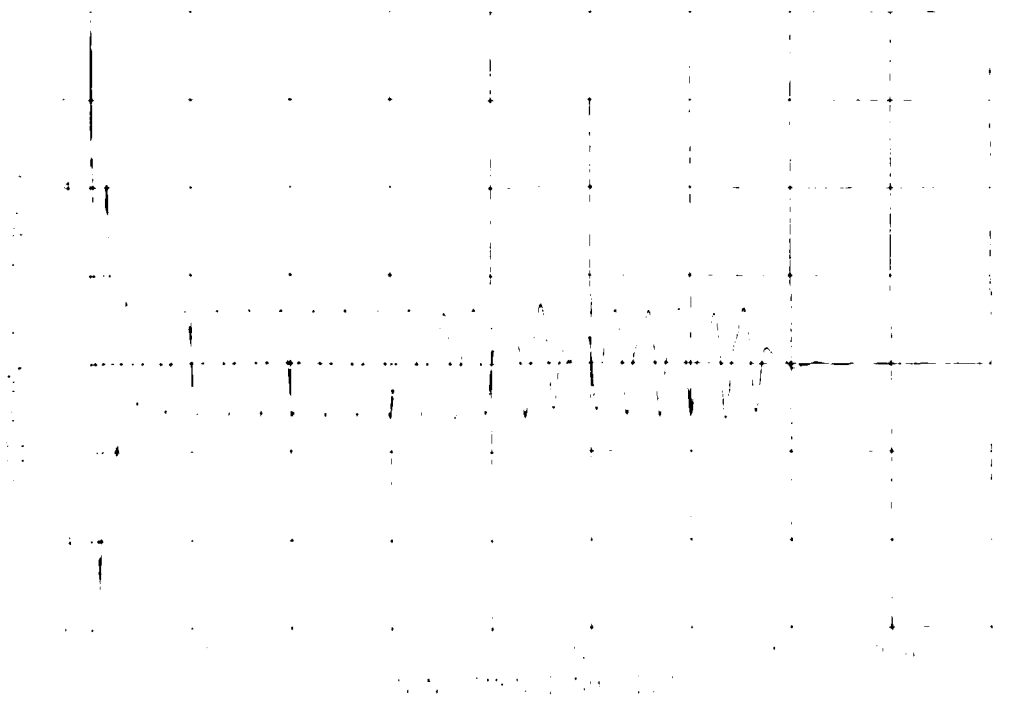

FIG. 6d: TIME VARIATION OF α FOR $\alpha(0) = 8$, $U^*/U_L^* = 0.82$
(CORRESPONDING TO LOCATION 4 IN FIG. 3)

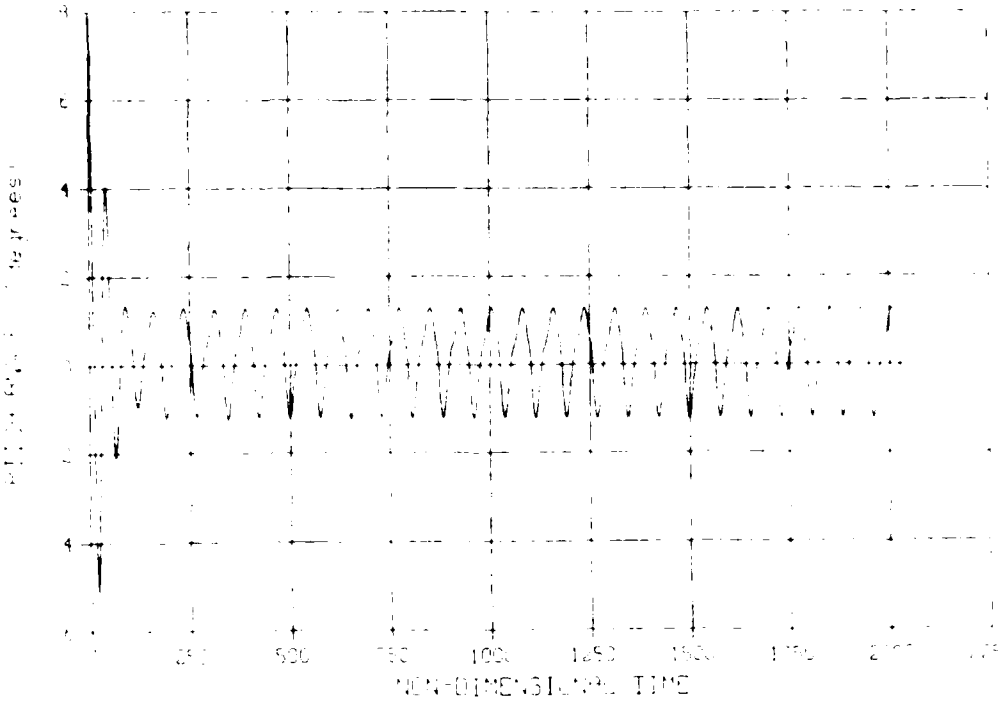

FIG. 6e: TIME VARIATION OF α FOR $\alpha(0) = 8^{\circ}$, $U^*/U_L^* = 0.83$
(CORRESPONDING TO LOCATION 5 IN FIG. 3)

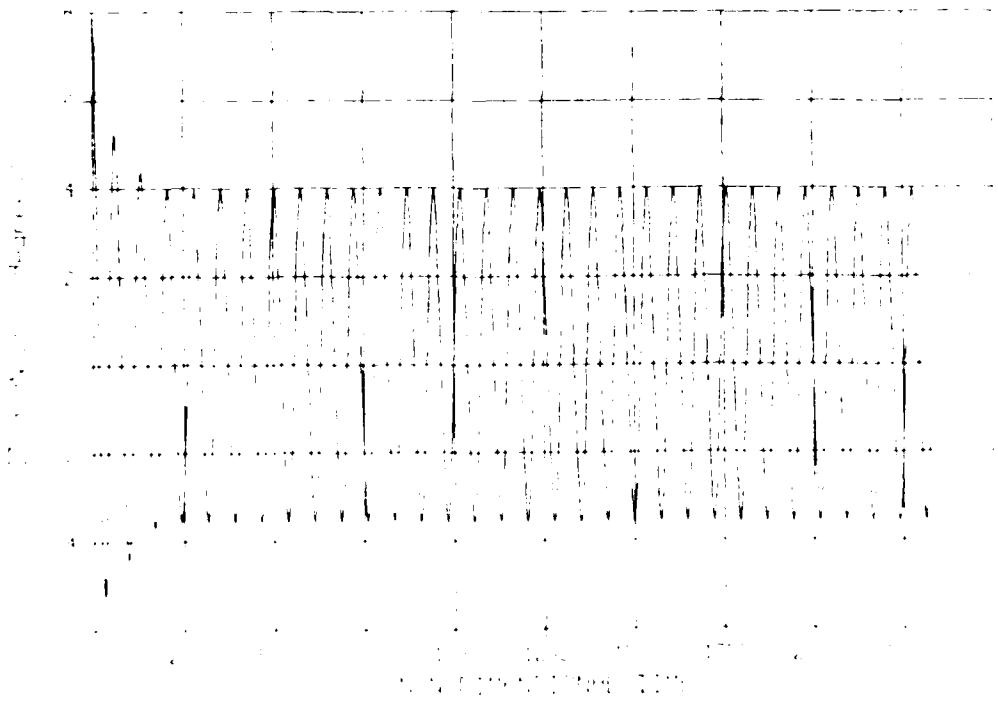

FIG. 6f: TIME VARIATION OF α FOR $\alpha(0) = 8$, U^*/U_L^* 0.95
(CORRESPONDING TO LOCATION 6 IN FIG. 3)

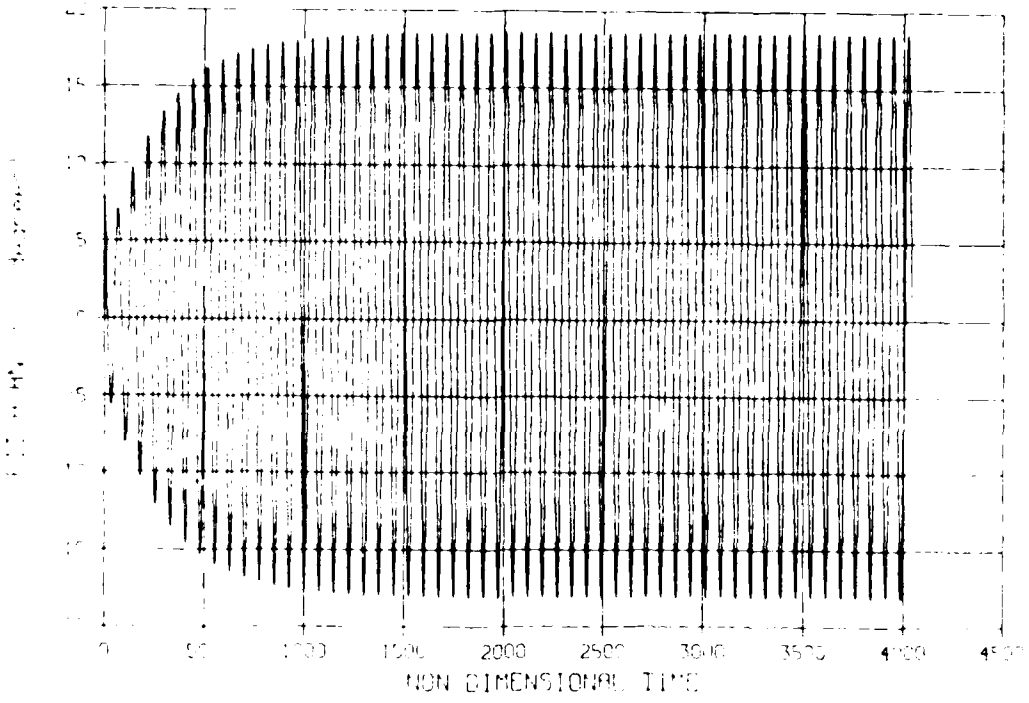

FIG. 6g: TIME VARIATION OF α FOR $\alpha(0) = 8^{\circ}$, $U^*/U_L^* = 0.99$
(CORRESPONDING TO LOCATION 7 IN FIG. 3)

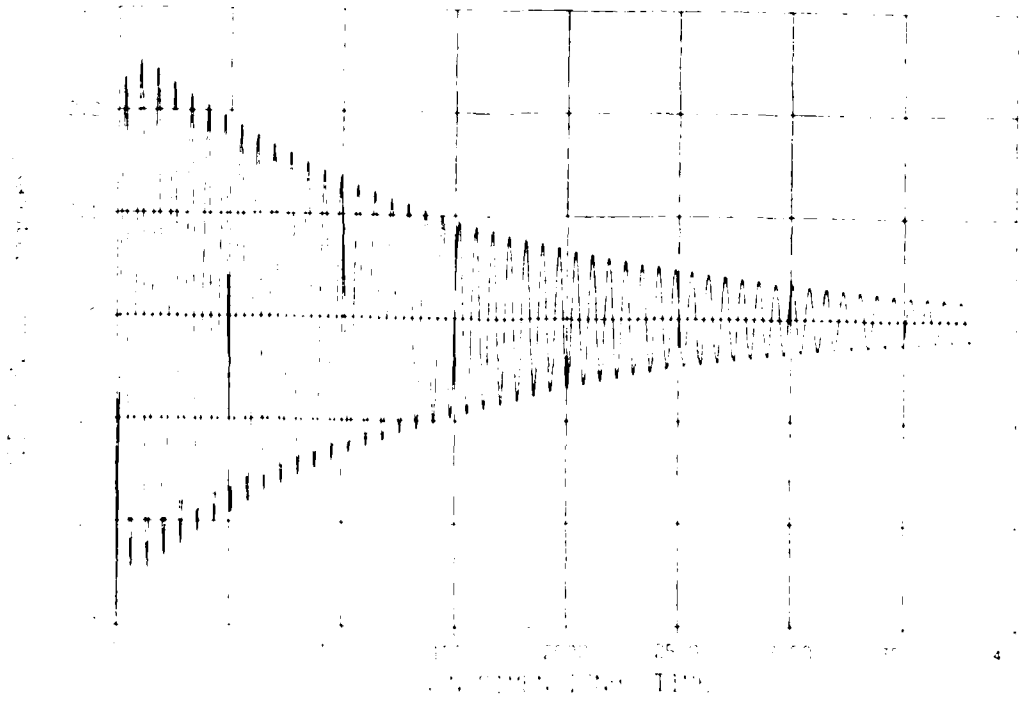

FIG. 6h: TIME VARIATION OF α FOR $\alpha(0) = -0.3^{\circ}$, $U^*/U_L^* = 0.99785$
(CORRESPONDING TO LOCATION 8 IN FIG. 3)

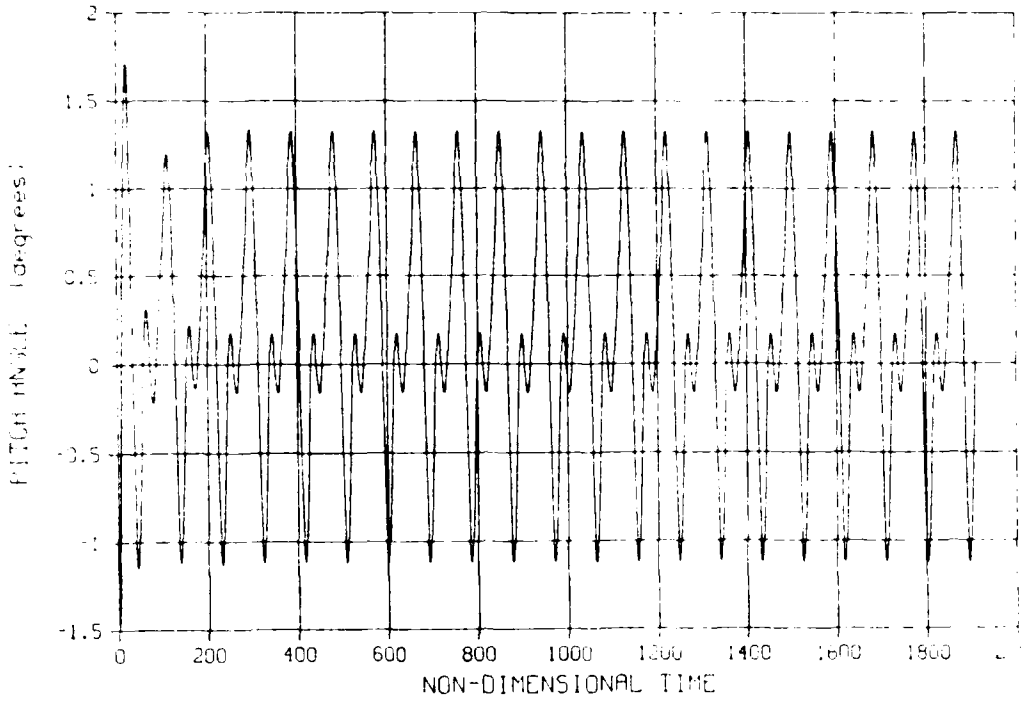

FIG. 6i: TIME VARIATION OF α FOR $\alpha(0) = -1.5°$, $U^*/U_L^* = 0.78$ (CORRESPONDING TO LOCATION 9 IN FIG. 3)

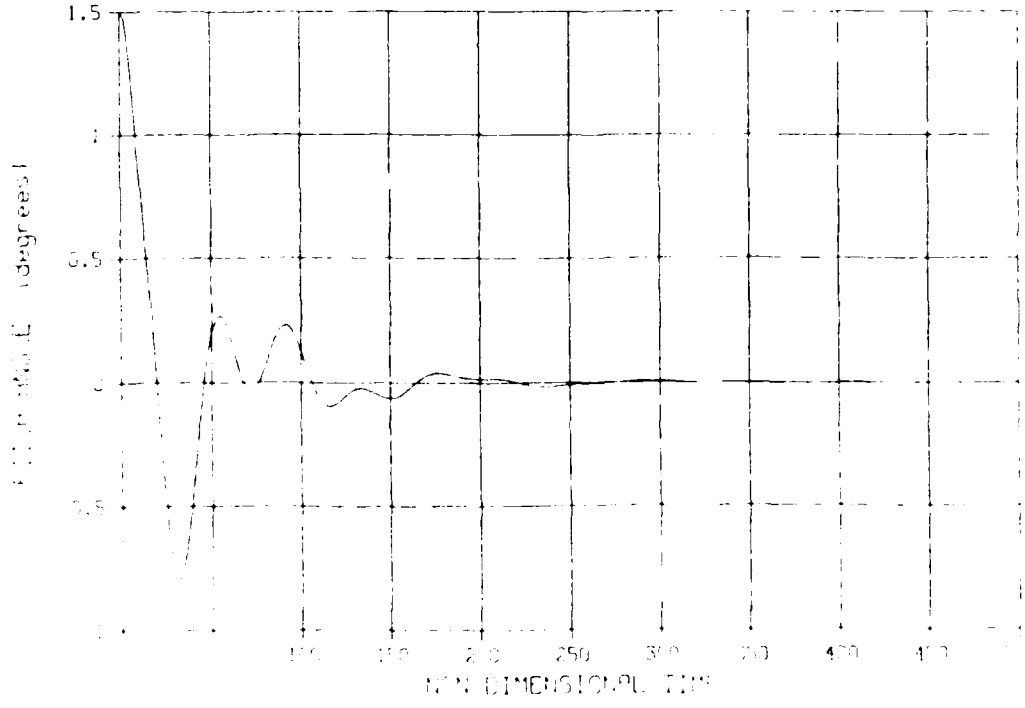

FIG. 6j: TIME VARIATION OF α FOR $\alpha(0) = 1.5$, $U^*/U_L^* = 0.84$ (CORRESPONDING TO LOCATION 10 IN FIG. 3)

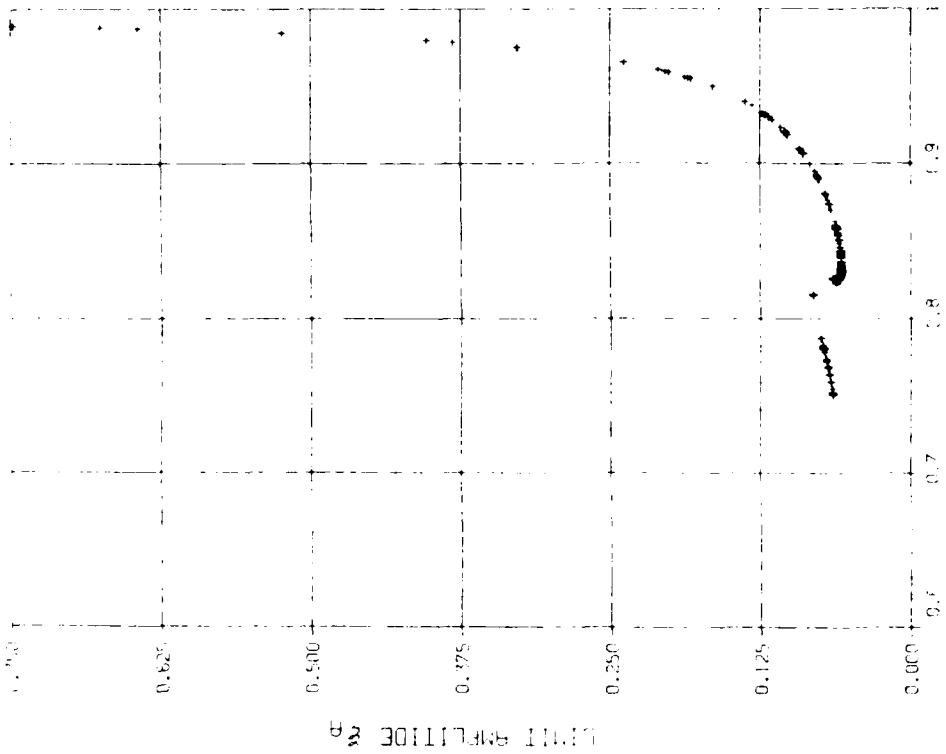

FIG. 7b: VARIATION OF LIMIT-AMPLITUDE ξ_A WITH SPEED RATIO FOR $\mu = 100$, $\bar{\omega} = 0.2$, $h_{f+} = 0.25^\circ$, $h_{f-} = 0.75^\circ$ AND $V_f = 0.25^\circ$

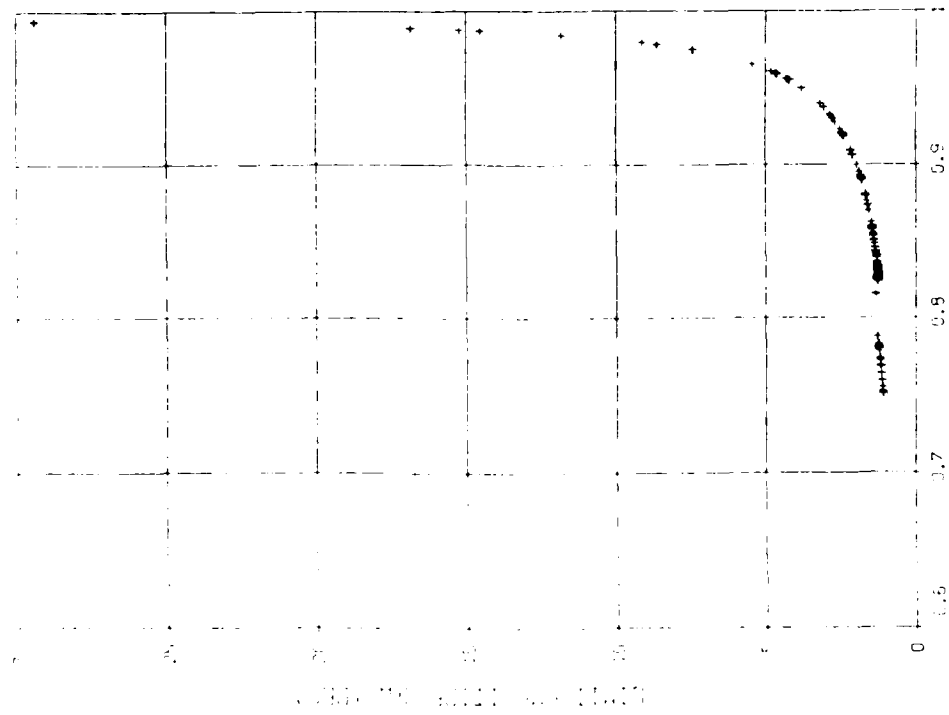

FIG. 7a: VARIATION OF LIMIT-AMPLITUDE α_A WITH SPEED RATIO FOR $\mu = 100$, $\bar{\omega} = 0.2$, $h_{f+} = 0.25^\circ$, $h_{f-} = 0.75^\circ$ AND $V_f = 0.25^\circ$

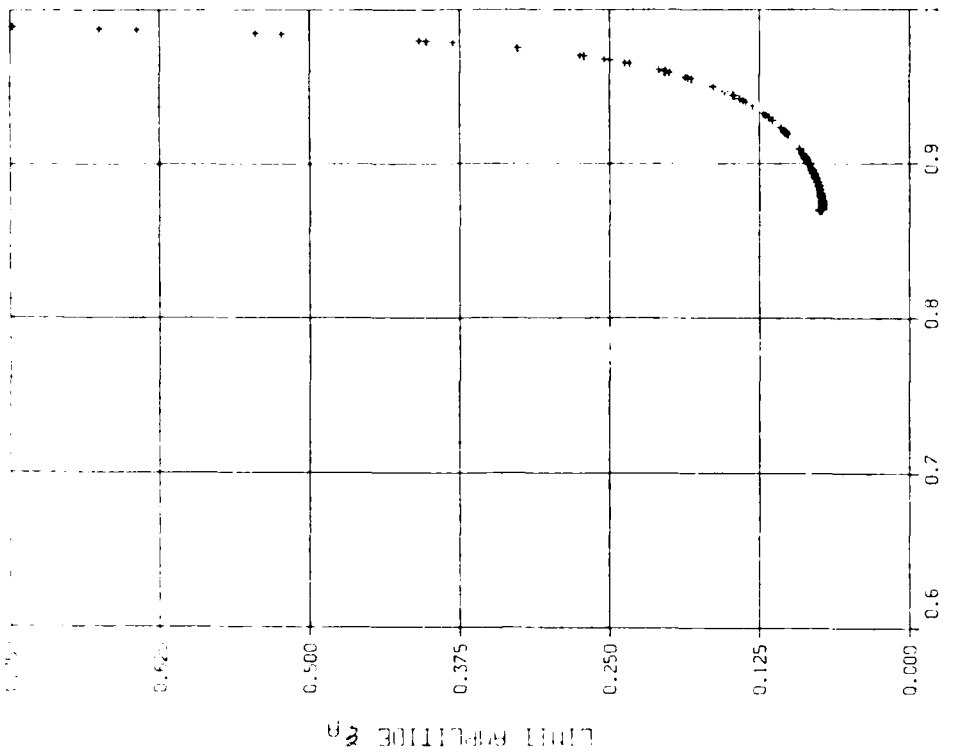

FIG. 8b: VARIATION OF LIMIT-AMPLITUDE ξ_A WITH SPEED RATIO FOR $\mu = 100$, $\bar{\omega} = 0.2$, $h_{f+} = 0.5^\circ$, $h_{f-} = 1.0^\circ$ AND $V_{f^-} = 0.5^\circ$

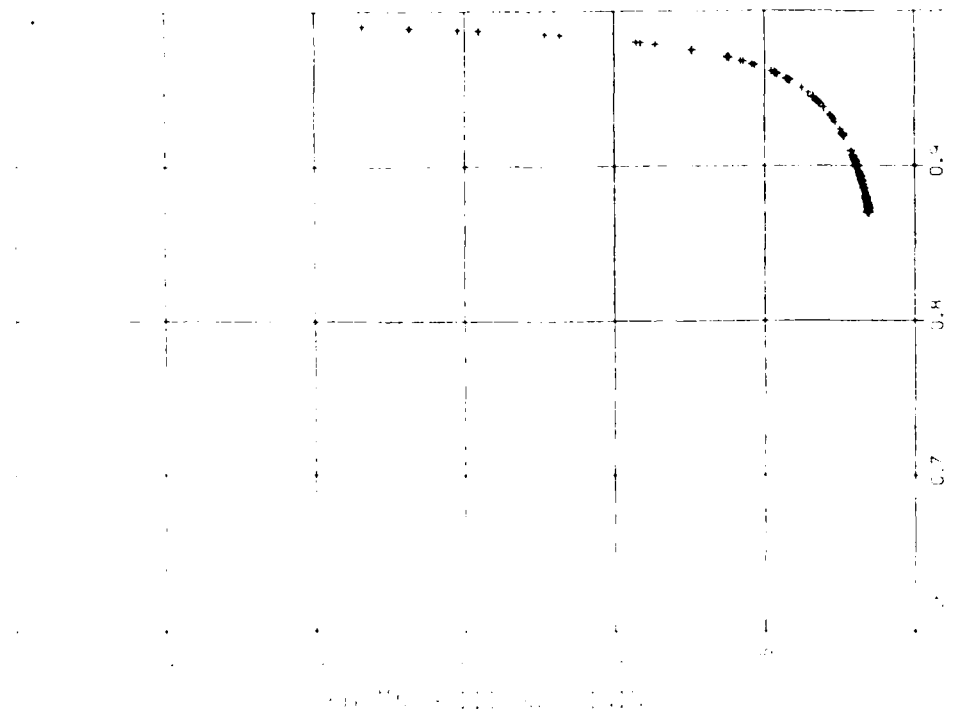

FIG. 8a: VARIATION OF LIMIT-AMPLITUDE α_A WITH SPEED RATIO FOR $\mu = 100$, $\bar{\omega} = 0.2$, $h_{f+} = 0.5^\circ$, $h_{f-} = 1.0^\circ$ AND $V_{f^-} = 0.5^\circ$

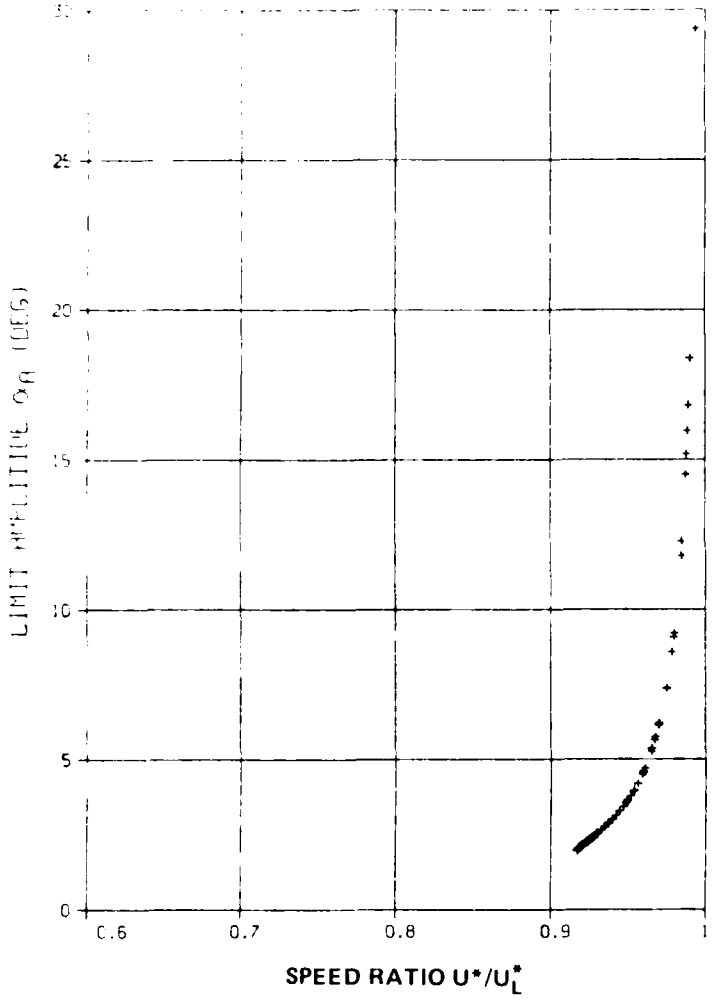

FIG. 9a: VARIATION OF LIMIT-AMPLITUDE α_A WITH SPEED RATIO FOR μ = 100, $\bar{\omega}$ = 0.2, h_{f+} = 1.0°, h_{f-} = 1.5° AND V_{f° = 1.0°

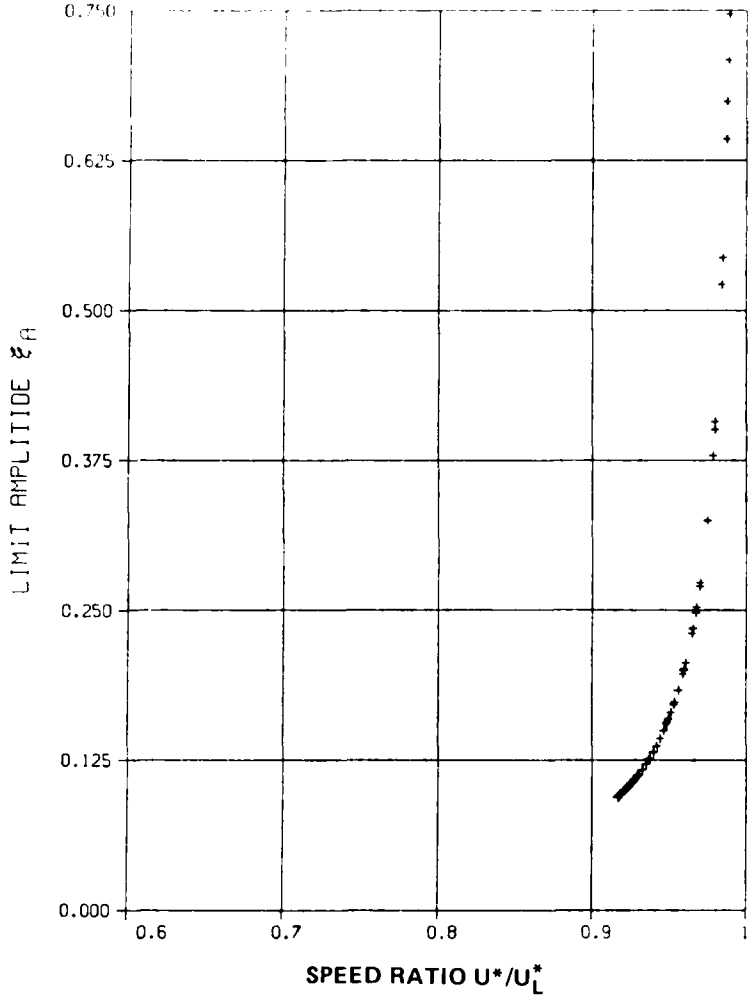

FIG. 9b: VARIATION OF LIMIT-AMPLITUDE ξ_A WITH SPEED RATIO FOR μ = 100, $\bar{\omega}$ = 0.2, h_{f+} = 1.0°, h_{f-} = 1.5° AND V_{f° = 1.0°

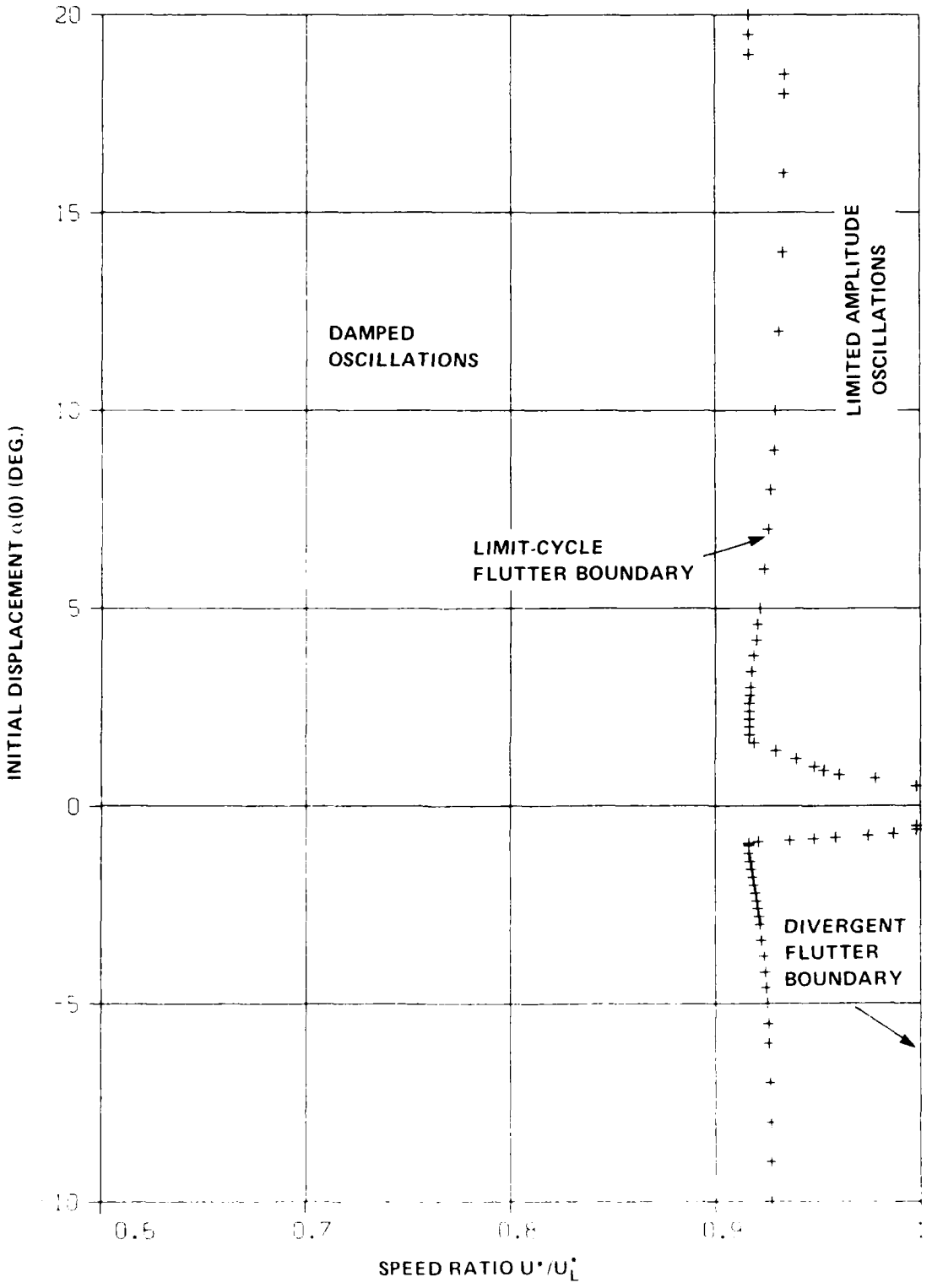

FIG. 10: FLUTTER BOUNDARY FOR $\mu = 100$, $\bar{\omega} = 0.2$, $h_{f+} = 0.5$, $h_{f-} = 0.75$ AND $V_f = 0.5$

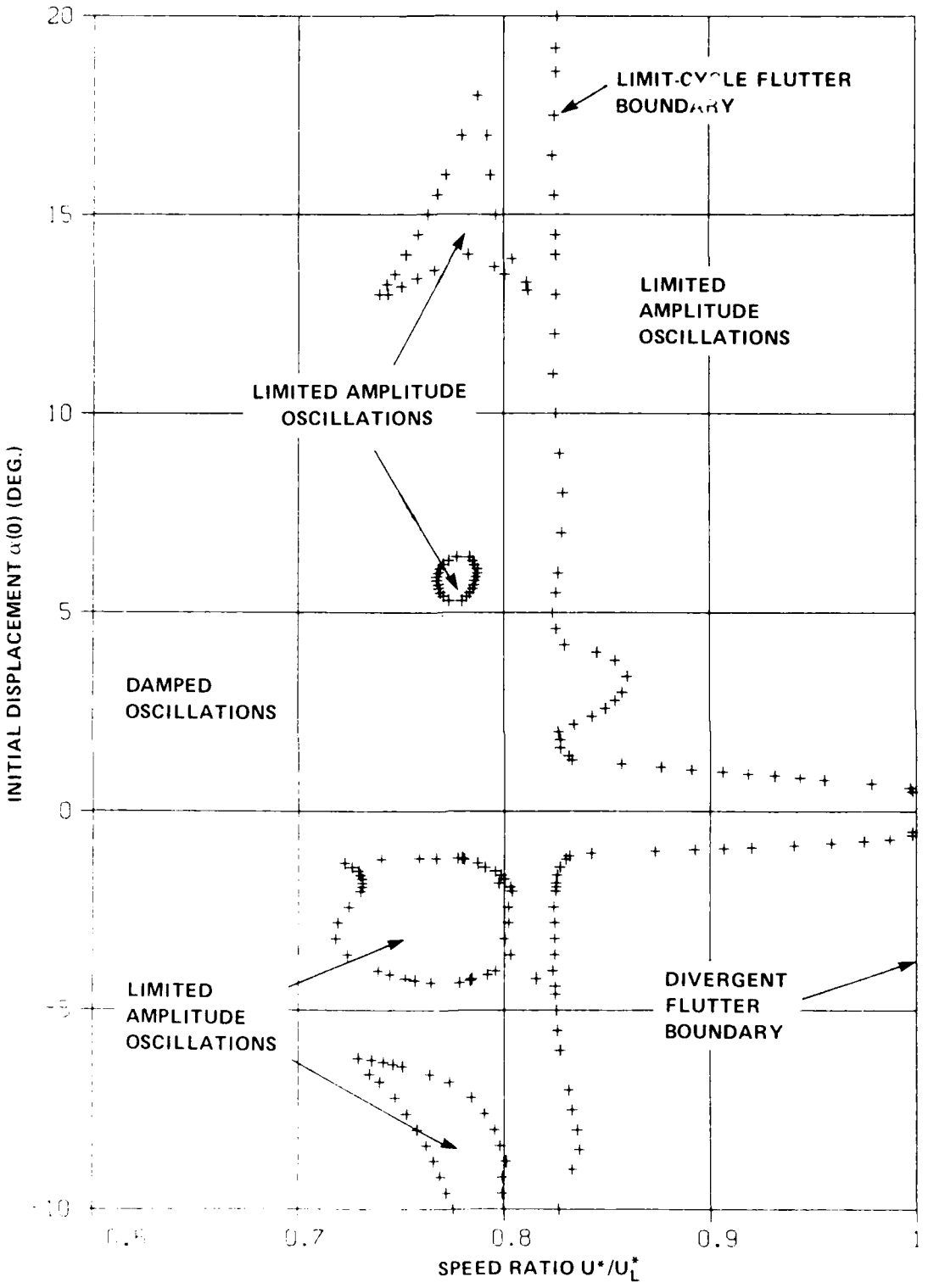

FIG. 11: FLUTTER BOUNDARY FOR $\mu = 100$, $\bar{\omega} = 0.2$, $h_{f+} = 0.5$, $h_{f-} = 1.5$ AND $V_{f_1} = 0.5$

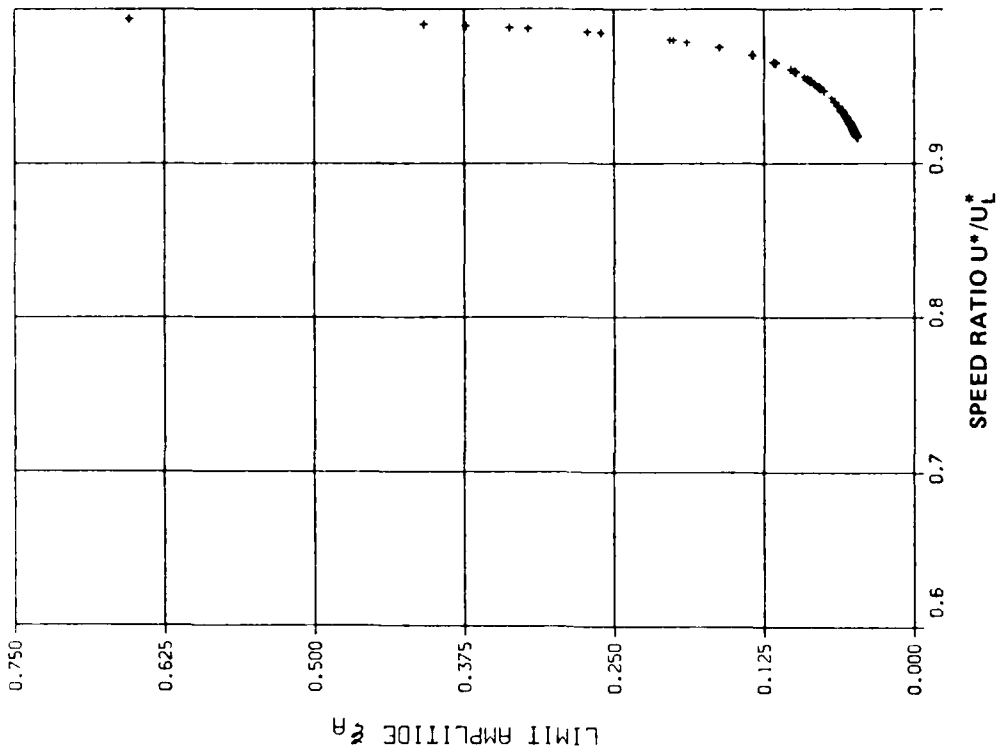

FIG. 12b: VARIATION OF LIMIT-AMPLITUDE ξ_A WITH SPEED RATIO FOR $\mu = 100$, $\bar{\omega} = 0.2$, $h_{f+} = 0.5^\circ$, $h_{f-} = 0.75^\circ$ AND $V_{f^\circ} = 0.5^\circ$

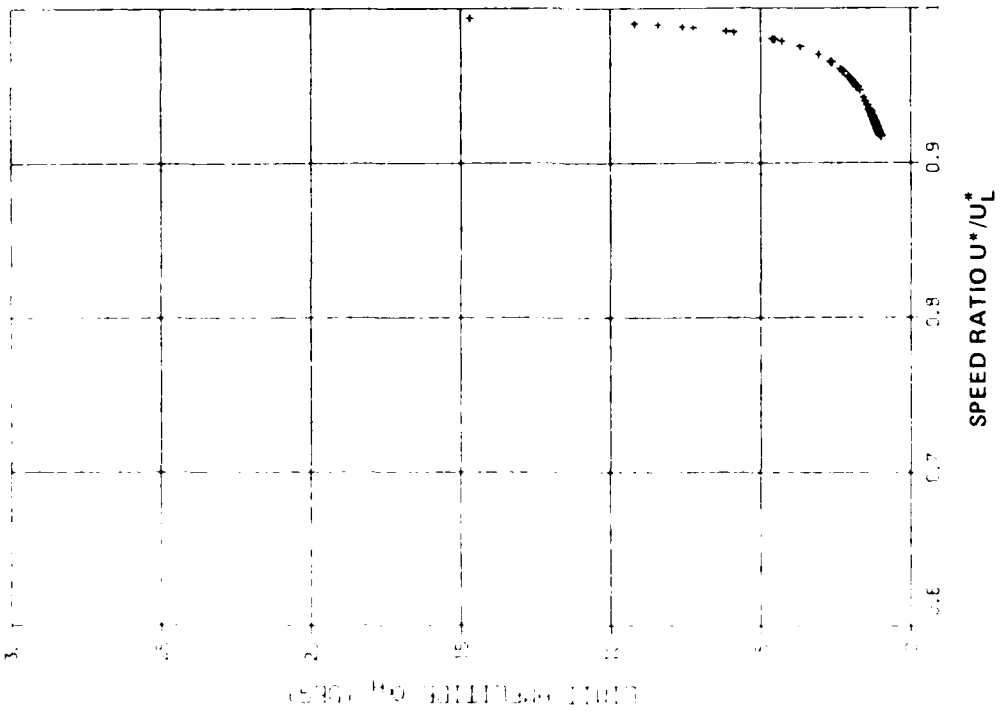

FIG. 12a: VARIATION OF LIMIT-AMPLITUDE α_A WITH SPEED RATIO FOR $\mu = 100$, $\bar{\omega} = 0.2$, $h_{f+} = 0.5^\circ$ $h_{f-} = 0.75^\circ$ AND $V_f = 0.5^\circ$

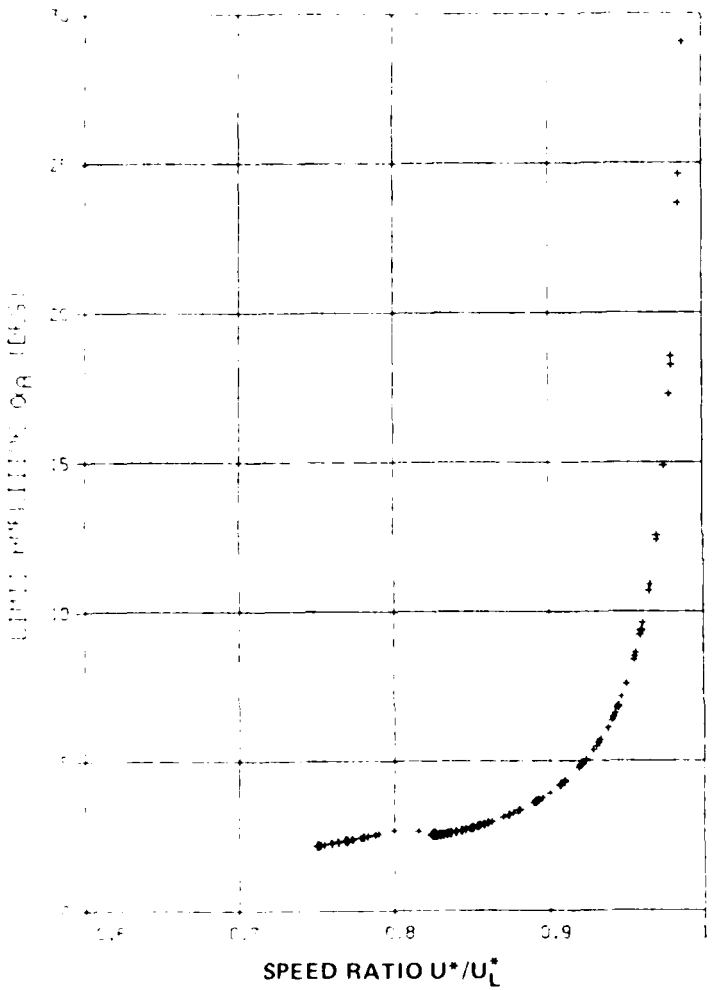

FIG. 13a: VARIATION OF LIMIT-AMPLITUDE α_A WITH SPEED RATIO FOR μ = 100, $\bar{\omega}$ = 0.2, h_{f+} = 0.5°, h_{f-} = 1.5° AND V_{f° = 0.5°

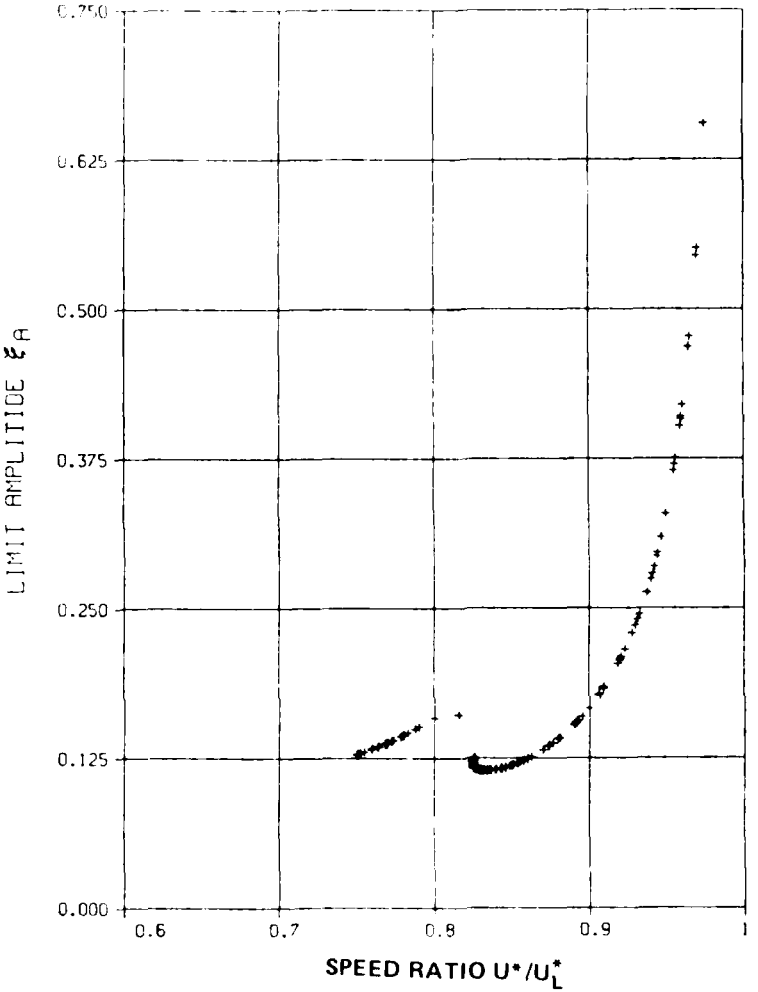

FIG. 13b: VARIATION OF LIMIT-AMPLITUDE ξ_A WITH SPEED RATIO FOR μ = 100, $\bar{\omega}$ = 0.2, h_{f+} = 0.5°, h_{f-} = 1.5° AND V_{f° = 0.5°

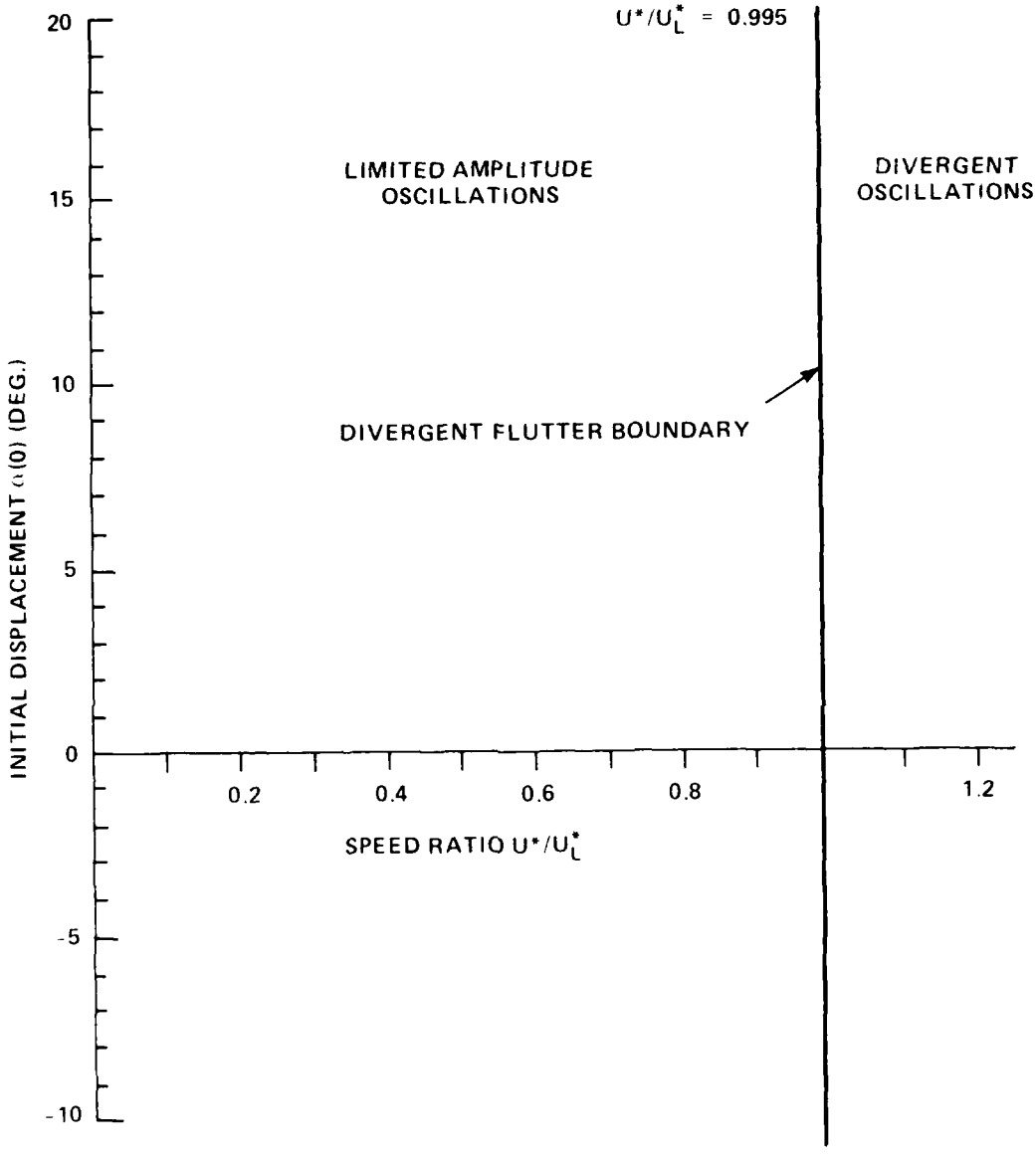

FIG. 14: FLUTTER BOUNDARY FOR $\mu = 100$, $\omega = 0.2$, $h_{f+} = 0°$, $h_{f-} = 1.0°$ AND $V_f = 0$

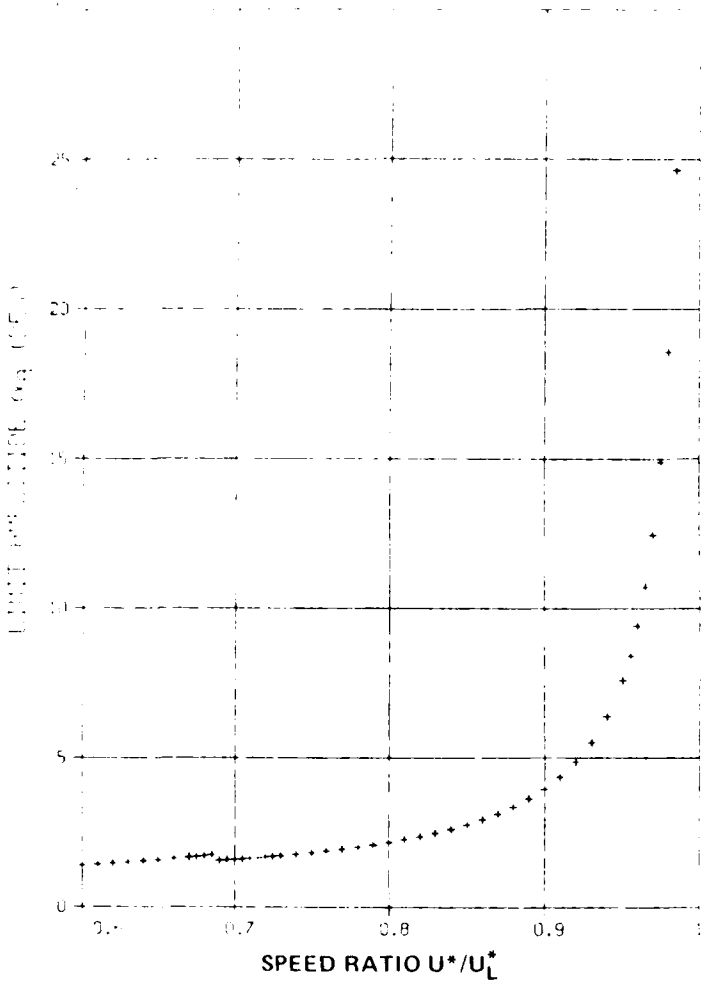

FIG. 15a: VARIATION OF LIMIT-AMPLITUDE α_A WITH SPEED RATIO FOR $\mu = 100$, $\bar{\omega} = 0.2$, $h_{f+} = 0^\circ$, $h_{f-} = 1.0^\circ$ AND $V_f = 0^\circ$

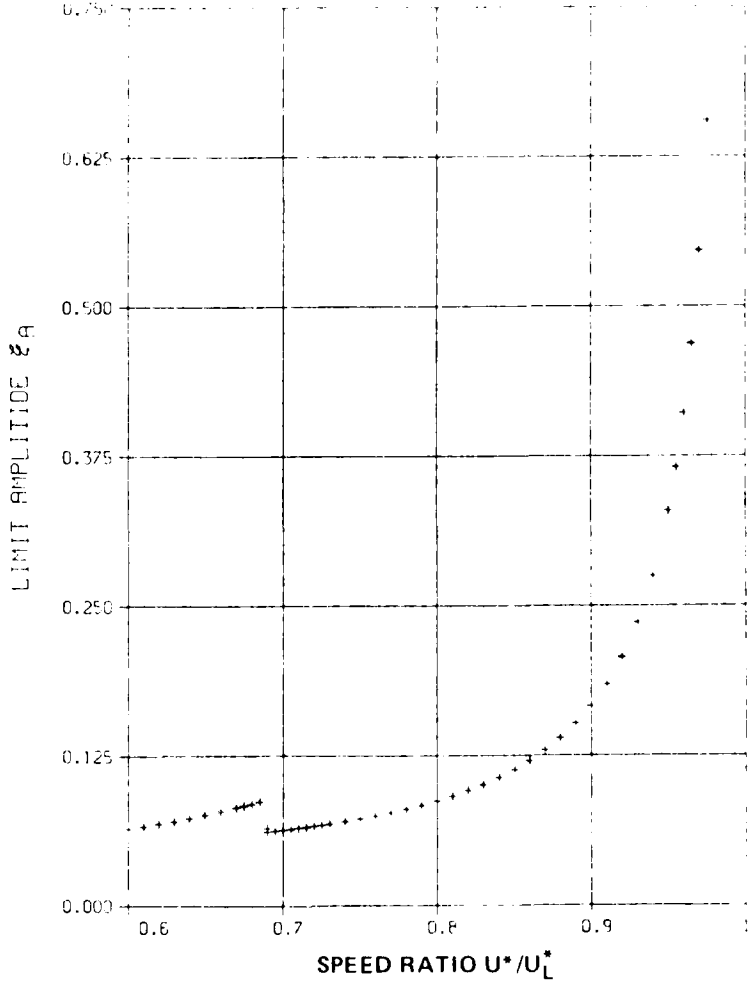

FIG. 15b: VARIATION OF LIMIT-AMPLITUDE ξ_A WITH SPEED RATIO FOR $\mu = 100$, $\bar{\omega} = 0.2$, $h_{f+} = 0^\circ$, $h_{f-} = 1.0^\circ$ AND $V_f = 0^\circ$

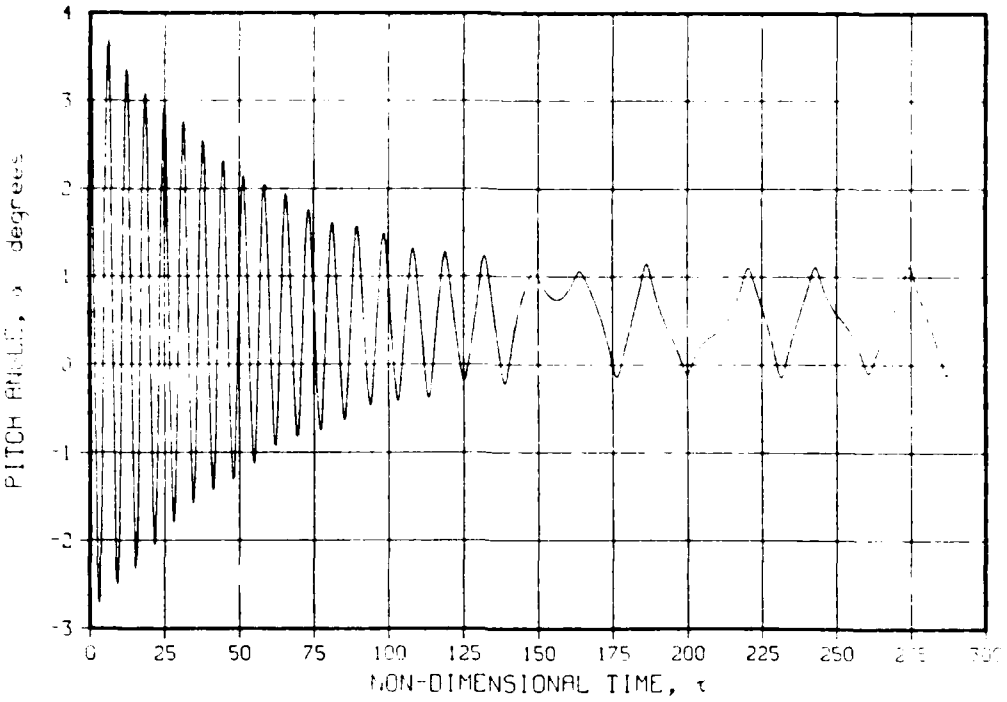

FIG. 16a: TIME VARIATION OF α FOR $\alpha(0) = 4^\circ$, $U^*/U_L^* = 0.16$, $h_{f+} = 0^\circ$, $h_{f-} = 1.0^\circ$ AND $V_{f^\circ} = 0^\circ$

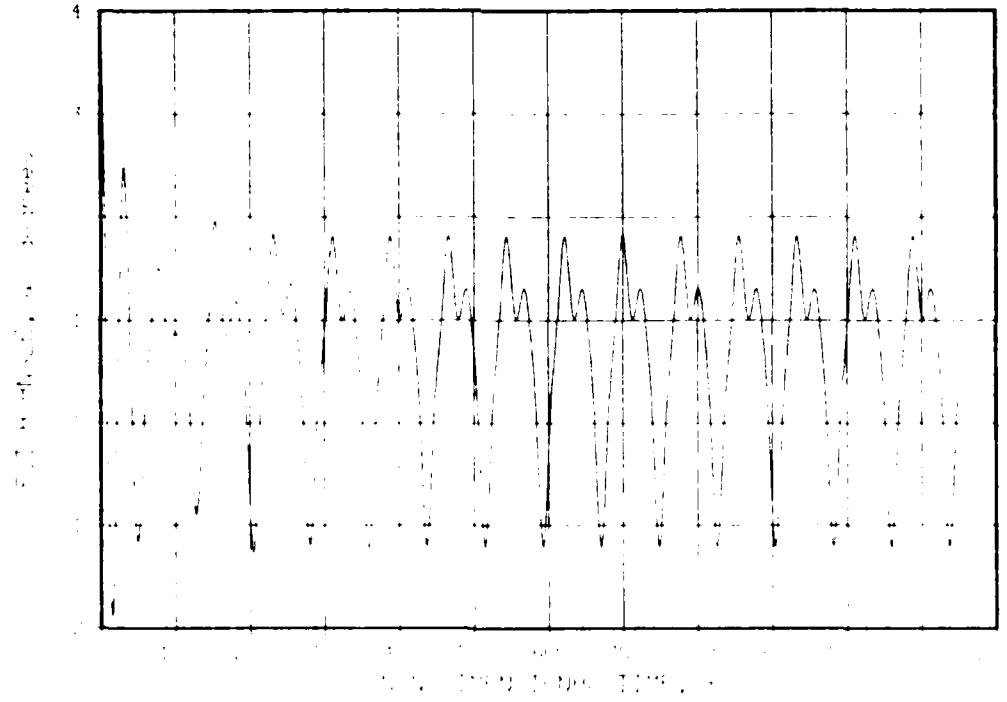

FIG. 16b: TIME VARIATION OF α FOR $\alpha(0) = 4$, $U^*/U_L^* = 0.636$, $h_{f+} = 0$, $h_{f-} = 1.0$ AND $V_f = 0$

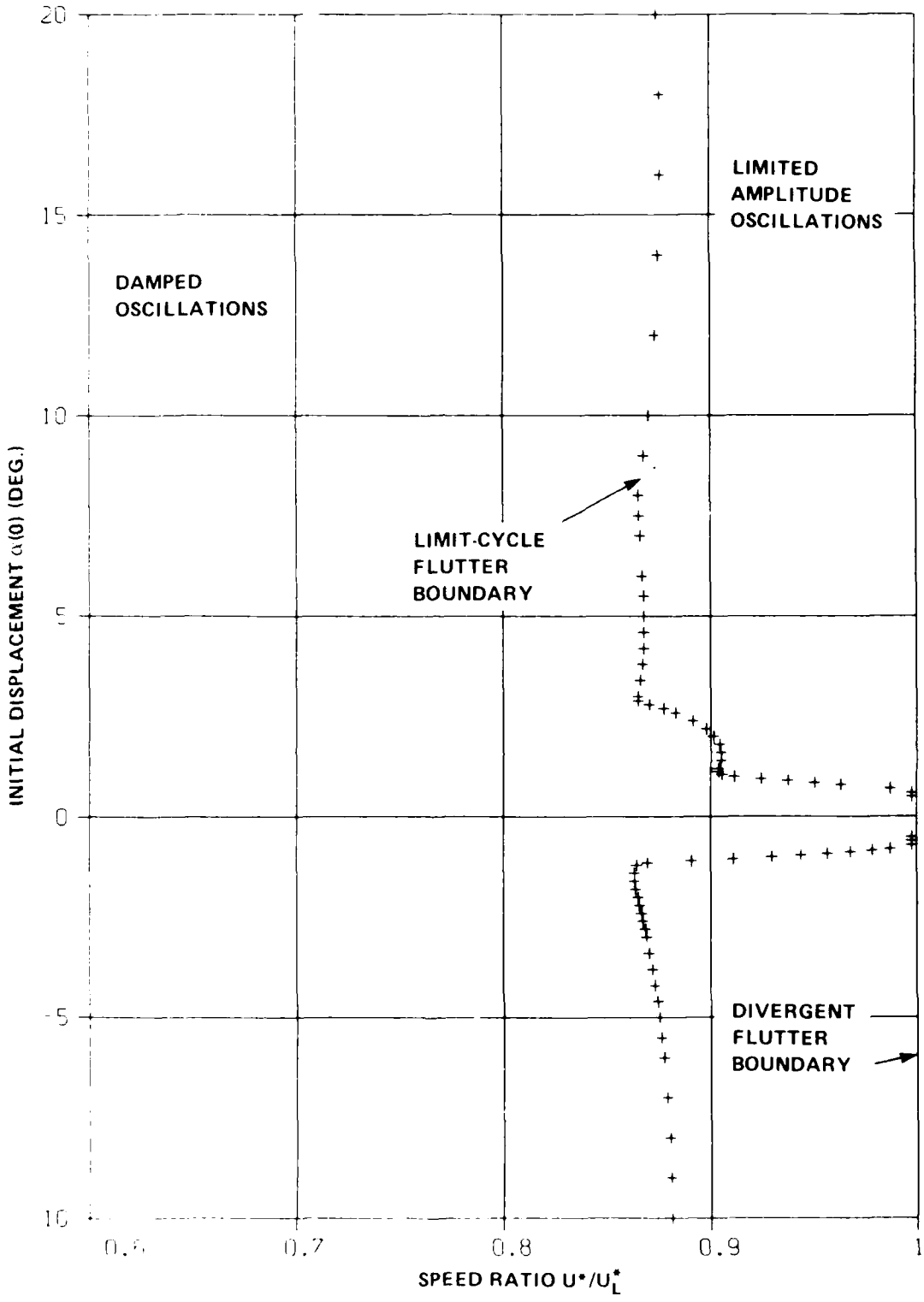

FIG. 17: FLUTTER BOUNDARY FOR $\mu = 50$, $\omega = 0.2$, $h_{f+} = 0.5°$, $h_{f-} = 1.0°$ AND $V_f = 0.5°$

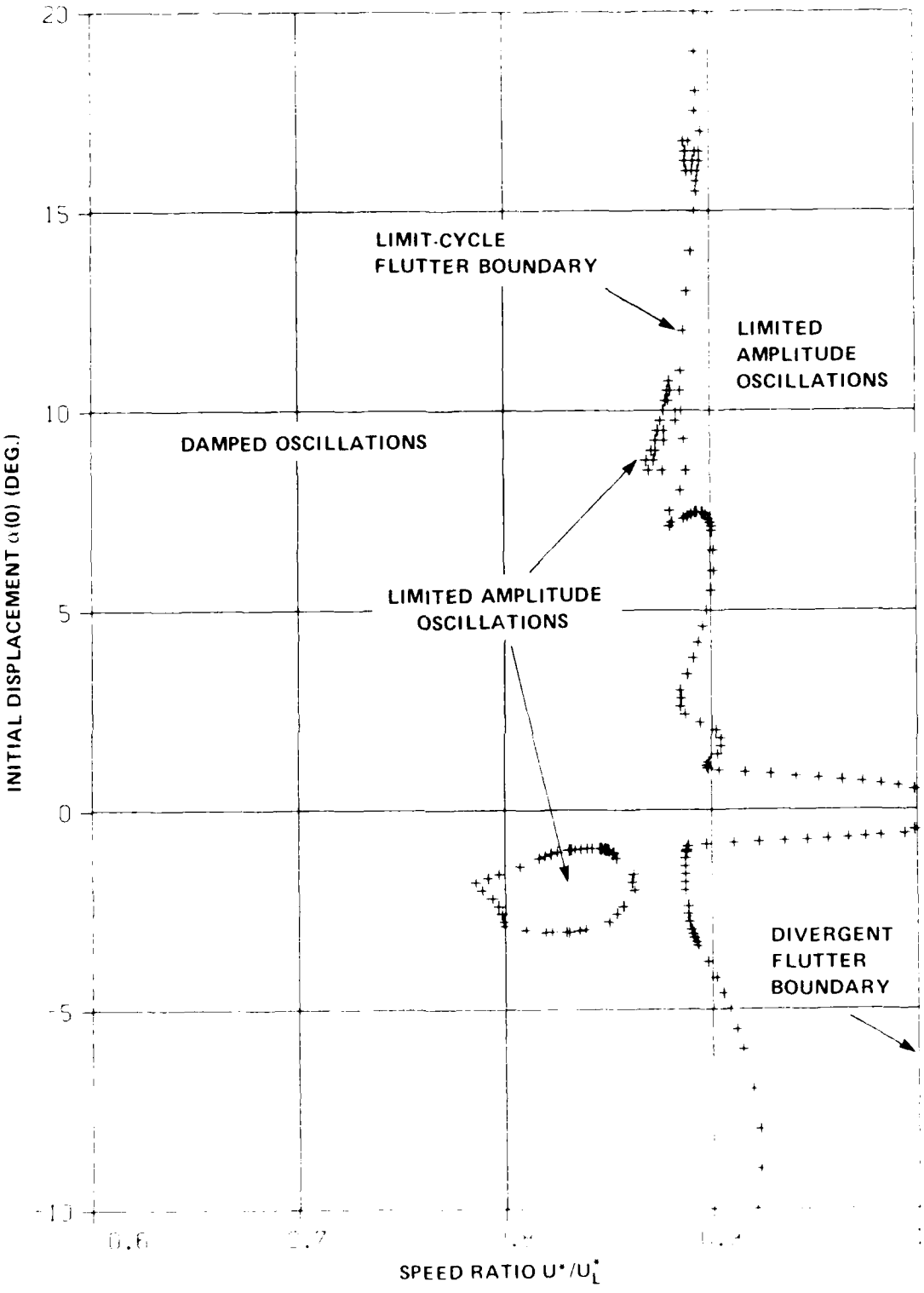

FIG. 18: FLUTTER BOUNDARY FOR $\mu = 250$, $\omega = 0.2$, $h_{f+} = 0.5$, $h_{f-} = 1.0$ AND $V_f = 0.5$

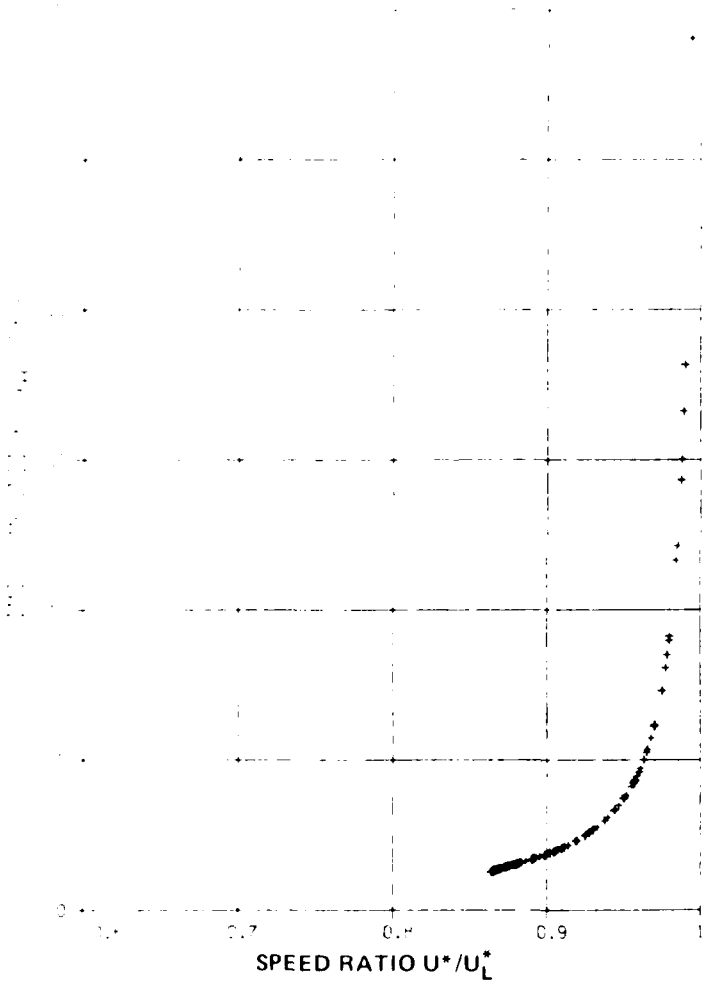

FIG. 19a: VARIATION OF LIMIT-AMPLITUDE α_A WITH SPEED RATIO FOR $\mu = 50$, $\bar{\omega} = 0.2$, $h_{f+} = 0.5^\circ$, $h_{f-} = 1.0^\circ$ AND $V_f = 0.5^\circ$

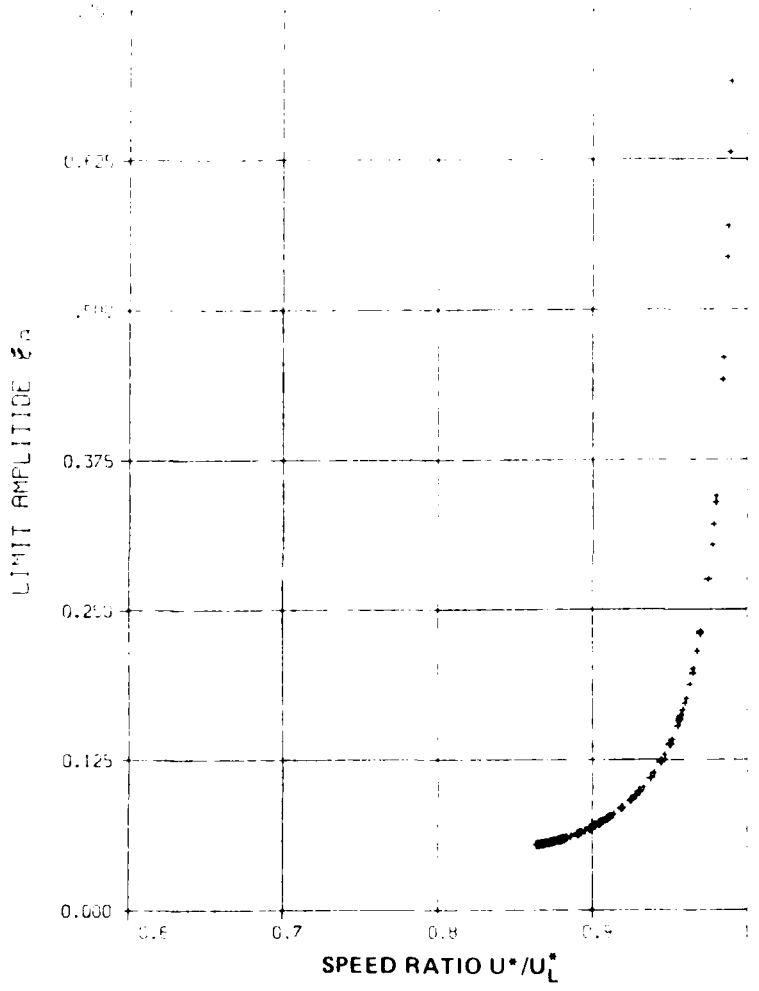

FIG. 19b: VARIATION OF LIMIT-AMPLITUDE ξ_A WITH SPEED RATIO FOR $\mu = 50$, $\bar{\omega} = 0.2$, $h_{f+} = 0.5^\circ$, $h_{f-} = 1.0^\circ$ AND $V_f = 0.5^\circ$

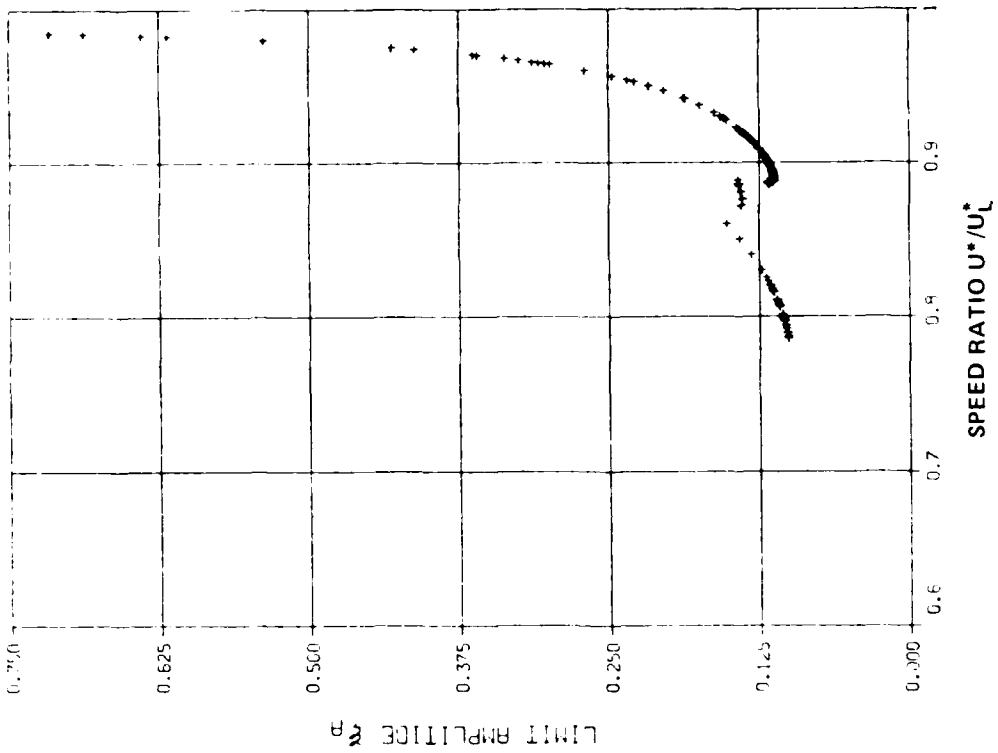

FIG. 20b: VARIATION OF LIMIT-AMPLITUDE ξ_A WITH SPEED RATIO FOR $\mu = 250$, $\bar{\omega} = 0.2$, $h_{f+} = 0.5°$, $h_{f-} = 1.0°$ AND $V_{f°} = 0.5°$

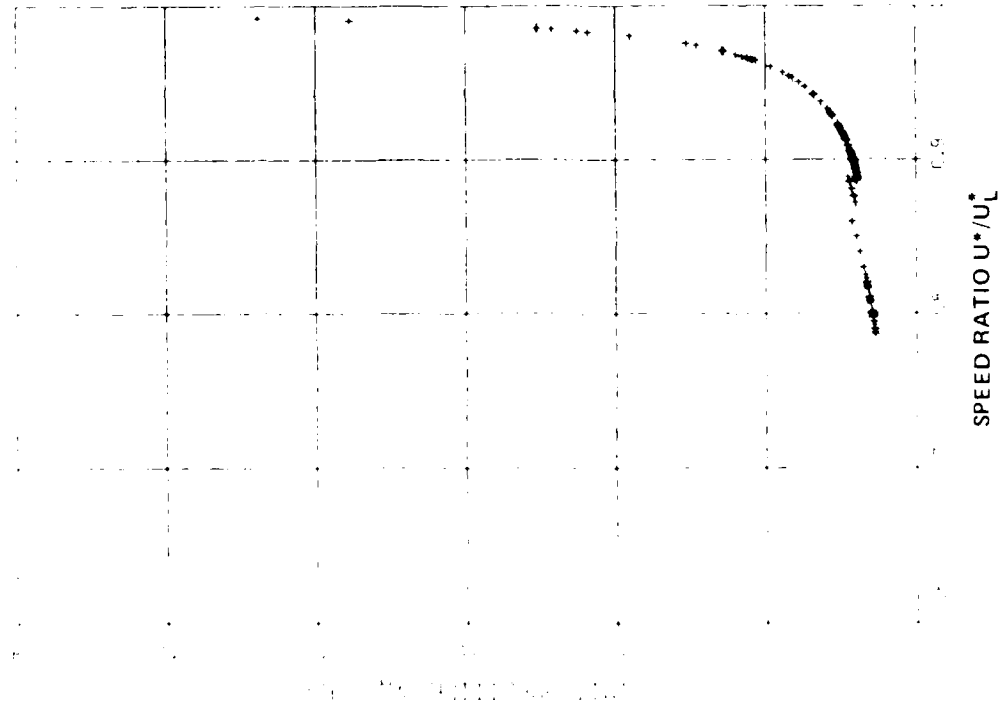

FIG. 20a: VARIATION OF LIMIT-AMPLITUDE α_A WITH SPEED RATIO FOR $\mu = 250$, $\bar{\omega} = 0.2$, $h_{f+} = 0.5$, $h_{f-} = 1.0$ AND $V_{f°} = 0.5$

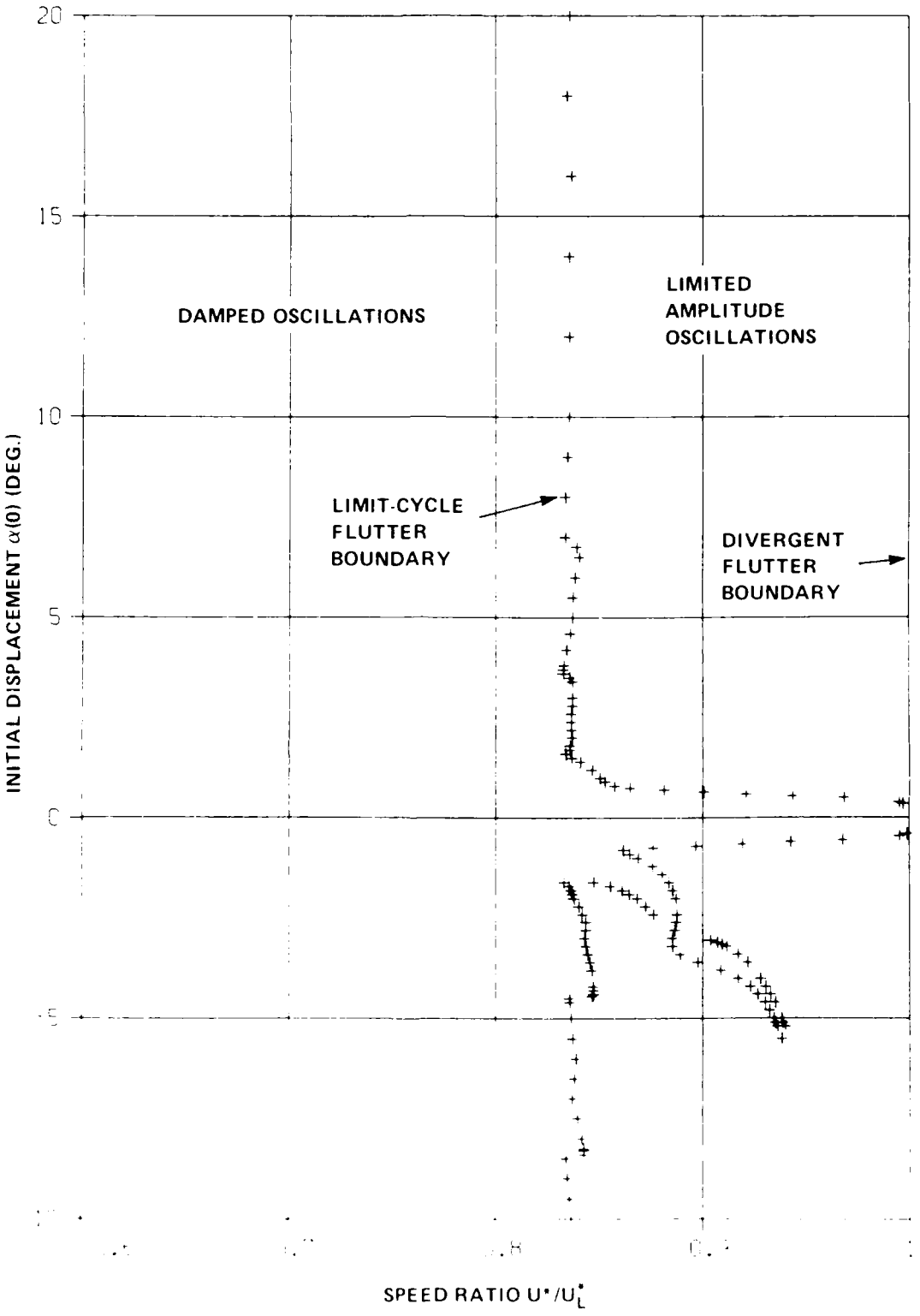

FIG. 21: FLUTTER BOUNDARY FOR $\mu = 100$, $\bar{\omega} = 0.8$, $h_{f+} = 0.25$, $h_{f-} = 0.75$ AND $V_{fr} = 0.25$

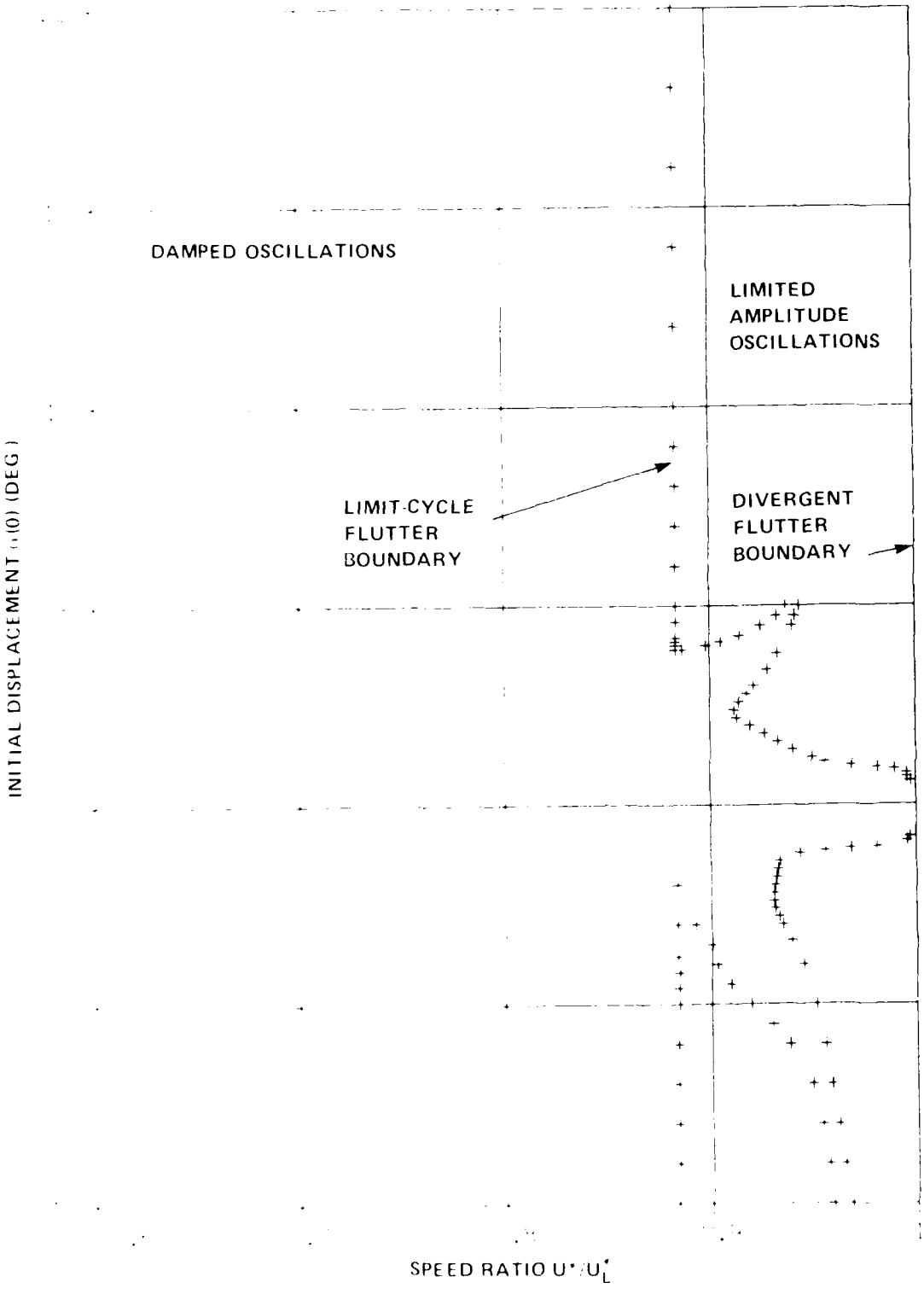

FIG. 22: FLUTTER BOUNDARY FOR μ = 100, ω = 0.8, h_f = 0.5, h_f = 1.0 AND V_f = 0.5

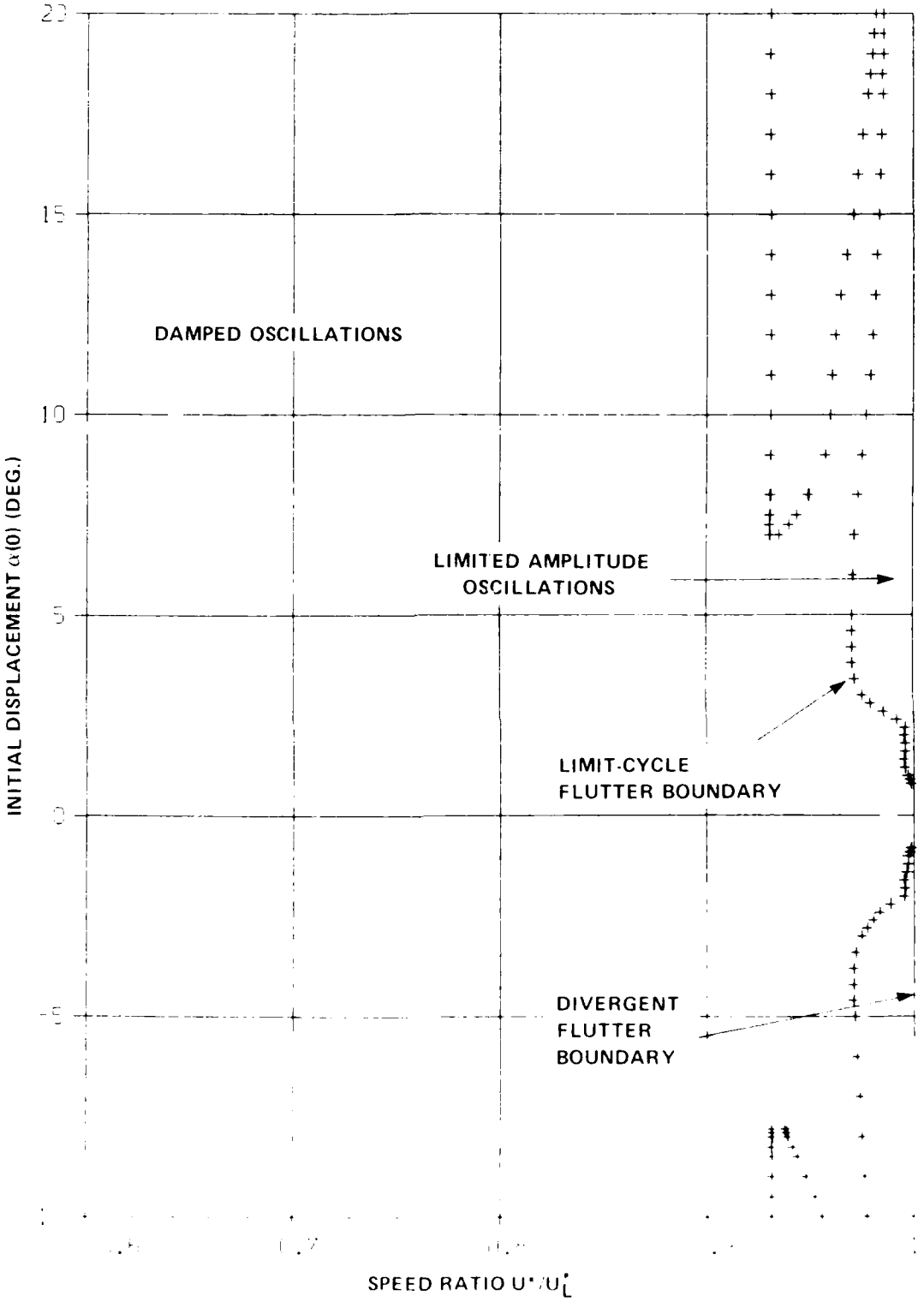

FIG. 23: FLUTTER BOUNDARY FOR μ = 100, $\bar{c}$ = 0.8, h_{f_1} = 1.0, h_{f_2} = 1.5 AND V_{f_2} = 1.0

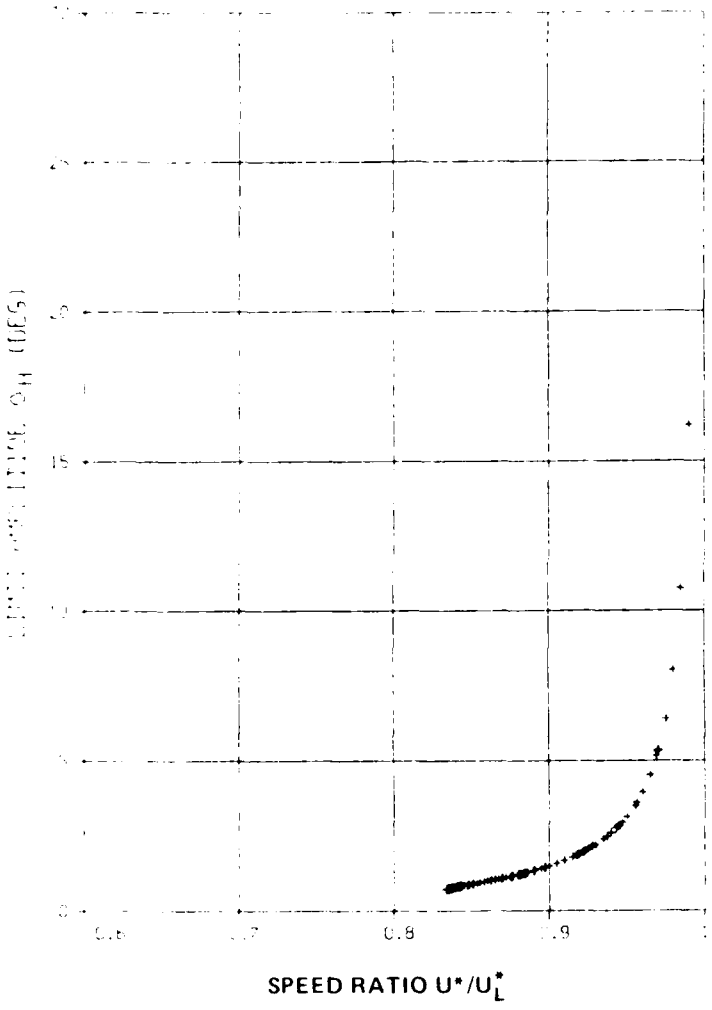

FIG. 24a: VARIATION OF LIMIT-AMPLITUDE α_A WITH SPEED RATIO FOR $\mu = 100$, $\bar{\omega} = 0.8$, $h_{f+} = 0.25^\circ$, $h_{f-} = 0.75^\circ$ AND $V_{f^\circ} = 0.25^\circ$

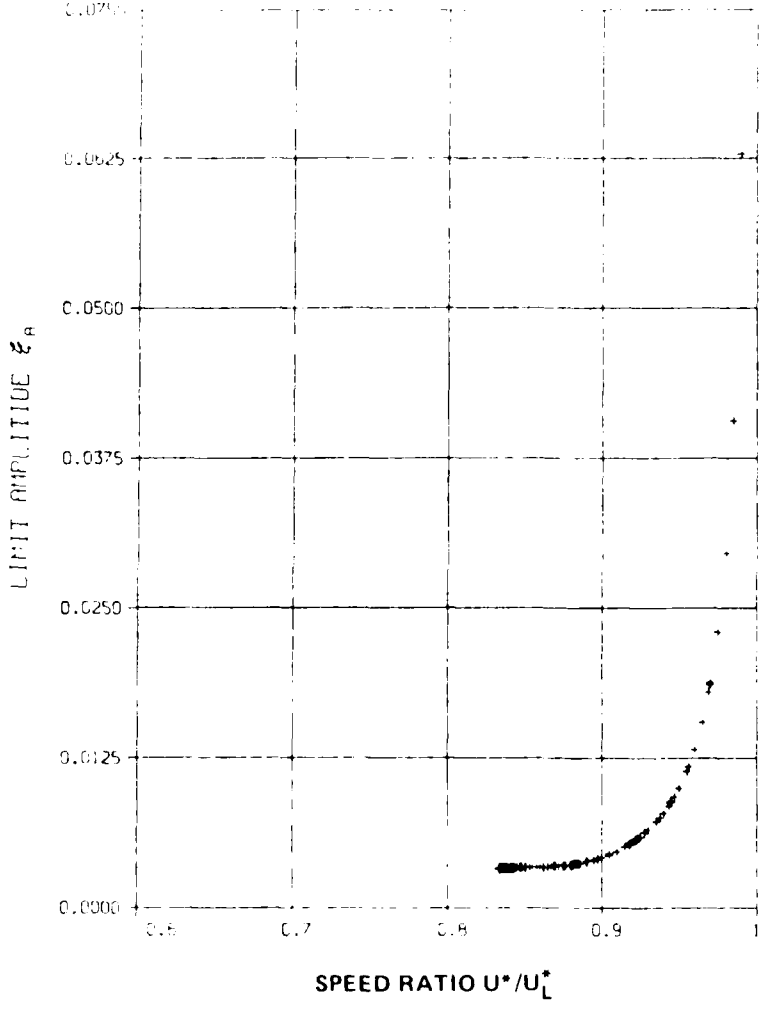

FIG. 24b: VARIATION OF LIMIT-AMPLITUDE ξ_A WITH SPEED RATIO FOR $\mu = 100$, $\bar{\omega} = 0.8$, $h_{f+} = 0.25^\circ$, $h_{f-} = 0.75^\circ$ AND $V_{f^\circ} = 0.25^\circ$

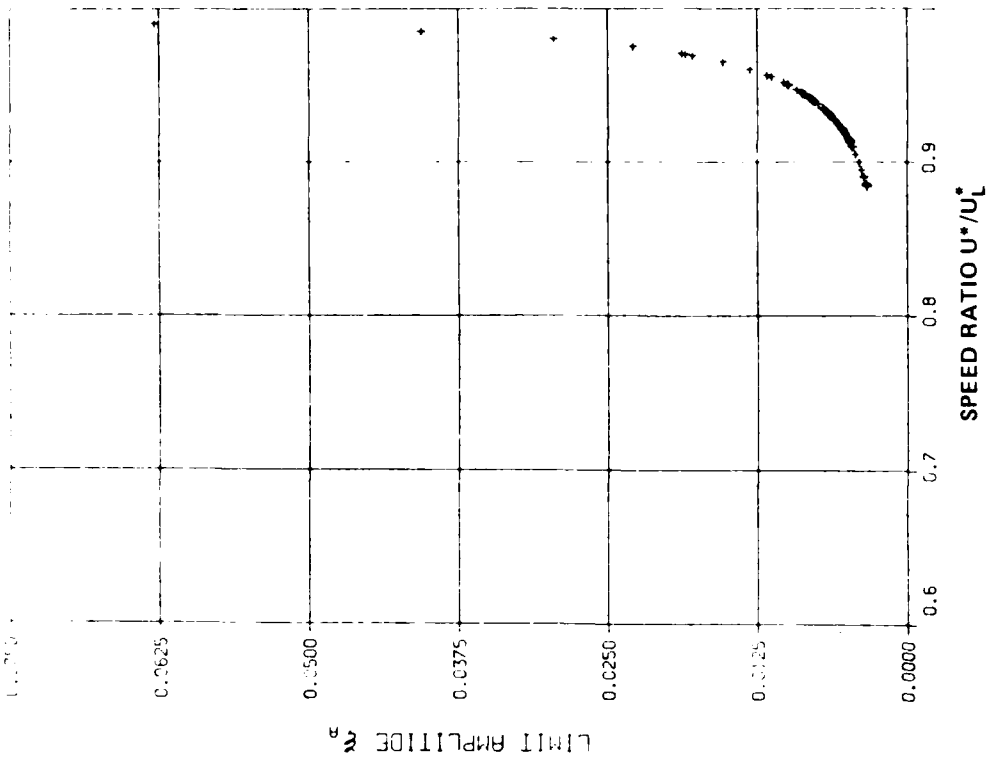

FIG. 25b: VARIATION OF LIMIT-AMPLITUDE ξ_A WITH SPEED RATIO FOR $\mu = 100$, $\bar{\omega} = 0.8$, $h_{f+} = 0.5^\circ$, $h_{f-} = 1.0^\circ$ AND $V_{f^\circ} = 0.5^\circ$

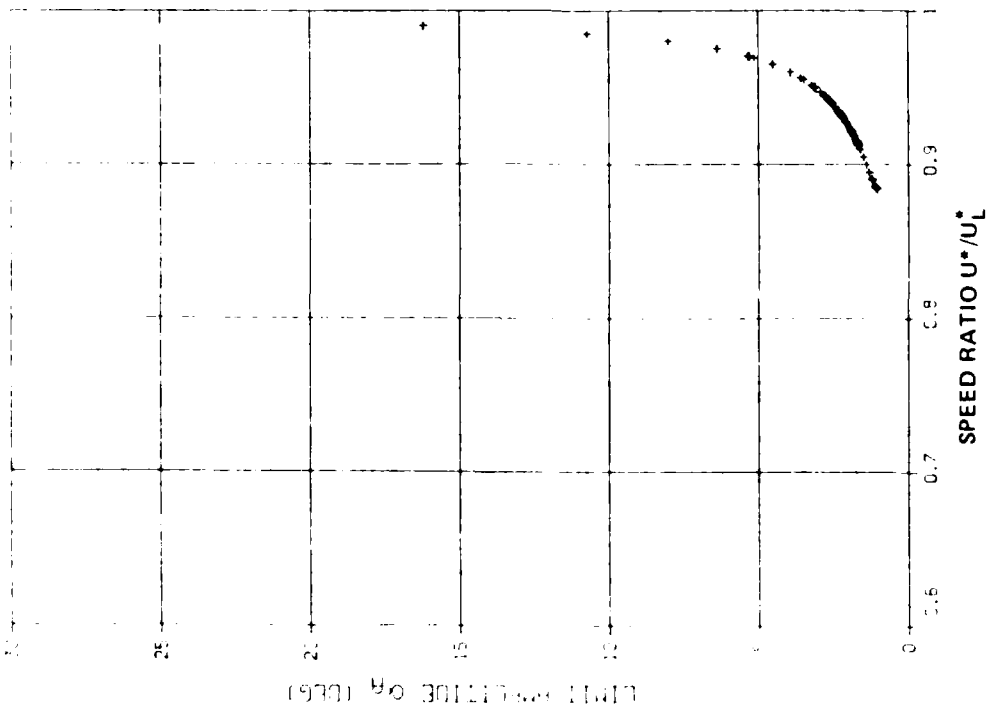

FIG. 25a: VARIATION OF LIMIT-AMPLITUDE α_A WITH SPEED RATIO FOR $\mu = 100$, $\bar{\omega} = 0.8$, $h_{f+} = 0.5^\circ$, $h_{f-} = 1.0^\circ$ AND $V_{f^\circ} = 0.5^\circ$

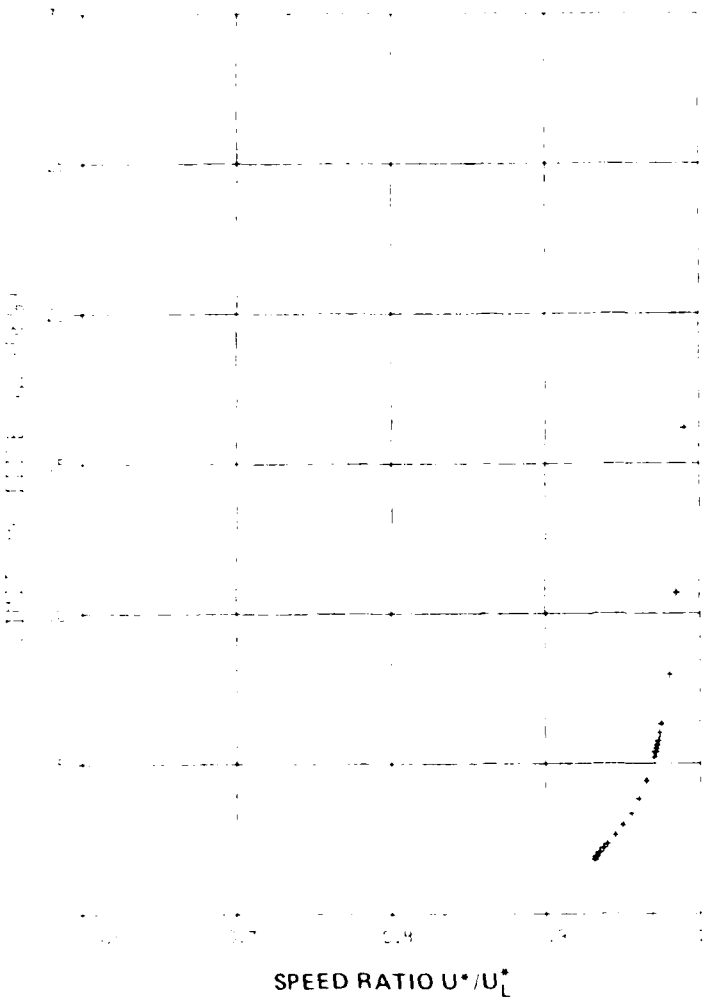

FIG. 26a: VARIATION OF LIMIT-AMPLITUDE α_A WITH SPEED RATIO FOR $\mu = 100$, $\bar{\omega} = 0.8$, $h_{f+} = 1.0^\circ$, $h_{f-} = 1.5$ AND $V_{f^\circ} = 1.0$

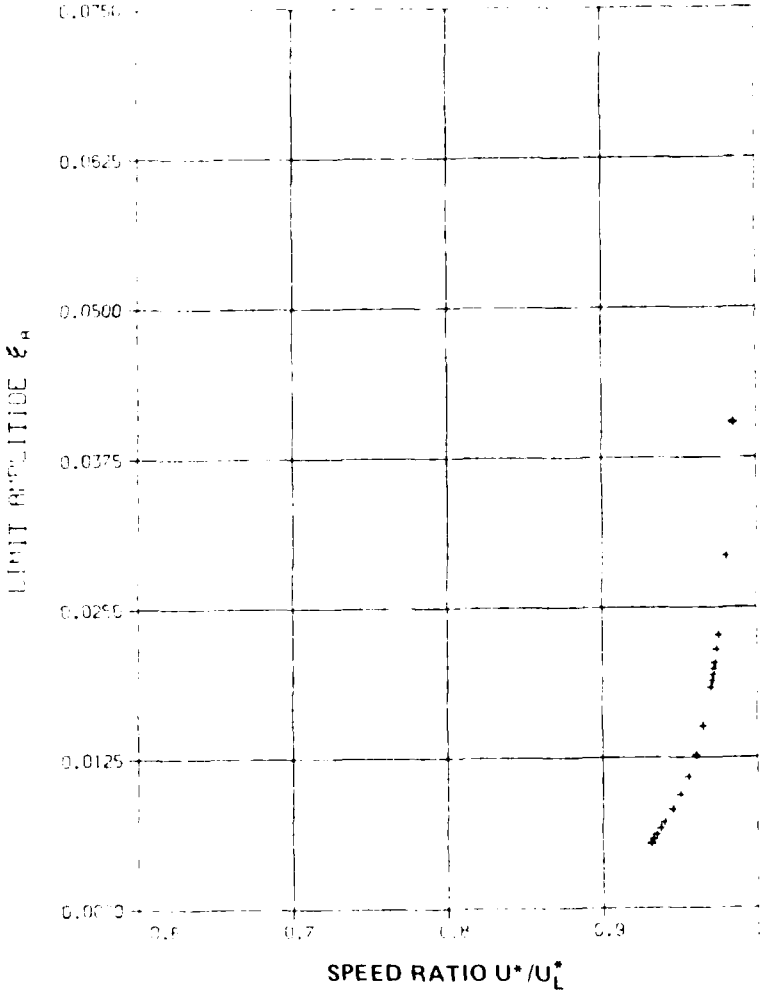

FIG. 26b: VARIATION OF LIMIT-AMPLITUDE ξ_A WITH SPEED RATIO FOR $\mu = 100$, $\bar{\omega} = 0.8$, $h_{f+} = 1.0^\circ$, $h_{f-} = 1.5^\circ$ AND $V_{f^\circ} = 1.0^\circ$

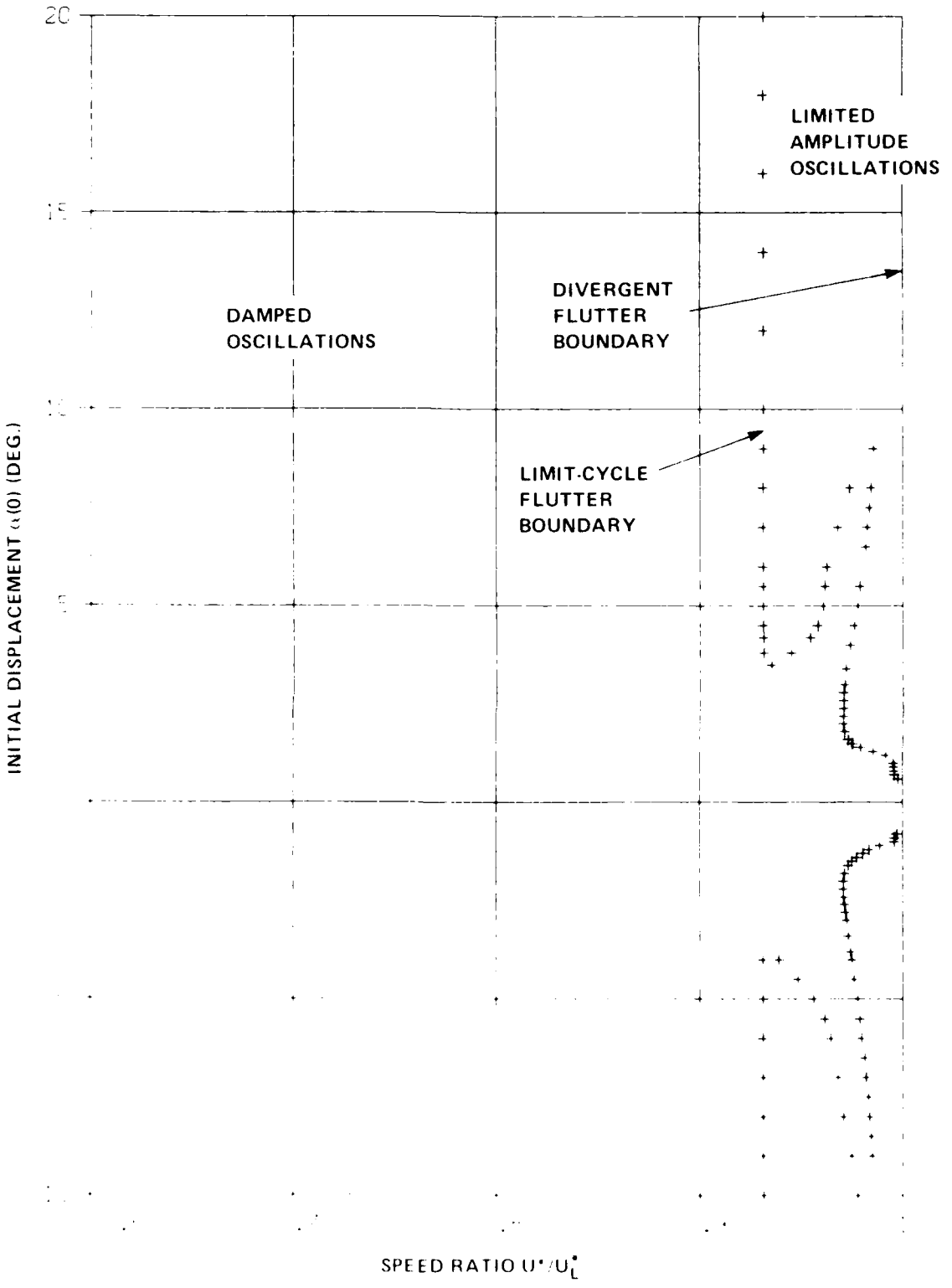

FIG. 27: FLUTTER BOUNDARY FOR μ = 100, $\bar{\omega}$ = 0.8, h_f = 0.5, h_f = 0.75 AND V_f = 0.5

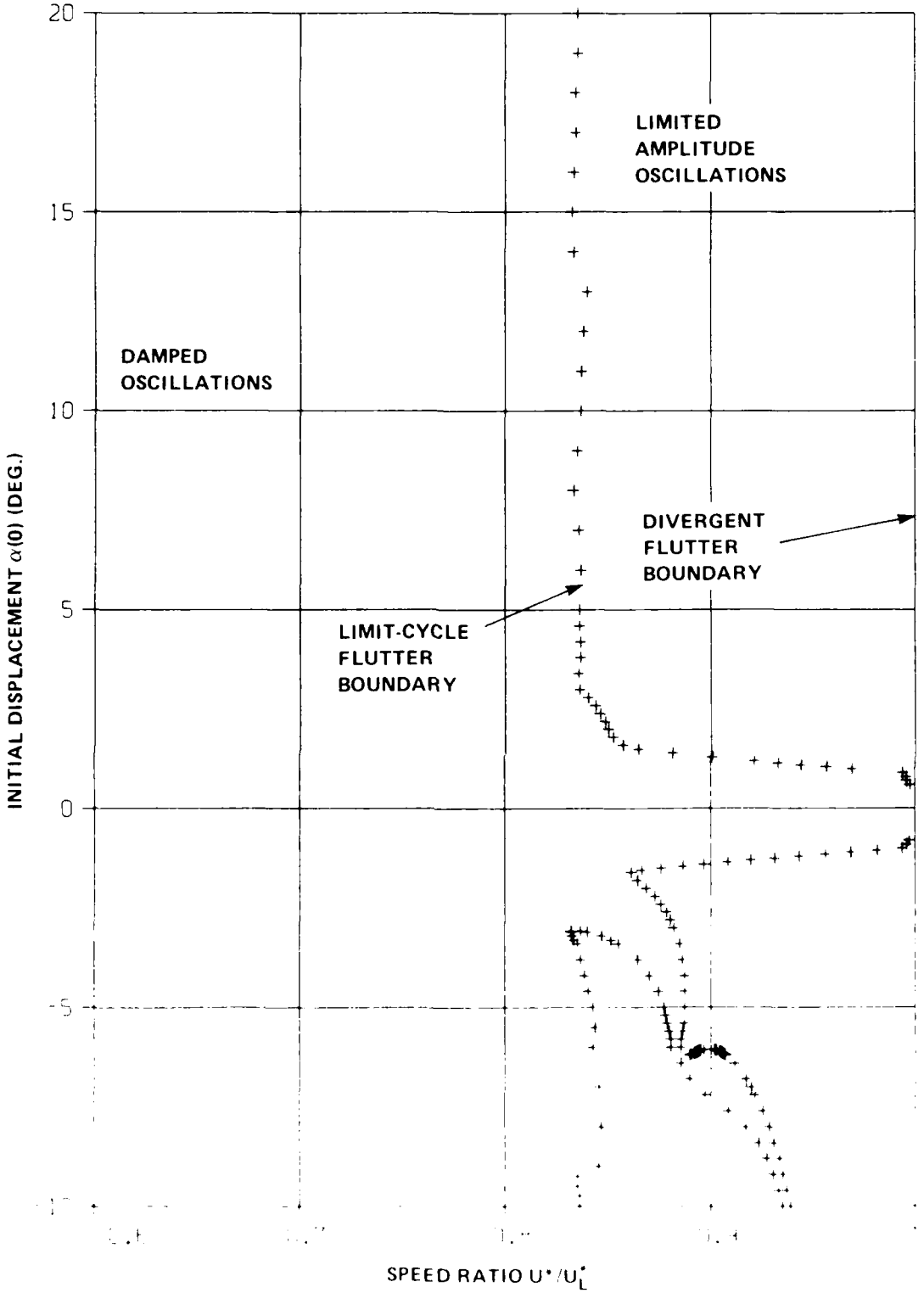

FIG. 28: FLUTTER BOUNDARY FOR μ = 100, ω = 0.8, h_f = 0.5, h_f = 1.5 AND V_f = 0.5

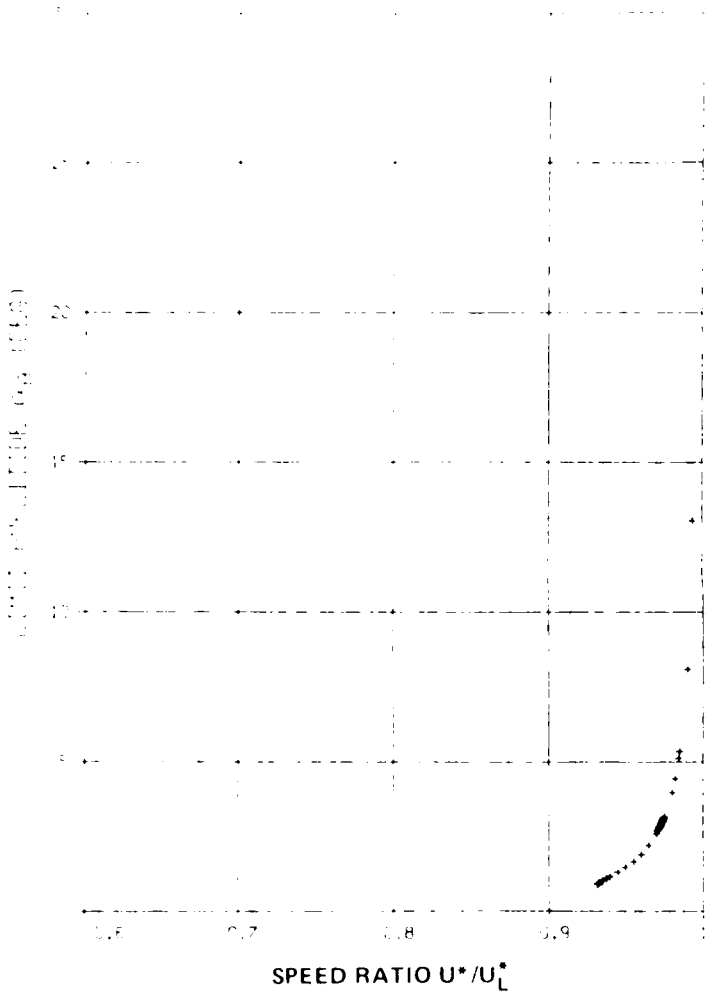

FIG. 29a: VARIATION OF LIMIT-AMPLITUDE α_A WITH SPEED RATIO FOR μ = 100, $\bar{\omega}$ = 0.8, h_{f+} = 0.5°, h_{f-} = 0.75° AND V_f = 0.5°

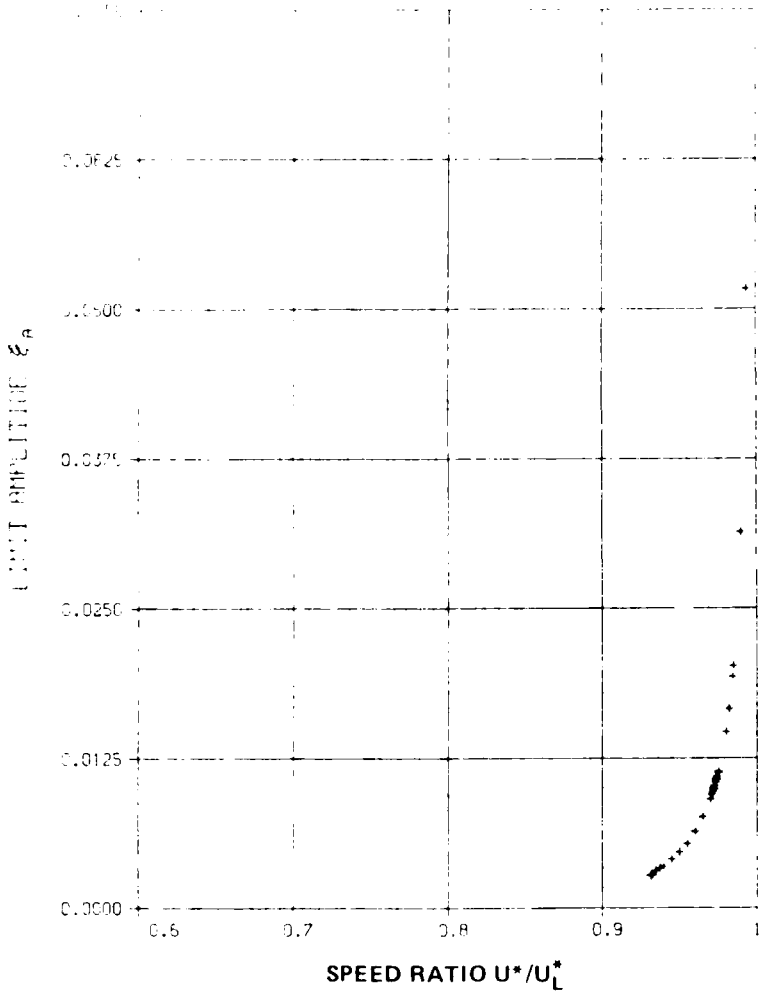

FIG. 29b: VARIATION OF LIMIT-AMPLITUDE ξ_A WITH SPEED RATIO FOR μ = 100, $\bar{\omega}$ = 0.8, h_{f+} = 0.5°, h_{f-} = 0.75° AND V_f = 0.5°

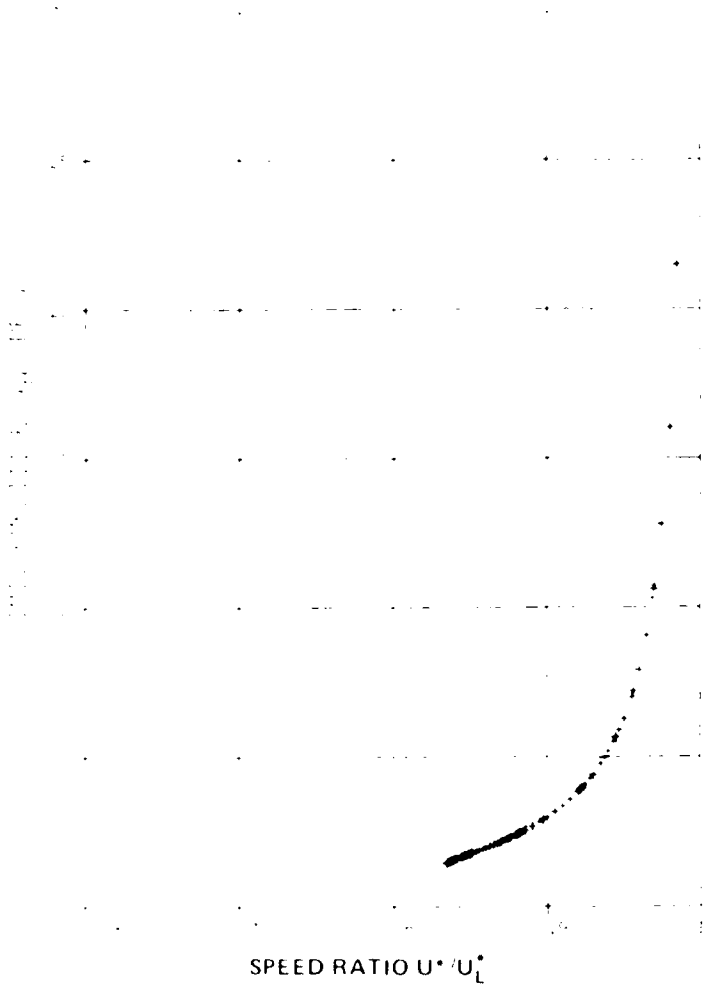

FIG. 30a: VARIATION OF LIMIT-AMPLITUDE α_A WITH SPEED RATIO FOR $\mu = 100$, $\bar{\omega} = 0.8$, $h_{f+} = 0.5$, $h_{f-} = 1.5$ AND $V_f = 0.5$

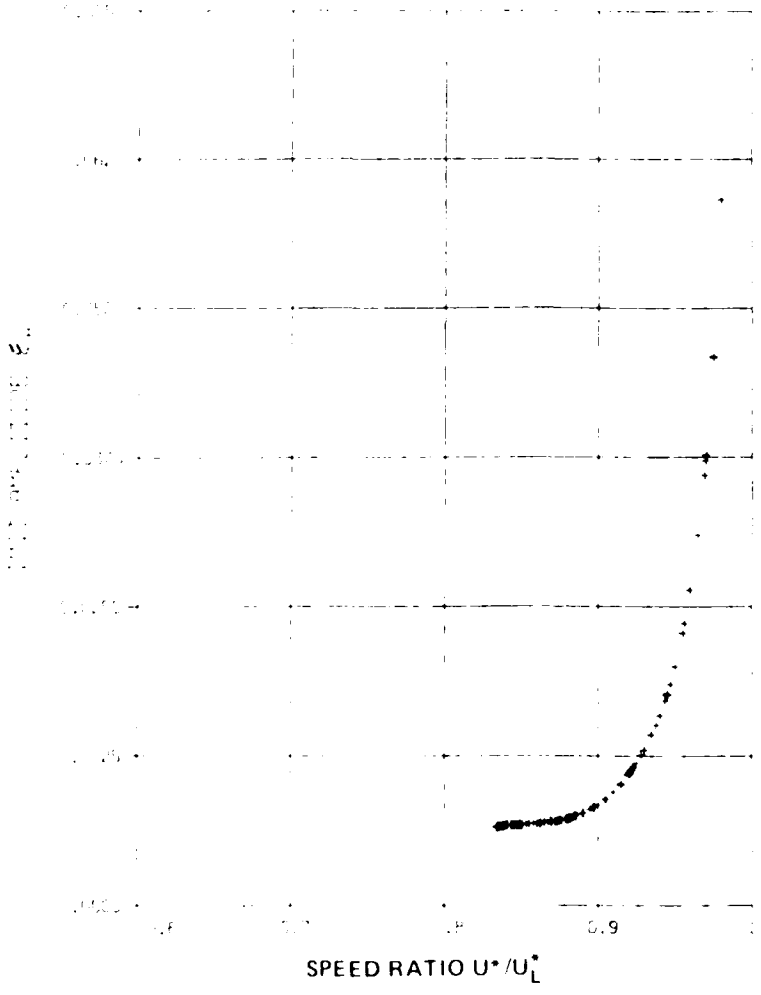

FIG. 30b: VARIATION OF LIMIT-AMPLITUDE ξ_A WITH SPEED RATIO FOR $\mu = 100$, $\bar{\omega} = 0.8$, $h_{f+} = 0.5$, $h_{f-} = 1.5$ AND $V_f = 0.5$

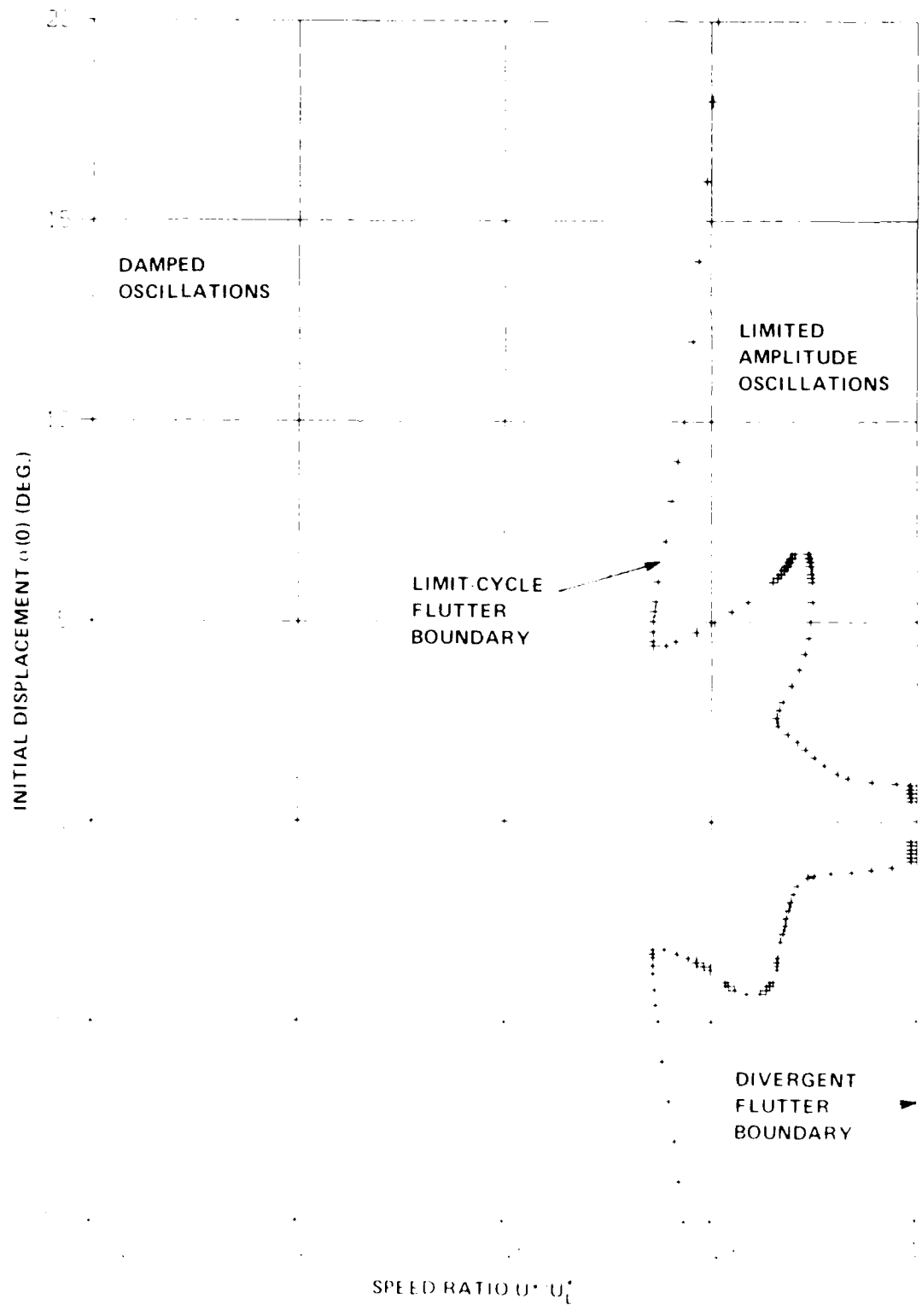

FIG 31 FLUTTER BOUNDARY FOR ... 50, ... 0.8, h_f 0.5, h_f 1.0 AND V_f 0.5

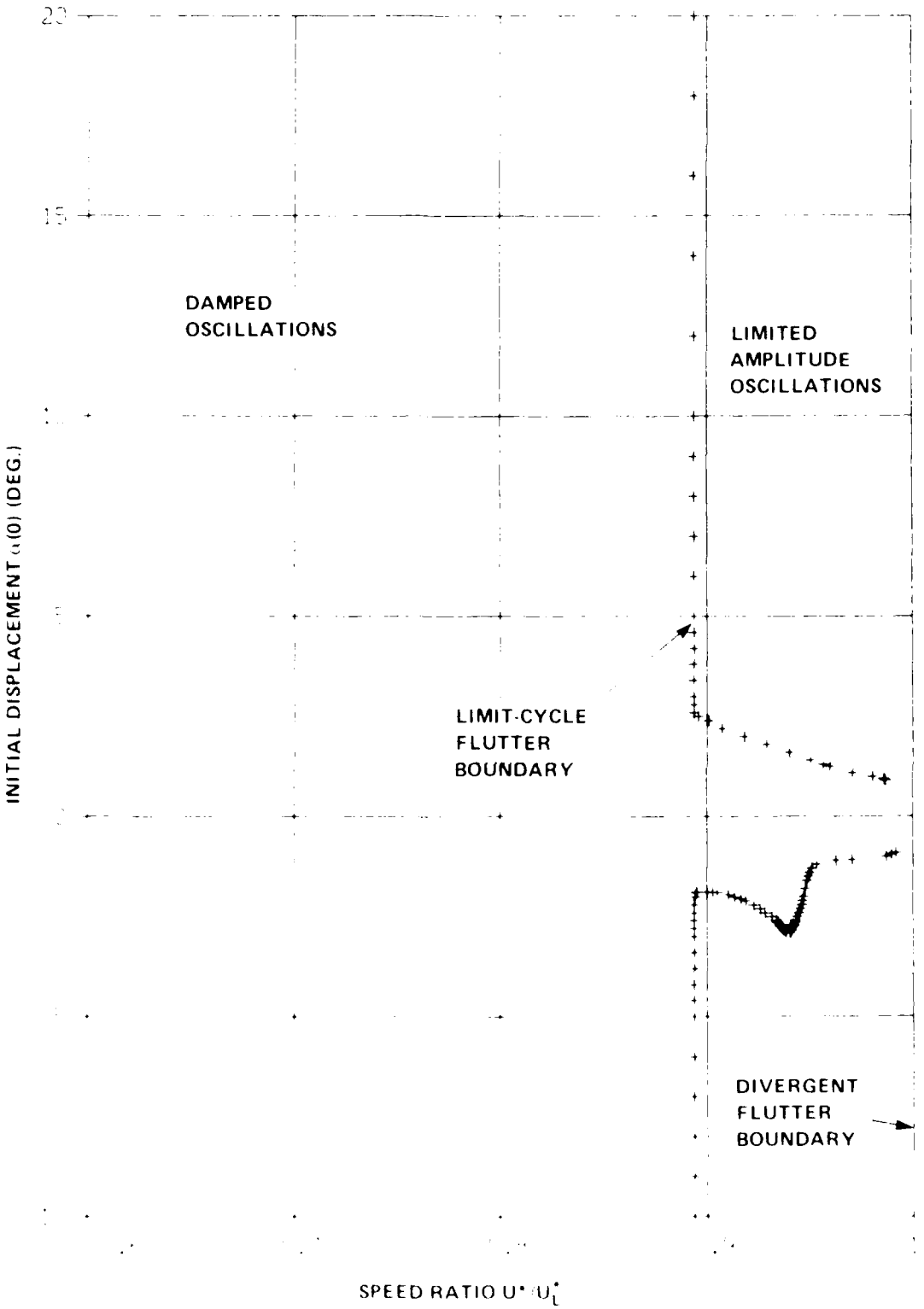

FIG. 32: FLUTTER BOUNDARY FOR μ 250, ω 0.8, h_f 0.5, h_f 1.0 AND V_f 0.5

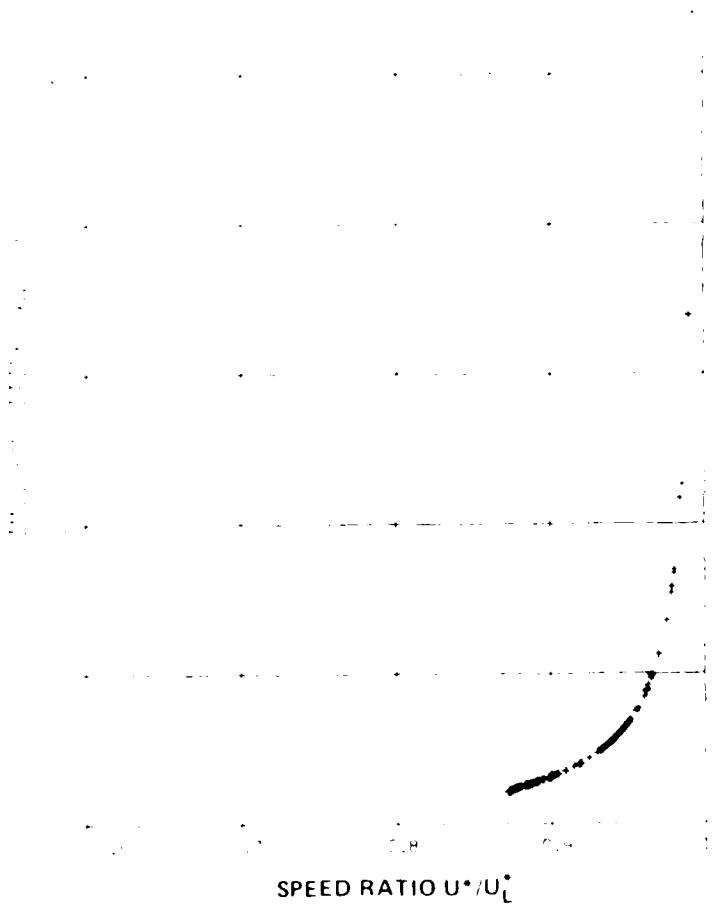

FIG. 33a: VARIATION OF LIMIT-AMPLITUDE α_A WITH SPEED RATIO FOR $\mu = 50$, $\bar{\omega} = 0.8$, $h_{f+} = 0.5^{\circ}$, $h_{f-} = 1.0^{\circ}$ AND $V_f = 0.5$

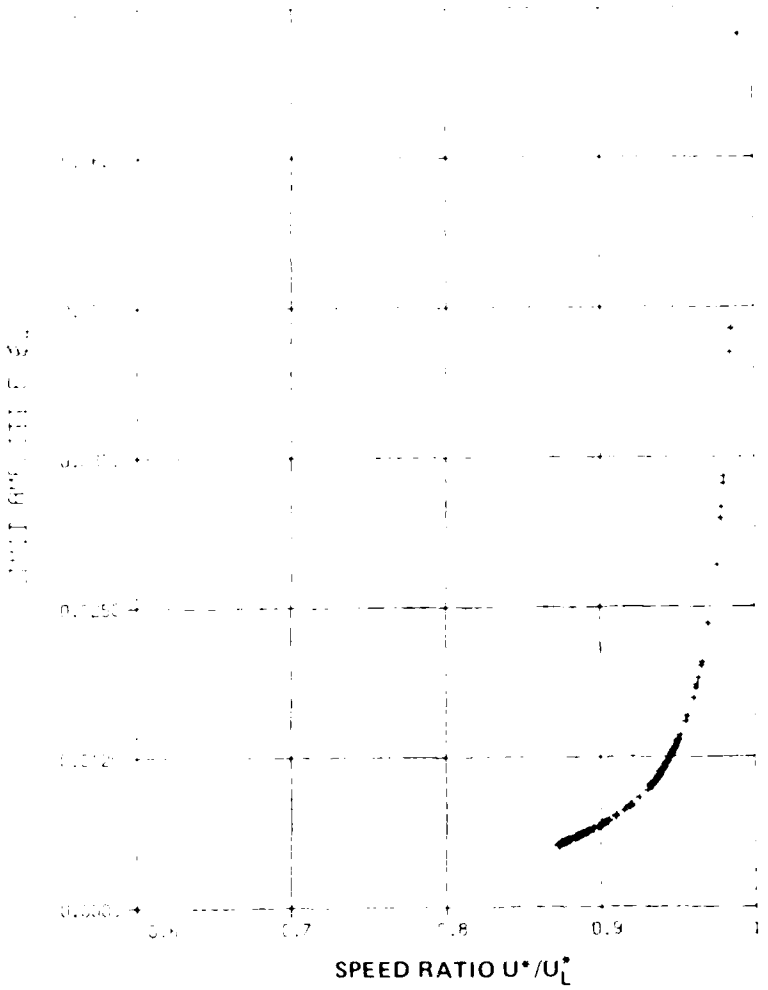

FIG. 33b: VARIATION OF LIMIT-AMPLITUDE ξ_A WITH SPEED RATIO FOR $\mu = 50$, $\bar{\omega} = 0.8$, $h_{f+} = 0.5^{\circ}$, $h_{f-} = 1.0^{\circ}$ AND $V_{f^{\circ}} = 0.5^{\circ}$

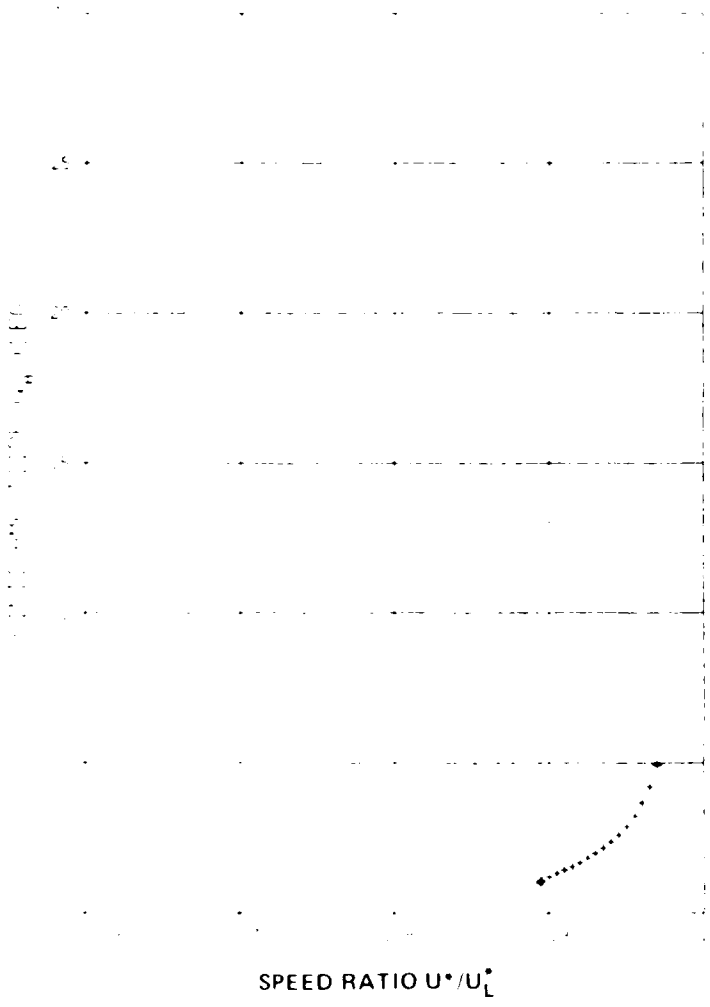

SPEED RATIO U^*/U_L^*

FIG. 34a: VARIATION OF LIMIT-AMPLITUDE α_A WITH SPEED RATIO FOR $\mu = 250$, $\bar{\omega} = 0.8$, $h_{f+} = 0.5^\circ$, $h_{f-} = 1.0^\circ$ AND $V_f = 0.5^\circ$

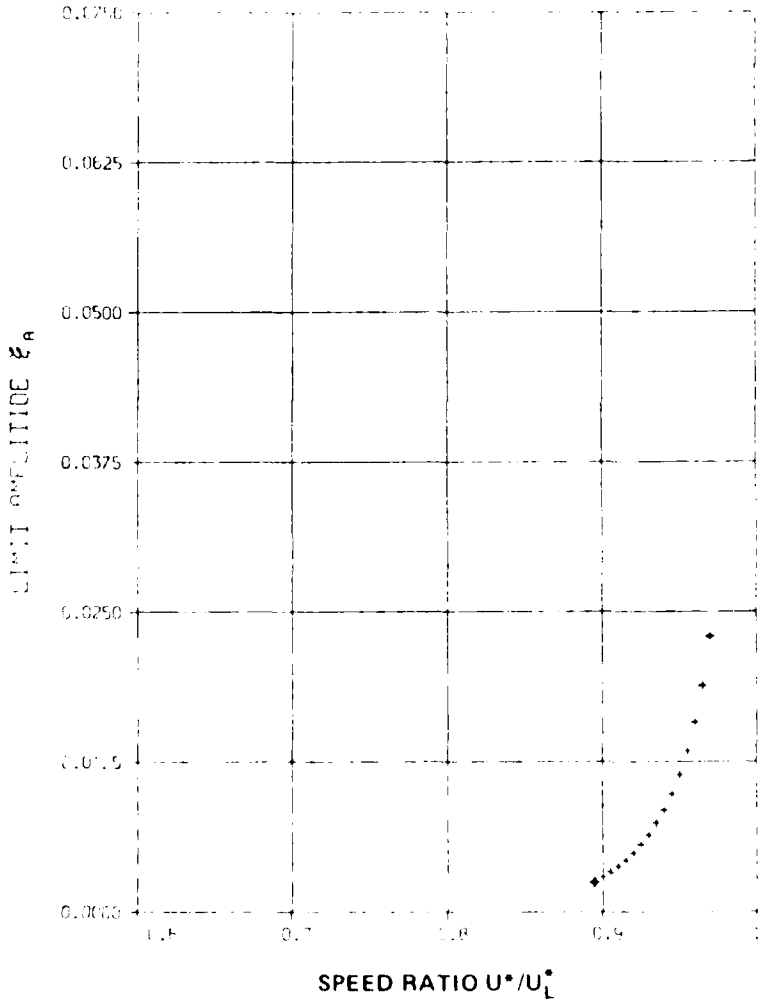

SPEED RATIO U^*/U_L^*

FIG. 34b: VARIATION OF LIMIT-AMPLITUDE ξ_A WITH SPEED RATIO FOR $\mu = 250$, $\bar{\omega} = 0.8$, $h_{f+} = 0.5^\circ$, $h_{f-} = 1.0^\circ$ AND $V_{f^\circ} = 0.5^\circ$

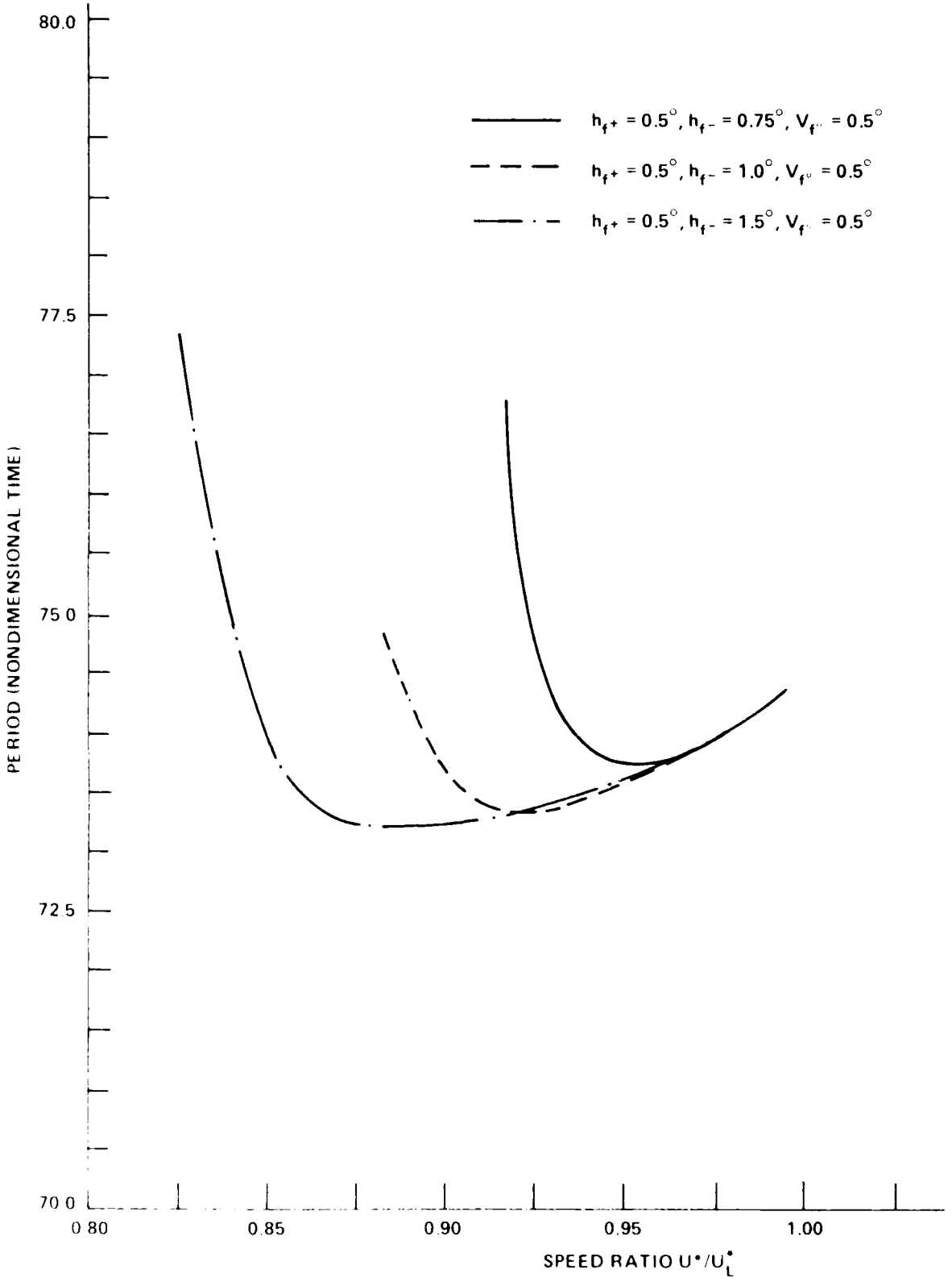

FIG. 35: PERIOD OF LIMITED AMPLITUDE OSCILLATIONS VERSUS SPEED RATIO FOR $\mu = 100$, $\bar{\omega} = 0.2$

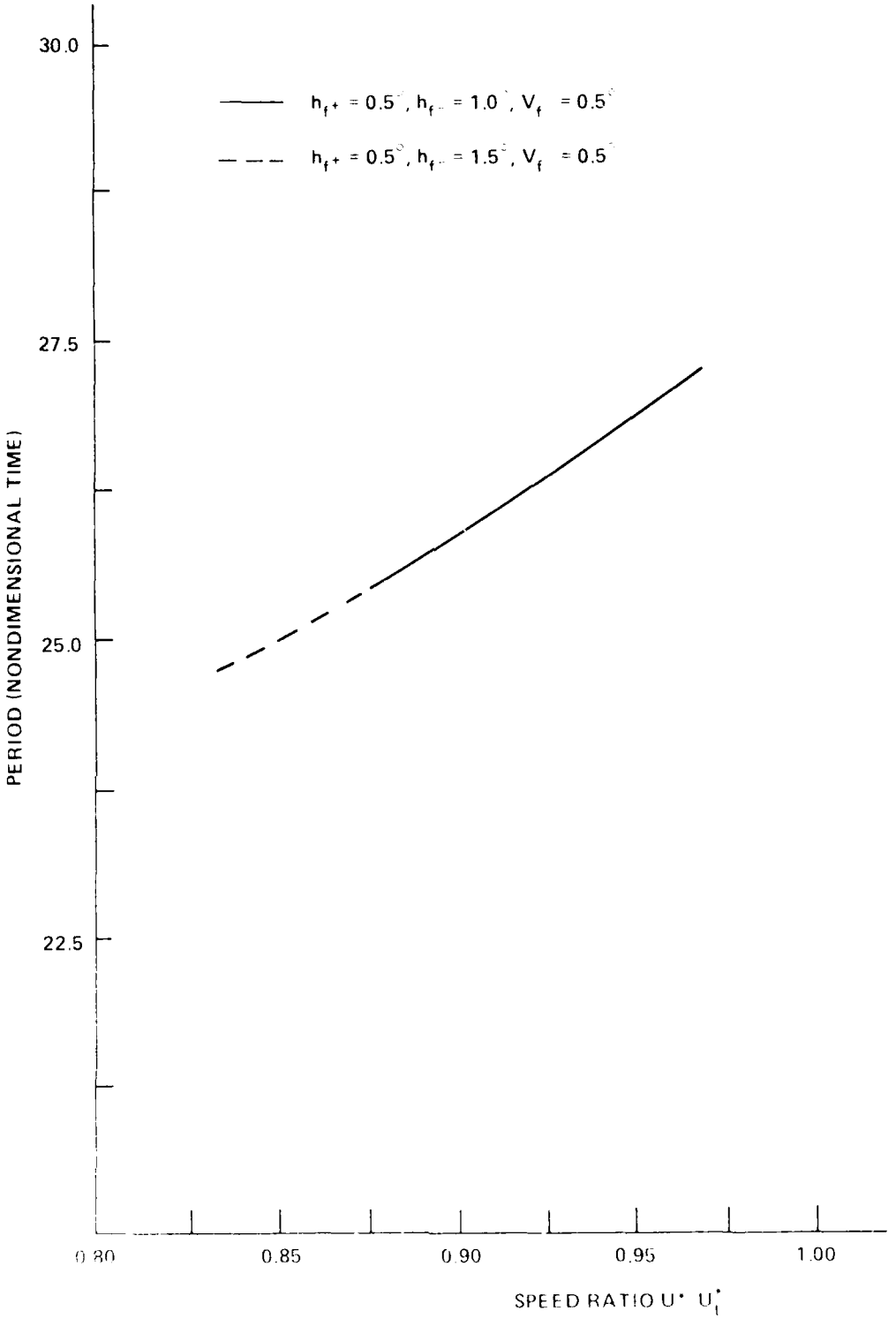

F IMITED AMPLITUDE OSCILLATIONS VERSUS SPEED RATIO
FOR μ 100, $\bar{\omega}$ 0.8

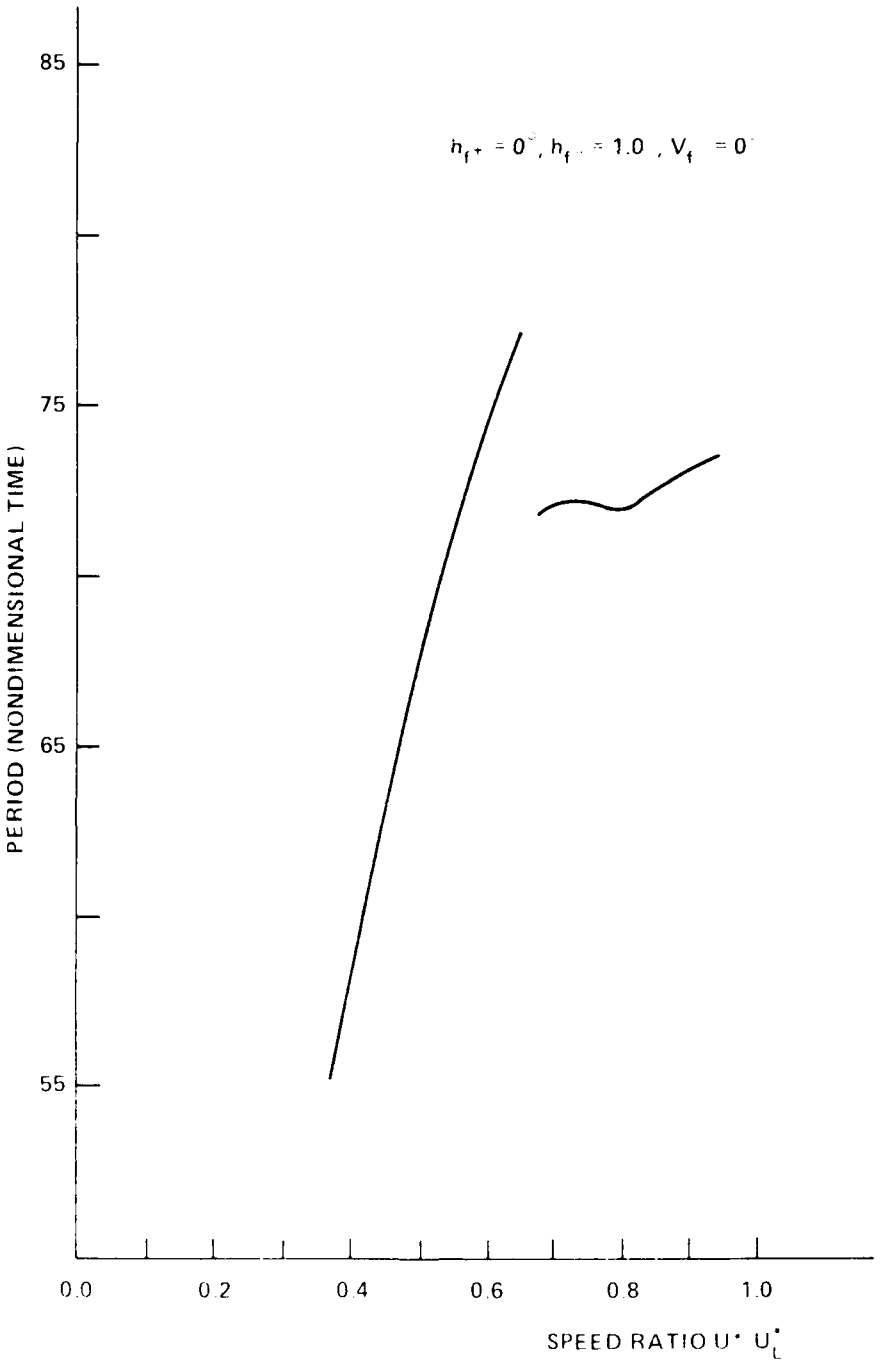

FIG. 37: PERIOD OF LIMITED AMPLITUDE OSCILLATIONS VERSUS SPEED RATIO FOR μ = 100, ω = 0.2

APPENDIX A

The coefficients $\bar{P}_{11}$, $\bar{P}_{12}$, $\bar{P}_{21}$, $\bar{P}_{22}$ and the terms $\bar{X}_1$ and $\bar{X}_2$ in Eqs. (14) and (15) are given as follows:

$$\bar{P}_{11} = \frac{2}{\mu(\Delta\tau)^2}\left[\mu x_\alpha - a_h\right] + \frac{1}{6\mu\Delta\tau}\left[11 + \left[\tfrac{1}{2}-a_h\right]\left[22\ell-9(a+c)\right]\right] + \frac{1}{8\mu}\left[16\ell - 11(a+c)\right] \tag{A-1}$$

$$\bar{P}_{12} = \frac{2}{\mu(\Delta\tau)^2}(1+\mu) + \frac{1}{6\mu\Delta\tau}\left[22\mu\,\zeta_\xi\,\frac{\bar{\omega}}{U^*} + 22\ell-9(a+c)\right] + \frac{\bar{\omega}^2}{U^{*2}} \tag{A-2}$$

$$\bar{P}_{21} = \frac{2}{\mu(\Delta\tau)^2}\left[\frac{1}{8}\left[r_\alpha^{-2}(1+8a_h^2)\right] + \mu\right] + \frac{1}{6\mu\Delta\tau}\left[22\,\mu\zeta_\alpha U^{*-1} + r_\alpha^{-2}\left(\tfrac{1}{2}-a_h\right)\left[11-\left(\tfrac{1}{2}+a_h\right)\{22\ell-9(a+c)\}\right]\right] - \frac{1}{8\mu}\,r_\alpha^{-2}\left(\tfrac{1}{2}+a_h\right)\left[16\ell-11(a+c)\right] \tag{A-3}$$

$$\bar{P}_{22} = \frac{2}{\mu(\Delta\tau)^2}\left[r_\alpha^{-2}(\mu x_\alpha - a_h)\right] - \frac{1}{6\mu\Delta\tau}\,r_\alpha^{-2}\left(\tfrac{1}{2}+a_h\right)\left[22\ell-9(a+c)\right] \tag{A-4}$$

$$\bar{X}_1 = \left\{\frac{5}{\mu(\Delta\tau)^2}(\mu x_\alpha - a_h) + \frac{3}{4\mu\Delta\tau}\left[4+\left(\tfrac{1}{2}-a_h\right)\left[8\ell-5(a+c)\right]\right] - \frac{9}{4\mu}(a+c)\right\}\alpha(\tau)$$

$$+ \left\{\frac{5}{\mu(\Delta\tau)^2}\ (1+\mu) + \frac{3}{4\mu\Delta\tau}\ [8\mu\zeta_\xi\bar{\omega}U^{*-1} + 8\ell-5(a+c)]\right\}\ \xi(\tau)$$

$$- \left\{\frac{4}{\mu(\Delta\tau)^2}\ (\mu x_\alpha - a_h) + \frac{3}{2\mu\Delta\tau}\ [1+(\tfrac{1}{2}-a_h)[2\ell-2(a+c)]] - \frac{9}{8\mu}\ (a+c)\right\}\ \alpha(\tau-\Delta\tau)$$

$$- \left\{\frac{4}{\mu(\Delta\tau)^2}\ (1+\mu) + \frac{3}{2\mu\Delta\tau}\ [2\zeta_\xi\mu\bar{\omega}U^{*-1} + 2\ell-2(a+c)]\right\}\ \xi(\tau-\Delta\tau)$$

$$+ \left\{\frac{1}{\mu(\Delta\tau)^2}\ (\mu x_\alpha - a_h) + \frac{1}{12\mu\Delta\tau}\ [4+(\tfrac{1}{2}-a_h)[8\ell-9(a+c)]] - \frac{1}{4\mu}\ (a+c)\right\}\ \alpha(\tau-2\Delta\tau)$$

$$+ \left\{\frac{1}{\mu(\Delta\tau)^2}\ (1+\mu) + \frac{1}{12\mu\Delta\tau}\ [8\mu\zeta_\xi\bar{\omega}U^{*-1} + 8\ell-9(a+c)]\right\}\ \xi(\tau-2\Delta\tau)$$

$$+ \frac{19\Delta\tau}{12\mu}\ [ae^{-b\Delta\tau} + ce^{-d\Delta\tau}]\ [\xi''(\tau) + (\tfrac{1}{2}-a_h)\ \alpha''(\tau) + \alpha'(\tau)]$$

$$- \frac{5\Delta\tau}{12\mu}\ [ae^{-2b\Delta\tau} + ce^{-2d\Delta\tau}]\ [\xi''(\tau-\Delta\tau) + (\tfrac{1}{2}-a_h)\ \alpha''(\tau-\Delta\tau) + \alpha'(\tau-\Delta\tau)]$$

$$+ \frac{\Delta\tau}{12\mu}\ [ae^{-3b\Delta\tau} + ce^{-3d\Delta\tau}]\ [\xi''(\tau-2\Delta\tau) + (\tfrac{1}{2}-a_h)\ \alpha''(\tau-2\Delta\tau) + \alpha'(\tau-2\Delta\tau)]$$

$$+ \frac{2}{\mu}\ [ae^{-b(\tau+\Delta\tau)} + ce^{-d(\tau+\Delta\tau)}]\ [\xi'(0) + (\tfrac{1}{2}-a_h)\ \alpha'(0) + \alpha(0)]$$

$$+ \frac{2}{\mu}\ ae^{-b\Delta\tau}\ I_1(\tau) + \frac{2}{\mu}\ ce^{-d\Delta t}\ I_2(\tau) \qquad \text{(A-5)}$$

where $$I_1(\tau) = \int_0^\tau \lambda(\sigma)\ e^{-b(\tau-\sigma)}\ d\sigma \qquad \text{(A-6)}$$

$$I_2(\tau) = \int_0^\tau \lambda(\sigma)\ e^{-d(\tau-\sigma)}\ d\sigma \qquad \text{(A-7)}$$

and $$\lambda(\sigma) = \xi''(\sigma) + (\tfrac{1}{2}-a_h)\,\alpha''(\sigma) + \alpha'(\sigma) \qquad \text{(A-8)}$$

$$\begin{aligned}
\bar{X}_2 = {} & \Big\{\frac{5}{\mu(\Delta\tau)^2}\Big[\frac{1}{8}\,[r_\alpha^{-2}(1+8a_h^2)] + \mu\Big] \\
& + \Big\{\frac{3}{4\mu\Delta\tau}\,[8\mu\zeta_\alpha U^{*-1} + r_\alpha^{-2}\,(\tfrac{1}{2}-a_h)\,[4-(\tfrac{1}{2}+a_h)\,(8\ell-5[a+c])]] \\
& + \frac{9}{4\mu}\,r_\alpha^{-2}\,(\tfrac{1}{2}+a_h)\,(a+c)\Big\}\alpha(\tau) \\
& + \Big\{\frac{5}{\mu(\Delta\tau)^2}\,r_\alpha^{-2}(\mu x_\alpha - \varepsilon_{..}) - \frac{3}{4\mu\Delta\tau}\,r_\alpha^{-2}\,(\tfrac{1}{2}+a_h)\,[8\ell-5(a+c)]\Big\}\xi(\tau) \\
& - \Big\{\frac{4}{\mu(\Delta\tau)^2}\Big[\frac{1}{8}\,[r_\alpha^{-2}\,(1+8a_h^2)] + \mu\Big] \\
& \quad + \frac{3}{2\mu\Delta\tau}\,[2\mu\zeta_\alpha U^{*-1} + r_\alpha^{-2}\,(\tfrac{1}{2}-a_h)\,[1-(\tfrac{1}{2}+a_h)\,(2\ell-2[a+c])]] \\
& \quad + \frac{9}{8\mu}\,r_\alpha^{-2}\,(\tfrac{1}{2}+a_h)\,(a+c)\Big\}\,a(\tau-\Delta\tau) \\
& - \Big\{\frac{4}{\mu(\Delta\tau)^2}\,r_\alpha^{-2}(\mu x_\alpha - a_h) - \frac{3}{2\mu\Delta\tau}\,r_\alpha^{-2}(\tfrac{1}{2}+a_h)\,[2\ell-2(a+c)]\Big\}\xi(\tau-\Delta\tau) \\
& + \Big\{\frac{1}{\mu(\Delta\tau)^2}\Big[\frac{1}{8}\,[r_\alpha^{-2}(1+8a_h^2)] + \mu\Big] \\
& \quad + \frac{1}{12\mu\Delta\tau}\,[8\mu\zeta_\alpha U^{*-1} + r_\alpha^{-2}(\tfrac{1}{2}-a_h)\,[4-(\tfrac{1}{2}+a_h)[8\ell-9(a+c)]]] \\
& \quad + \frac{1}{4\mu}\,r_\alpha^{-2}(\tfrac{1}{2}+a_h)\,(a+c)\Big\}\,\alpha(\tau-2\Delta\tau) \\
& + \Big\{\frac{1}{\mu(\Delta\tau)^2}\,r_\alpha^{-2}(\mu x_\alpha - a_h) - \frac{1}{12\mu\Delta\tau}\,r_\alpha^{-2}(\tfrac{1}{2}+a_h)\,[8\ell-9(a+c)]\Big\}\,\xi(\tau-2\Delta\tau) \\
& - \frac{19\Delta\tau}{12\mu}\,r_\alpha^{-2}\,(\tfrac{1}{2}+a_h)\,(ae^{-b\Delta\tau}+ce^{-d\Delta\tau})\,[\xi''(\tau)+(\tfrac{1}{2}-a_h)\,\alpha''(\tau)+\alpha'(\tau)] \\
& + \frac{5\Delta\tau}{12\mu}\,r_\alpha^{-2}(\tfrac{1}{2}+a_h)\,[ae^{-2b\Delta\tau}+ce^{-2d\Delta\tau}]\,[\xi''(\tau-\Delta\tau)+(\tfrac{1}{2}-a_h)\,\alpha''(\tau-\Delta\tau)+\alpha'(\tau-\Delta\tau)]
\end{aligned}$$

$$- \frac{\Delta\tau}{12\mu} r_\alpha^{-2(\frac{1}{2}+a_h)} \left(ae^{-3b\Delta\tau}+ce^{-3d\Delta t}\right) \left[\xi''(\tau-2\Delta\tau)+(\tfrac{1}{2}-a_h)\alpha''(\tau-2\Delta\tau) + \alpha'(\tau-2\Delta\tau)\right]$$

$$- \frac{2}{\mu} r_\alpha^{-2(\frac{1}{2}+a_h)} \left(ae^{-b(\tau+\Delta\tau)}+ce^{-d(\tau+\Delta\tau)}\right) \left[\xi'(0)+(\tfrac{1}{2}-a_h)\alpha'(0)+\alpha(0)\right]$$

$$- \frac{2}{\mu} r_\alpha^{-2(\frac{1}{2}+a_h)} ae^{-b\Delta\tau} I_1(\tau) - \frac{2}{\mu} r_\alpha^{-2(\frac{1}{2}+a_h)} ce^{-d\Delta\tau} I_2(\tau)$$

(A-9)

APPENDIX B

In Eq. (26), the elements of [Q] and $\{Y^{(n)}\}$ are:

$$Q_{11} = \frac{1}{\mu} (\mu x_\alpha - a_h) \tag{B-1}$$

$$Q_{12} = \frac{1}{\mu} (1+\mu) \tag{B-2}$$

$$Q_{21} = \frac{1}{\mu} \left[\frac{1}{r_\alpha^2} \left(\frac{1}{8}+a_h^2\right) + \mu\right] \tag{B-3}$$

$$Q_{22} = \frac{1}{\mu} r_\alpha^{-2} (\mu x_\alpha - a_h) \tag{B-4}$$

$$\begin{aligned} Y_1^{(2)} = & - \frac{1}{\mu} \left[1+\left(\tfrac{1}{2}-a_h\right) [2\ell-2(a+c)]\right] \alpha'(0) \\ & - \frac{1}{\mu} \left[2\mu\zeta_\xi \bar{\omega} U^{*^{-1}} + 2\ell-2(a+c)\right] \xi'(0) - \frac{1}{\mu} [2\ell-(a+c)]\alpha(0) \\ & - \frac{1}{U^{*^2}} \xi(0) \end{aligned} \tag{B-5}$$

$$\begin{aligned} Y_2^{(2)} = & - \frac{1}{\mu} \left[2\mu\zeta_\alpha U^{*^{-1}} + r_\alpha^{-2}\left(\tfrac{1}{2}-a_h\right) \left[1-\left(\tfrac{1}{2}+a_h\right)[2\ell-2(a+c)]\right]\right] \alpha'(0) \\ & + \frac{1}{\mu} \left[r_\alpha^{-2}\left(\tfrac{1}{2}+a_h\right) [2\ell-2(a+c)]\right] \xi'(0) + \frac{1}{\mu} r_\alpha^{-2}\left(\tfrac{1}{2}+a_h\right) [2\ell-2(a+c)] \alpha(0) \\ & - \frac{1}{U^{*^2}} F[\alpha(0)] \end{aligned} \tag{B-6}$$

$$Y_1^{(3)} = -\frac{1}{\mu}\left[1+(\tfrac{1}{2}-a_h)\left[2\ell-2(a+c)\right]\right]\alpha''(0) - \frac{1}{\mu}\left[2\mu\zeta_\xi\bar{\omega}U^{*-1}+2\ell-2(a+c)\right]\xi''(0)$$

$$-\frac{1}{\mu}\left[2\ell-2(a+c)+(\tfrac{1}{2}-a_h)(2ab+2cd)\right]\alpha'(0) - \left\{\frac{1}{\mu}\left[2ab+2cd\right]+\frac{\bar{\omega}^2}{U^{*2}}\right\}\xi'(0)$$

$$-\frac{1}{\mu}(2ab+2cd)\,\alpha(0) \qquad \text{(B-7)}$$

$$Y_2^{(3)} = -\frac{1}{\mu}\left[2\mu\zeta_\alpha U^{*-1} + r_\alpha^{-2}(\tfrac{1}{2}-a_h)\left[1-(\tfrac{1}{2}+a_h)\left[2\ell-2(a+c)\right]\right]\right]\alpha''(0)$$

$$+\frac{1}{\mu}r_\alpha^{-2}(\tfrac{1}{2}+a_h)\left[2\ell-2(a+c)\right]\xi''(0)$$

$$+\frac{1}{\mu}r_\alpha^{-2}(\tfrac{1}{2}+a_h)\left[2\ell-2(a+c)+(\tfrac{1}{2}-a_h)(2ab+2cd)\right]\alpha'(0)$$

$$+\frac{1}{\mu}r_\alpha^{-2}(\tfrac{1}{2}+a_h)(2ab+2cd)\left[\xi'(0)+\alpha(0)\right] - \frac{1}{U^{*2}}\frac{d}{d\tau}F[\alpha(0)]$$

$$\text{(B-8)}$$

$$Y_1^{(4)} = -\frac{1}{\mu}\left[1+(\tfrac{1}{2}-a_h)\left[2\ell-2(a+c)\right]\right]\alpha'''(0)$$

$$-\frac{1}{\mu}\left[2\mu\zeta_\xi\bar{\omega}U^{*-1}+2\ell-2(a+c)\right]\xi'''(0)$$

$$-\frac{1}{\mu}\left[2\ell-2(a+c)+(\tfrac{1}{2}-a_h)(2ab+2cd)\right]\alpha''(0)$$

$$-\left\{\frac{1}{\mu}\left[2ab+2cd\right]+\frac{\bar{\omega}^2}{U^{*2}}\right\}\xi''(0)$$

$$-\frac{1}{\mu}\left[2ab+2cd-(\tfrac{1}{2}-a_h)(2ab^2+2cd^2)\right]\alpha'(0)$$

$$+\frac{1}{\mu}\left[2ab^2+2cd^2\right]\left[\xi'(0)+\alpha(0)\right] \qquad \text{(B-9)}$$

$$
\begin{aligned}
Y_2^{(4)} = &- \frac{1}{\mu}\left[2\mu\zeta_\alpha U^{*-1} + r_\alpha^{-2}\left(\tfrac{1}{2}-a_h\right)\left[1-\left(\tfrac{1}{2}+a_h\right)[2\ell-2(a+c)]\right]\right]\alpha'''(0) \\
&+ \frac{1}{\mu}\left[r_\alpha^{-2}\left(\tfrac{1}{2}+a_h\right)\left[2\ell-2(a+c)>\right]\right]\xi'''(0) \\
&+ \frac{1}{\mu}\left[r_\alpha^{-2}\left(\tfrac{1}{2}+a_h\right)\left[2\ell-2(a+c) + \left(\tfrac{1}{2}-a_h\right)(2ab+2cd)\right]\right]\alpha''(0) \\
&+ \frac{1}{\mu} r_\alpha^{-2}\left(\tfrac{1}{2}+a_h\right)(2ab+2cd)\,\xi''(0) \\
&+ \frac{1}{\mu}\left[r_\alpha^{-2}\left(\tfrac{1}{2}+a_h\right)\left[2ab+2cd - \left(\tfrac{1}{2}-a_h\right)(2ab^2+2cd^2)\right]\right]\alpha'(0) \\
&- \frac{1}{\mu} r_\alpha^{-2}\left(\tfrac{1}{2}+a_h\right)(2ab^2+2cd^2)\left[\xi'(0)+\alpha(0)\right] \\
&- \frac{1}{U^{*2}}\frac{d^2}{d\tau^2}\,F[\alpha(0)] \qquad\qquad (B\text{-}10)
\end{aligned}
$$

REPORT DOCUMENTATION PAGE / PAGE DE DOCUMENTATION DE RAPPORT

REPORT/RAPPORT	REPORT/RAPPORT
LR-618 (1a)	NRC No. 27833 (1b)
REPORT SECURITY CLASSIFICATION / CLASSIFICATION DE SÉCURITÉ DE RAPPORT	DISTRIBUTION (LIMITATIONS)
Unclassified (2)	Unlimited (3)

TITLE/SUBTITLE/TITRE/SOUS-TITRE

4 Flutter Analysis of a Two-Dimensional Airfoil Containing Structural Nonlinearities

AUTHOR(S)/AUTEUR(S)

5 B.H.K. Lee, J. Desrochers*

* Summer Student, McGill University

SERIES/SÉRIE

6 Aeronautical Report

CORPORATE AUTHOR/PERFORMING AGENCY/AUTEUR D'ENTREPRISE/AGENCE D'EXÉCUTION

7 National Research Council Canada
National Aeronautical Establishment — High Speed Aerodynamics Laboratory

SPONSORING AGENCY/AGENCE DE SUBVENTION

8

DATE	FILE/DOSSIER	LAB. ORDER / COMMANDE DU LAB.	PAGES	FIGS/DIAGRAMMES
87-05			92	37
9	10	11	12a	12b

NOTES

13

DESCRIPTORS (KEY WORDS)/MOTS-CLÉS

1. Aerofoils — flutter

14

SUMMARY/SOMMAIRE

Nonlinear flutter of a two-dimensional airfoil undergoing plunging and pitching motions is studied using a time marching finite difference scheme. The structural nonlinearity considered is of the type [illegible] with preload and freeplay. Flutter is determined from [illegible] the structural dynamic [illegible] when [illegible] divergent or limited amplitude oscillations are [illegible]. Case studies using various [illegible] preload and freeplay are carried out. The effect of initial conditions, which [illegible], is investigated by varying the displacement from equilibrium of the pitch angle [illegible]. For nonzero values of the preload, three types of oscillatory motion are possible, namely, damped, limit cycle and divergent. The divergent flutter boundary is practically identical to that for the linear [illegible] case. The location of the limit cycle flutter boundary varies for different [illegible] and [illegible] parameters. [illegible] are not encountered [illegible] study. The limited amplitude of the pitch [illegible] displacement. The characteristics of [illegible] the flutter boundaries [illegible] are [illegible].

15

END

10-87

DTIC